

PEOPLE'S DEMOCRATIC REPUBLIC OF ALGERIA
MINISTRY OF HIGHER EDUCATION AND SCIENTIFIC RESEARCH
NATIONAL POLYTECHNIC SCHOOL



Electronics Department
Final Studies Project to obtain
Electronics Engineer Diploma

Topic:

**Field Oriented Control of Induction Motors
Based on DSP Controller**

Presented By:

BOUKHTACHE Seyfeddine

MESSINI Merouane

Dissertation Committee:

Mr. C.LERBES	Professor	ENP	Supervisor
Mr. M.S. AIT-CHEIKH	Professor	ENP	President
Mr. M.HADDADI	Professor	ENP	Examiner

ENP June 2016

ملخص

في هذا العمل، طُور نموذج رياضي للمحرك اللامتزامن. أُستعملت تقنية تطبيع عرض النبض الشعاعية من أجل التحكم في المموج. التحكم الشعاعي طُور من أجل فصل التدفق والعزم. المضبطات PI صُممت من أجل ضبط السرعة والتيار. التيارات Matlab/Simulink. أُستعمل من أجل المحاكاة لإظهار سير الخوارزمية FOC. أخيرا الخوارزمية FOC تُثبتت على البطاقة DSP F28335.

كلمات مفتاحية: محرك لا متزامن، تقنية تطبيع عرض النبض الشعاعية، التحكم الشعاعي.

RESUME

Dans ce travail, un modèle mathématique du moteur asynchrone a été développé. La technique MLI vectorielle a été utilisée pour commander l'onduleur. La commande vectorielle a été développée pour découpler le flux et le couple. Des régulateurs PI ont été conçus pour régler la vitesse et le courant. La simulation par Matlab/Simulink a été employée pour montrer le fonctionnement de l'algorithme FOC. Enfin, l'algorithme FOC a été implémenté sur DSP F28335.

Mots clés : Moteur à induction, MLI vectorielle, Commande vectorielle.

ABSTRACT

In this work, a mathematical model was developed for induction motor. The space vector PWM technique was implemented for controlling the three-phase inverter switches. Field oriented control (FOC) method was developed to get the decoupled control of flux and torque. PI based controllers were designed for speed and current control loop. The computer simulation Matlab/Simulink was used to show the efficacy of the FOC algorithm. The field oriented control algorithm was implemented on DSP F28335.

Key words: Induction motor, SVPWM, Inverter, FOC, DSP.

ACKNOWLEDGEMENTS

We wish to express our sincere gratitude to our supervisor Pr C.LARBES, who has been a constant source of guidance, support and encouragement throughout our graduate studies. His extensive knowledge, rigorous research attitude, diligent working and creative thinking have inspired us and will definitely benefit our future career.

Finally we would like to thank our parents for their love and support.

They are the strength behind our success.

DEDICATION

To our parents, our families, our teachers and anyone who ever shared their knowledge with us.

TABLE OF CONTENTS

ABSTRACT

ACKNOWLEDGEMENTS

DEDICATION

LIST OF FIGURES

LIST OF TABLES

LIST OF SYMBOLS

INTRODUCTION.....	1
1. Background.....	1
2. Power plant Characteristics.....	1
3. Electric motor.....	3
4. Research Objectives and Thesis Outline.....	7
CHAPTER1: THE MODELING OF INDUCTION MOTOR.....	9
1.1 Introduction.....	9
1.2 Induction motor construction, principles and operation.....	10
1.3 The Equivalent Circuit of Induction Motor.....	16
1.4 The System Equations in abc Reference Frame.....	18
1.5 Determination of Machine Inductances.....	19
1.6 3phase to 2phase Transformation.....	21
1.7 Dynamic Model of Induction Motor.....	26
1.8 Power and Torque.....	32
1.9 Simulation.....	34
1.10 Conclusion.....	36

CHAPTER 2: SPACE VECTOR PULSE WIDTH MODULATION.....	37
2.1 INVERTERS.....	37
2.1.1 Current Source Inverter (CSI).....	37
2.1.2 Voltage Source Inverter (VSI).....	38
2.1.3 120 ⁰ conduction mode.....	38
2.2 PWM.....	39
2.2.1 Principle of Sinusoidal Pulse Width Modulation (SPWM).....	39
2.2.2 Space Vector PWM.....	40
2.3 Implementation of Space Vector PWM.....	42
2.4 SVPWM Simulation.....	49
3.5 Summary.....	51
CHAPTER 3: FIELD ORIENTED CONTROL.....	52
3.1 Introduction.....	52
3.1.1 Model of field oriented control.....	53
3.1.2 FOC algorithm.....	57
3.2 Rotor field oriented scheme.....	59
3.2.1 PI current controller design.....	61
3.2.2 PI speed controller design.....	63
3.3 Simulation.....	66
3.4 Conclusion.....	70
CHAPTER 4: DSP PROGRAMMING.....	71
4.1 Introduction.....	71
4.1.1 Approach1.....	71

4.1.2 Approach2.....	72
4.2 DSP Programming and CCS.....	73
4.2.1 Description of the F28335 DSP and the Used Hardware.....	73
4.2.2 FOC Implementation.....	75
4.3 Testing and Evaluation.....	93
4.4 Summary.....	96
CONCLUSION.....	97
REFERENCES.....	98
APPENDIX.....	100

LIST OF FIGURES

Figure	page
Fig 1: Ideal performance characteristics for a vehicle traction power plant.....	2
Fig 2: Typical characteristics of a gasoline engine.....	2
Fig 3: Classification of electric motor.....	3
Fig 4: Permanent magnet synchronous motor.....	4
Fig 5: Switched reluctance motors	5
Fig 6: Induction motors	5
Fig 1.1: Cross section of an induction machine.....	10
Fig 1.2: Resultant vector representation of the three phase currents.....	10
Fig 1.3: Conducting rotor bars without the rotor.....	11
Fig 1.4: Short-Circuited rotor bars of the squirrel cage induction motor.....	11
Fig 1.5: Squirrel cage induction motor cross section.....	12
Fig 1.6: The Simple Construction of Two Pole Stator.....	12
Fig 1.7: At $\omega t = 0^\circ$	13
Fig 1.8: At $\omega t = 90^\circ$	14
Fig 1.9: The Per Phase Equivalent Circuit of Induction Motor.....	16
Fig 1.10: The Per Phase Equivalent Circuit of Induction Motor.....	17
Fig 1.11: The Modified Per Phase Equivalent Circuit of Induction Motor.....	18
Fig 1.12: Clarke's Transformation.....	22
Fig 1.13: Clarke transformation of three-phase currents.....	23
Fig 1.14: Park transformation of two-phase currents.....	25
Fig 1.15: The total Transformation from abc to dq coordinates.....	25

Fig 1.16: The stator current I_{ds}	34
Fig 1.17: The stator current I_{qs}	34
Fig 1.18: The torque (T_e).....	35
Fig 1.19: The speed.....	35
Fig 2.1: Current Source Inverter.....	37
Fig 2.2: Voltage Source Inverter.....	38
Fig 2.3: Operation of switches over a cycle.....	39
Fig 2.4: Voltage state.	39
Fig 2.5: Circuit model of a single-phase inverter.....	39
Fig 2.6: Pulse Width Modulation.....	40
Fig 2.7: The eight inverter voltage vectors (V_0 to V_7).....	42
Fig 2.8: Clarke's Transformation.....	43
Fig 2.9: Hexagon Representation of Space Vectors.....	43
Fig 2.10: The V_{ref} in $\alpha \beta$ axis.....	44
Fig 2.11: The reference voltage in sector 1.....	44
Fig 2.12: The Switching Pattern of SVPWM at each Sector.....	48
Fig 2.13: SVPWM simulation model.....	49
Fig 3.14: SVPWM duty cycle (T_a, T_b, T_c).....	49
Fig 2.15: SVPWM duty cycle (T_a-T_b).....	50
Fig 2.16: The output line to neutral voltage (V_{an}).....	50
Fig 2.17: The output line to line voltage (V_{ab}, V_{bc}, V_{ca}).....	50
Fig 2.18: The filtered output line to line voltage (V_{ab}, V_{bc}, V_{ca}).....	51
Fig 3.1: A simple representation of DC motor.....	52

Fig 3.2: The vector representation of rotor field oriented scheme.....	56
Fig 3.3: The flow chart of the FOC algorithm.....	57
Fig 3.4: The basic scheme of field oriented control.....	58
Fig 3.5: Block diagram of indirect rotor field oriented control.....	59
Fig 3.6: The block diagram of direct axis current control.....	61
Fig 3.7: The block diagram of the quadrature axis current control.....	62
Fig 3.8: The block diagram of the speed control.....	64
Fig 3.9: FOC Simulink Model.....	66
Fig 3.10: Test results for scenario 1.....	67
Fig 3.11: Test results for scenario 2.....	68
Fig 3.12: Test results for Scenario 3.....	69
Fig 4.1: Illustration of two different approaches that can be used in the DSP project.....	71
Fig 4.2: Programming Languages used in Embedded Designs	72
Fig 4.3: Block Diagram of F28335	74
Fig 4.4: The used F28335 modules.....	75
Fig 4.5: Design of vector control pwn for induction motor	75
Fig 4.6: Flow chart of the DSPF28335 program.....	76
Fig 4.7: Block diagram of ADC module.....	78
Fig 4.8: ADC module configuration.....	79
Fig 4.9: The sub-modules of each ePWM module	80
Fig 4.10: Time-base submodule structure in each ePWM module.....	83
Fig 4.11: Time base counter synchronization scheme for F28335.....	83
Fig 4.12: Counter-compare event, up-down counter mode.....	84

Fig 4.13: Block diagram of ePWM dead band sub-module.....	86
Fig 4.14: Waveform of PWM with dead band inserted.....	86
Fig 4.15: Block diagram of eQEP module.....	89
Fig 4.16: Example waveforms of the eQEP.....	90
Fig 4.17: Four memory sections of DATALOG module.....	92
Fig 4.18: The graphical waveforms of the observed variables.....	92
Fig 4.19: Clarke voltage (V_{α} and V_{β}).....	93
Fig 4.20: Duty cycles (T_a, T_b, T_c).....	94
Fig 4.21: The three uppers PWM signals.....	95
Fig 4.22: The Motor speed.....	96

LIST OF TABLES

Table	page
Table 1: Comparison of three AC motors.....	6
Table 2.1: Switching vectors, phase voltages and output line to line voltages.....	41
Table 2.2: Calculation of Switching Time at each Sector.....	47
Table 4.1: ADC input channels and corresponding addresses.....	78
Table 4.2: Encoder Truth table.....	91

LIST OF SYMBOLS

EVs	Electric vehicles.
HEVs	Hybrid Electric Vehicles.
DC	Direct Current.
AC	Alternative Current.
PMSM	Permanent Magnet Synchronous Motor.
SRM	Switched Reluctance Motor.
DSP	Digital Signal Processor.
PWM	Pulse Width Modulation.
SVPWM	Space Vector Pulse Width Modulation.
FOC	Field Oriented Control.
IGBT	Insulated Gate Bipolar Transistor
IGCT	integrated gate-commutated thyristor
MOSFET	Metal Oxide Semiconductor Field Effect Transistor
VSI	Voltage Source Inverter
CSI	Current Source Inverter
EMF	Electromotive force
DFOC	Direct Field Oriented Control
IFOC	Indirect Field Oriented Control
CCS	Code Composer Studio
ADC	Analog to digital converter
FPU	Floating Point Unit
PLL	Phase Locked Loop

SARAM	Single Access Random Access Memory
ROM	Read Only Memory
OTP	One Time Programmable memory
DMA	Direct Memory Access
QEP	Quadrature Encoder Pulse
PIE	Peripheral Interrupt Expansion
MUX	Multiplexer
SOC	Start Of Conversion
GPIO	General Purpose Input/Output
TI	Texas Instruments
R	Magnetic circuit reluctance.
i_a	Phase a current.
I_b	Phase b current.
i_c	Phase c current.
i_m	Current magnitude.
H_a	Phase a magnetic field intensity.
H_b	Phase b magnetic field intensity.
H_c	Phase c magnetic field intensity.
H_m	Magnetic field intensity magnitude.
B_a	Phase a magnetic flux density.
B_b	Phase b magnetic flux density.
B_c	Phase c magnetic flux density.
B_m	Magnetic flux density magnitude.

N_{sync}	Synchronous speed.
f	Frequency.
P	Number of poles.
N_{slip}	Slip speed.
S	Slip.
a_{eff}	Equivalent turns ratio
n_s	Number of turns per stator phase
n_r	Number of turns per rotor phase
V_{abc}^s	Three phase stator voltage
i_{abc}^s	Three phase stator current
λ_{abc}^s	Three phase stator flux
V_{abc}^r	Three phase rotor voltage
i_{abc}^r	Three phase rotor current
λ_{abc}^r	Three phase rotor flux
r_s	Stator resistance
r_r	Rotor resistance
$L_{\text{as,bs,cs}}$	Total self inductance of phase as,bs,cs
L_{ls}	Self inductance of stator phase
L_{ms}	Magnetizing inductance of stator phase
$L_{\text{abs}}, L_{\text{bcs}}, L_{\text{cas}}$	The mutual inductance between stator three phase
θ_r	Angle from the rotor to the stator phase
(a,b,c)	Three coordinate system
(α,β)	Two coordinate stationary frame

(d,q)	Two coordinate rotating frame
K	Clarke transformation matrix.
Q	Park transformation matrix
θ_s	Angle of stator magnetic field
T_e	Torque
ω_s	Electrical speed
ω_r	Mechanical speed
P_e	Electric power
T_L	Load torque
J	Rotor's moment of inertia
m	Modulation index
ω	Angular velocity
T_a, T_b, T_c	Duty cycles
T_0, T_1, T_2	Time durations
V_{an}, V_{bn}, V_{cn}	Line to neutral voltages
V_{ab}, V_{bc}, V_{ca}	Line to line voltages
S_1 to S_6	Switching variable vectors
V_0 to V_7	Space voltage vectors
V_{dc}	DC main bus Voltage

INTRODUCTION

INTRODUCTION

1 Background

The development of internal combustion engine vehicles is one of the greatest achievements in the automotive industry for the past a few centuries. Automobiles have made great contributions to the growth of technology, economy, even cultures by satisfying many of the needs for mobility in our daily life.

However, the large numbers of automobiles which are being used all around the world have caused serious problems to the environment and human life. Air pollution, global warming, and the rapid depletion of the earth's petroleum resources are now problems of primary concern. The environmental issues and oil crisis compel people to develop clean, efficient vehicles solutions for urban transportation.

In the past few decades, lots of research and development activities related to the automotive industry started emphasizing the development of clean, low/zero emission, and high efficiency transportation. So electric vehicles (EVs), hybrid electric vehicles (HEVs), and fuel cell vehicles became popular and have been typically proposed to replace conventional vehicles in the near future. The electric vehicle is the first consideration for its zero emissions feature [1,2].

2 Power plant Characteristics

For vehicular applications, the ideal performance characteristic of a power plant is a constant power output over the full speed range. Consequently, the torque varies with speed hyperbolically as shown in Fig 1. With this ideal profile, the maximum power of the power plant will be available at any vehicle speed, therefore yielding the optimal vehicle performance [2].

INTRODUCTION

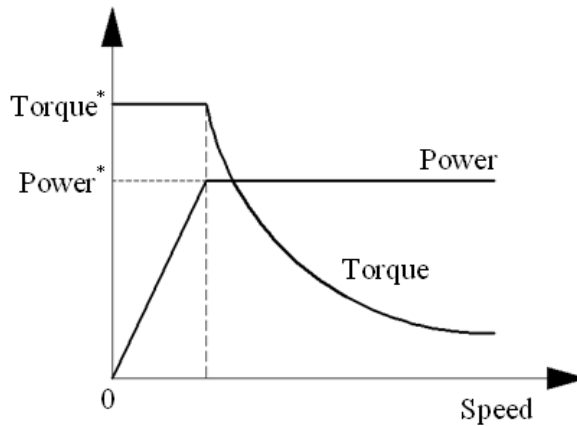


Fig 1: Ideal performance characteristics for a vehicle traction power plant.

The most commonly used power plants for vehicles are no doubt the internal combustion engine. The typical characteristics of an internal combustion engine are shown in Fig 2. Obviously, it is far from the ideal torque–speed profile curve.

At the idle speed region, it operates in a smooth condition, but the maximum torque is achieved at an intermediate speed. With the speed further increasing, the torque decreases.

Instead of occurring at the very beginning, the maximum power happens at a high speed. Beyond this speed, the engine power decreases. Furthermore, the internal combustion engine has a relatively flat torque–speed profile, as compared with an ideal power plant shown in Fig2.

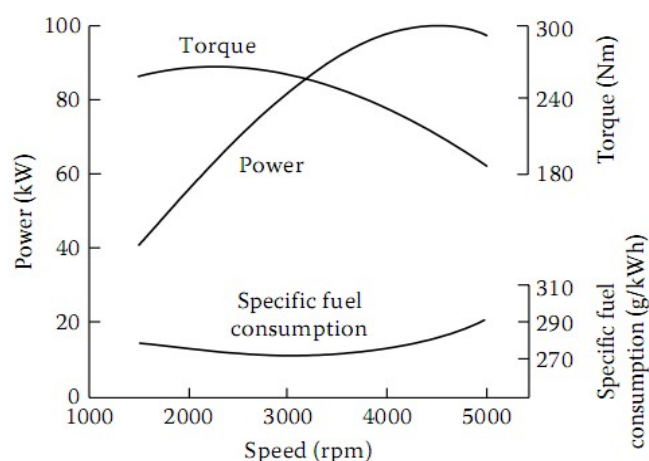


Fig 2: Typical characteristics of a gasoline engine.

INTRODUCTION

The electric motor is another candidate as a vehicle power plant, and it is becoming more and more important with the rapid development of electric and hybrid electric vehicles.

Electric motors are the work horses of electric vehicles drive systems. An electric motor converts electrical energy from the energy storage unit to mechanical energy that drives the wheels of the vehicle. In the traditional vehicle case, the engine must ramp up before full torque can be provided [2]. However, in the case of electric motor the full torque could be provided at low speed ranges. This characteristic is very important; it gives the vehicle an excellent acceleration at the beginning. Also, other important characteristics of the motor include good control abilities and high efficiency [3].

The speed–torque characteristics of electric motors are much closer to the ideal one, as shown in Fig 2. The speed starts from zero and generally increases to its nominal value. During this process, the voltage increases to its rated value as well, and the flux remains constant. A constant torque is generated in this speed range from zero to nominal speed. Beyond the nominal speed, the voltage remains constant and the output power will also remain constant. Thus, the output torque declines hyperbolically with the increasing speed.

3 Electric Motors

The motor drives for EVs can be classified into two groups, as shown in Fig 3:

- Commutator motors (also known as DC motors)
- Commutatorless motors (known as AC motors)

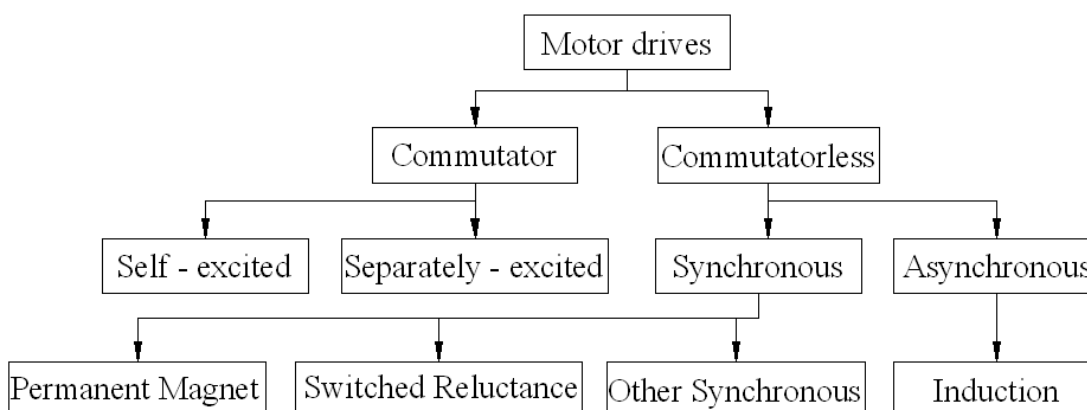


Fig 3: Classification of electric motor

INTRODUCTION

3.1 Permanent Magnet Synchronous Motor (PMSM)

Instead of using the windings for the rotor, the PMSM's rotor is made of magnetic materials. So the operating principle of a PMSM is quite different from an induction motor. The magnetic flux in a PMSM is generated from the magnetic materials on rotor. And absence of rotor windings gives PMSMs some advantages such as high efficiency and higher power density.

On the other side, the absence of field windings makes the flux weakening capability of PMSM's constrained, and eventually limits their speed ranges in the constant power region. Also, the permanent magnet is very sensitive to the temperature, this will certainly lead to a demagnetization problem, and sometimes a special cooling system is necessary for a PMSM drive system [4].



Fig 4: Permanent magnet synchronous motor.

3.2 Switched Reluctance Motor

The switched reluctance motor is an electric motor which runs by reluctance torques. It is another potential candidate due to some important features such as rugged structure, high power density and insensitivity to high temperatures.

The wound field coils are fixed on the stator, but the rotor has no magnets or coils attached. When the opposite poles of the stator get energized, the rotor will become aligned. In order to achieve a full rotation of the motor, the windings must be energized in the right sequence.

The disadvantages of switched reluctance motors are high torque ripples, acoustic noise, and instabilities caused by the energizing sequence [5].

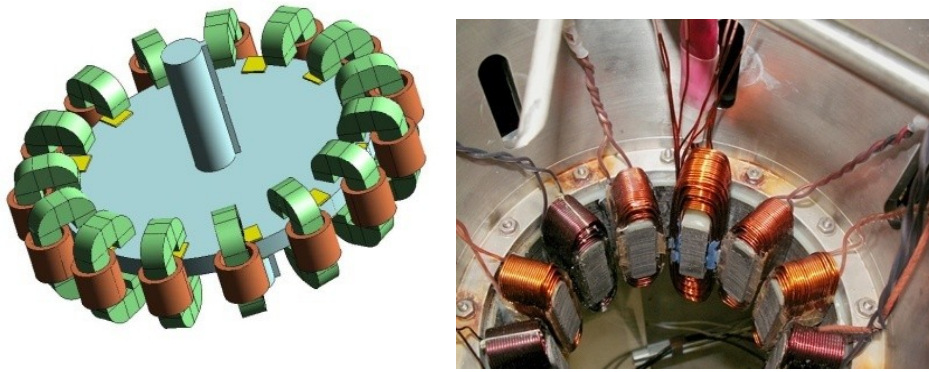


Fig 5: Switched reluctance motors

3.3 Induction Motor

The induction motor is a type of AC motors; it is called an induction motor because the working principles are based on electromagnetic induction. The energy is transformed through the rotating magnetic fields in induction motor. The three-phase currents in the stator side create an electromagnetic field which interacts with the electromagnetic field in the rotor bars, and then the resultant torque will be produced by the Lorentz' law. Therefore, the electrical energy could be transformed into mechanical energy.

Induction motors are the preferred choice for industrial applications due to their rugged structure, low price and easy maintenance [6].

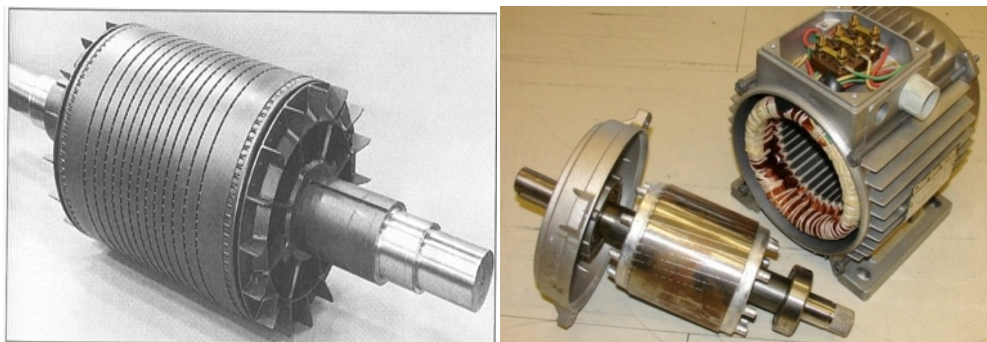


Fig 6: Induction motors

INTRODUCTION

3.4 Comparison of Three AC Motors

Table 1: Comparison of three AC motors [4-7]

Item	Induction Motor	PM Motor	SR Motor
Power density	Medium	High	Higher
Overload capacity (%)	300-500	300	300-500
Peak efficiency (%)	94-95	95-97	90
Load efficiency (%)	90-92	85-97	78-86
Range of speeds (r/min)	12K-20K	4K-10K	More than 15K
Reliability	Good	Better	Good
Volume	Medium	Small	Small
Mass	Medium	Light	Light
Control Performance	Good	Good	Good
Manufacturing costs	Medium	High	Medium

The PMSM is a popular candidate because of its high power density, high efficiency and compact volume. Its disadvantage, the magnetic materials used in the PMSM are really expensive and they need to be well maintained for the reason of magnet corrosion or demagnetization. The SRM is another promising candidate for EV applications, because of its simple structure, fault tolerant operation, and wide speed range at constant power. However, the disadvantages of the SRM are its high torque ripples and low efficiency.

As a result of these researches, the induction motor is considered as the best candidate for most of EVs applications. Intelligent, reliable and commercialized control systems of AC induction motors are being developed based on power electronic devices and digital signal processing (DSP) technology.

4 Research Objectives and Thesis Outline

Since an induction motor is a complicated nonlinear system, the electric rotor variables are not measurable directly and the physical parameters of an induction motor are often imprecisely known. Meanwhile, the induction motor used in electric vehicle applications usually requires both fast transient responses and excellent steady state speed performance. All of these make the control of induction motor a challenging problem.

The speed of induction motor can be controlled by different methods. (V/f) control is most commonly used scalar control method for speed control in which both voltage and frequency are varied to keep the ratio and flux constant. The scalar control gives the slower response, more overshoots and suffers instability for higher order harmonics. However, field oriented control or vector control has better performances than scalar control methods. The speed control of induction motor must be done through Adjustable Speed Drives. The growth and availability of power electronic devices made speed control affordable. This thesis considers the adjustable speed drives based on Space Vector PWM three-phase voltage source inverter as the induction motor drive.

The main focus of this work is to design an induction motor control system using FOC algorithm. This algorithm will be validated by Matlab/Simulink then experimentally by a digital signal processor (DSP F28335).

INTRODUCTION

Project outlines

The structure of this project is as follows:

Chapter1: presents the induction motor modeling basics, including the modeling tools and the modeling equations.

Chapter2: describes the details for the Inverter and presents the Matlab/Simulink simulations results.

Chapter3: the theory of field orientation control for an induction motor and the simulation results using Matlab/Simulink will be introduced in this chapter.

Chapter4: focuses on the DSP programming and the different modules and shows the experimental results.

And finally the conclusion.

CHAPTER 1

THE MODELING OF INDUCTION MOTOR

1.1 Introduction

The asynchronous machines operate below the synchronous speed when motoring and above the synchronous speed when generating. They are the most popular machine used in industry today. Induction motor is cheap to produce, easy to maintain and robust.

In general, induction motors consist of two main parts the stator and the rotor, the stator is connected to voltage source to create the rotating magnetic field between stator and rotor. The rotor winding is short circuited or connected to an external variable resistance for motor speed control purposes.

Based on construction of the rotor, the induction motor can be classified into two types: the wound induction motor and the squirrel cage induction motor. The latter is less expensive and more robust. In this thesis, the squirrel cage induction motors are discussed. Since they are the most commonly used in industry and household [8,9].

Unlike the DC separately excited machine and the synchronous machine in the induction machine the rotor is supplied through the rotating stator magnetic field, which makes the construction simple and reliable.

Induction machines have a wide variety of applications such as blowers, cranes, traction and many other industrial applications, because of their high robustness and reliability.

In this chapter, induction motor construction is detailed. The rotating field concept is explained, the model of Induction Motor is presented and finally the simulation of an induction motor by Matlab/Simulink.

1.2 Induction motor construction, principles and operation

1.2.1 Construction:

1.2.1.1 Stator:

The stator is made up of thin laminations of highly permeable steel that together yield high magnetic flux density and low core losses. The stator windings are wound and placed 120° apart in space. These are wound so as to create stator magnetic poles when current flows through them. The number of stator poles in conjunction with the frequency of the applied three phase power determine the speed of rotation of the stator's magnetic [10].

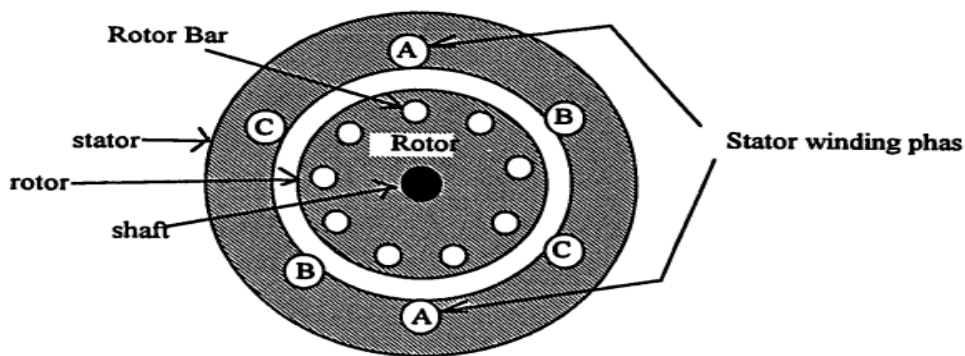


Fig 1.1: Cross section of an induction machine

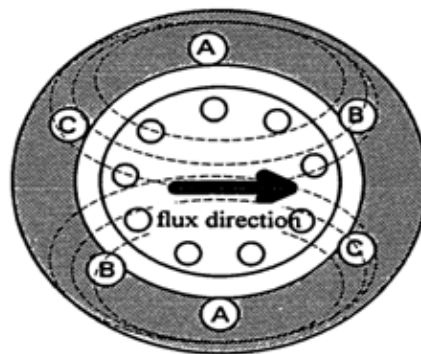


Fig 1.2: Resultant vector representation of the three phase currents.

Fig 1.2 shows a static picture of the flux and current directions when only winding A of the stator is energized. During normal operation, three currents, oriented 120 degrees apart in time, are applied to the three windings and can be combined to form a stator vector.

1.2.1.2 The Squirrel Cage Rotor

The squirrel cage rotor is also made up of thin laminations of highly permeable steel that together yield high magnetic flux density and low core losses. The rotor of a squirrel cage induction motor consists of aluminum bars which are short circuited by connecting them to two end rings as shown in Fig 1.3, so that rotor generates the induction current and magnetic field by itself. This makes the AC induction motor robust, rugged and inexpensive candidate for motor drive systems. The rotor is mounted on a shaft so that it can rotate and is placed inside the stator [7].

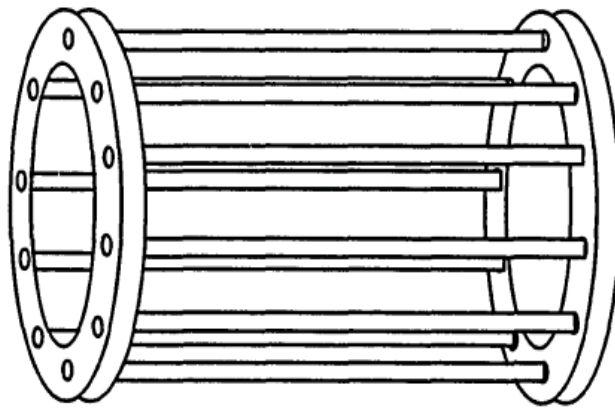


Fig 1.3: Conducting rotor bars without the rotor

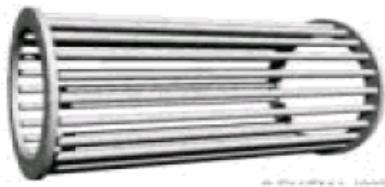


Fig 1.4: Short-circuited rotor bars of the squirrel cage induction motor

The bearings serve to position the rotor (keep it centered inside the stator) and allow it to rotate freely. Since air has very high magnetic reluctance, the rotor must be positioned very close to the stator to achieve maximum flux coupling and high efficiency [10]. The structure of a squirrel cage induction motor is shown in Fig 1.5.

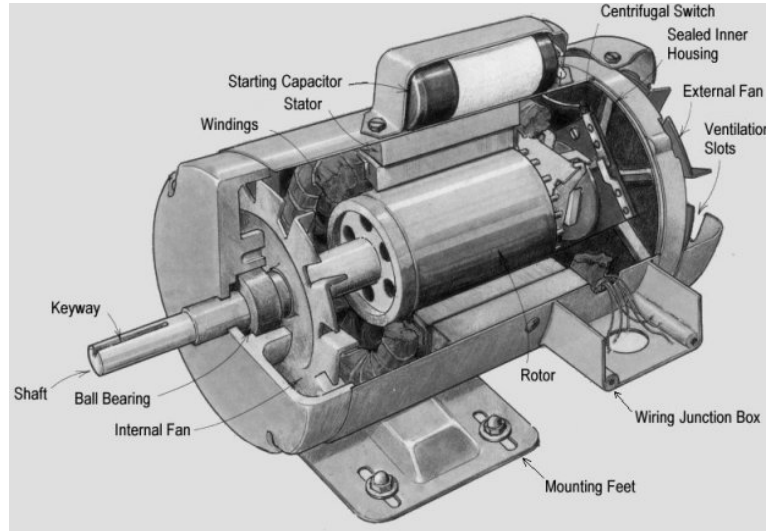


Fig 1.5: Squirrel cage induction motor cross section

1.2.2 Principles and operation (Rotating Magnetic Field)

The windings of stator are supplied with a balanced and symmetric three phase currents having equal magnitude and phase difference of 120° , which are shown in (1.1), (1.2) and (1.3) [13].

$$i_a = i_m \cos(\omega t) \quad (1.1)$$

$$i_b = i_m \cos\left(\omega t - \frac{2\pi}{3}\right) \quad (1.2)$$

$$i_c = i_m \cos\left(\omega t + \frac{2\pi}{3}\right) \quad (1.3)$$

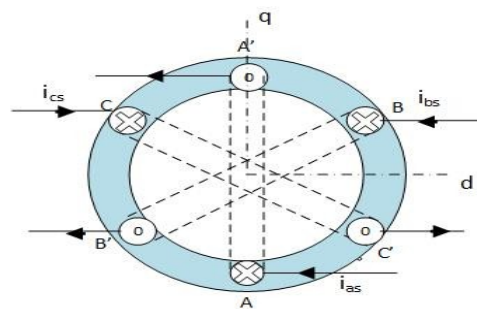


Fig 1.6: The Simple Construction of Two Pole Stator.

When the three-phase stator windings are fed by a three phase supply, a magnetic flux of a constant magnitude rotating at synchronous speed is created inside the motor [7].

The closed-loop coils carrying AC current produce magnetic field intensity based on Ampere's law. The magnetic field intensities of three currents coils are:

$$H_a = H_m \cos(\omega t) \sin(\theta) \quad (1.4)$$

$$H_b = H_m \cos\left(\omega t - \frac{2\pi}{3}\right) \sin\left(\theta - \frac{2\pi}{3}\right) \quad (1.5)$$

$$H_c = H_m \cos\left(\omega t + \frac{2\pi}{3}\right) \sin\left(\theta + \frac{2\pi}{3}\right) \quad (1.6)$$

From magnetic flux intensity, we can obtain magnetic flux densities based on $B = \mu H$.

$$B_a = B_m \cos(\omega t) \sin(\theta) \quad (1.7)$$

$$B_b = B_m \cos\left(\omega t - \frac{2\pi}{3}\right) \sin\left(\theta - \frac{2\pi}{3}\right) \quad (1.8)$$

$$B_c = B_m \cos\left(\omega t + \frac{2\pi}{3}\right) \sin\left(\theta + \frac{2\pi}{3}\right) \quad (1.9)$$

At time $\omega t = 0^\circ$, they have a phase shift of 120° from each other. The net magnetic field density can be obtained by summing up of all three coils magnetic field density vectors.

$$B_{net} = B_a + B_b + B_c = 1.5 B_m \sin(\theta - \omega t) \quad (1.10)$$

For θ constant, at $\omega t = 0^\circ$ $B_{net} = 1.5 B_m \angle 0^\circ$ which is shown in Fig 1.7

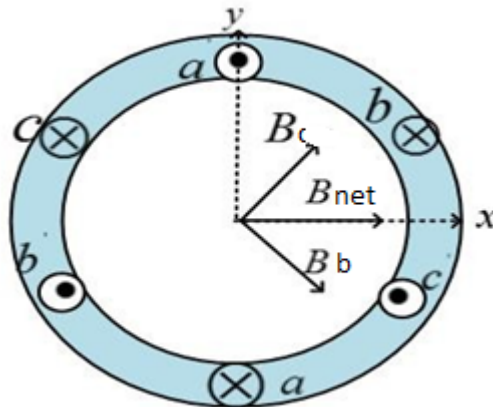


Fig 1.7: At $\omega t = 0$

At $\omega t = 90^\circ$ $B_{net} = 1.5B_m \angle -90^\circ$ which is shown in Fig 1.8

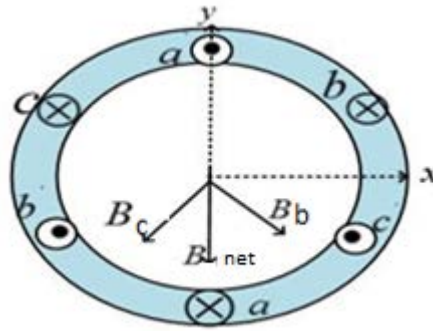


Fig 1.8: At $\omega t = 90^\circ$

The magnitude of B_{net} remains constant, but the direction of magnetic field density has changed and will continue to rotate with an angular velocity of ω . The rotating speed of this magnetic field is defined as synchronous speed, and it is related to the number of poles of the induction motor and the frequency of power source.

$$N_{sync} = \frac{120f}{p} \text{ rpm} \quad (1.11)$$

Where f is the power source frequency, P is the number of poles and N_{sync} is the synchronous speed in revolutions per minute.

Due to the relative speed between the rotating flux and the stationary conductors, an electromotive force (EMF) is induced in the rotor in accordance with Faraday's laws of electromagnetic induction. The frequency of the induced EMF is the same as the supply frequency, and the magnitude is proportional to the relative velocity between the flux and the conductors. The direction of this EMF is given by Fleming's right-hand rule [14].

Since the rotor bars form a closed path, a rotor current is produced which, according to Lenz's law, is opposite to that of the relative velocity between the rotating flux and the conductors. Therefore, the rotor current develops in the same direction as the flux and tries to catch up with the rotating flux (stator magnetic field) [14].

This induced rotor current will then induce a force when placed in the external stator magnetic field

Based on the right hand rule, the direction of the force acting on the conductor is the same as the motion of the rotor magnetic field. The induced EMF is proportional to the change of flux linking to the rotor conductors.

If the rotor rotates at synchronous speed, then the relative motion of the rotor to the stator is stationary and the voltage induced is zero. If the induced voltage is zero, then there is no induced current [7]. This is why induction motors are also called asynchronous motors because the rotor speed will never equal the synchronous speed.

The operation of induction motor mainly depends upon the relative motion between the stator magnetic field and rotor. The synchronous speed N_{sync} of the motor is denoted as the stator magnetic field speed, N_r is denoted as the rotor speed. The induction machine works as a motor when the rotor moves slower than the synchronous speed. The difference in rpm is defined as slip speed:

$$N_{slip} = N_{sync} - N_r \quad (1.14)$$

When slip speed is expressed in per unit or percentage value, slip is defined by

$$s = \frac{N_{sync} - N_r}{N_{sync}} \times 100\% \quad (1.15)$$

It may also be expressed in angular velocity ω

$$\omega_{syn} = \frac{2\pi N_{sync}}{60} \quad (1.16)$$

Substituting (1.11) with (1.16) we get

$$\omega_{sync} = \frac{4\pi f}{p} \quad (1.17)$$

$$s = \frac{\omega_{syn} - \omega_r}{\omega_{syn}} \times 100\% \quad (1.18)$$

Notice that, if the rotor runs at synchronous speed $s = 0$ (1.19)

If the rotor stops moving

$$s = 1 \quad (1.20)$$

1.3 The Equivalent Circuit of Induction Motor

The working principle of an induction motor is similar to a transformer. It is also called a rotating transformer. The stator winding is considered as primary winding and rotor as secondary winding which is always shortened. The voltage induced from primary winding to the secondary winding is just as the voltage induced in transformers. There are a few characteristics such as frequency and air gap, which differentiate induction machine from the

real transformers. The air gap exists between the stator and rotor for induction motors. The frequency induced in the rotor varies in induction machine when the rotor is loaded. However, in the transformer, no air gap is presented between the primary and secondary winding and the electrical frequency is the same on both sides. The per-phase equivalent circuit of induction machine is represented in Fig. 1.9 [12].

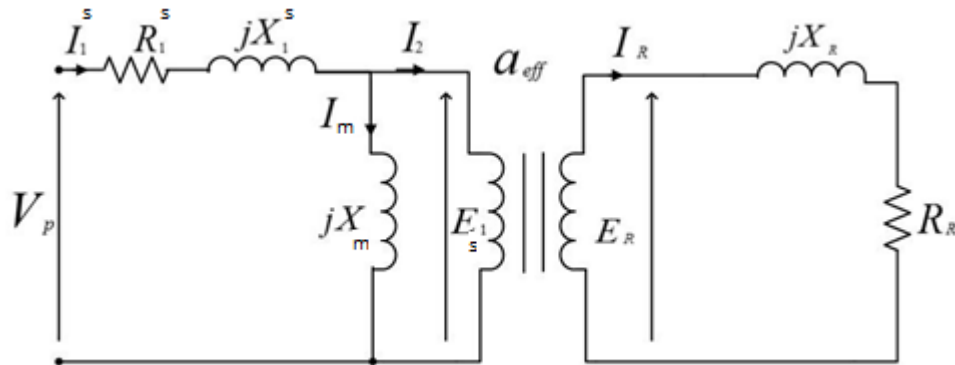


Fig 1.9: The Per Phase Equivalent Circuit of Induction Motor

Where R_1^s, R_R stator and rotor resistances

X_1^s, X_R stator and rotor leakage reactances

X_m magnetizing reactance

V_p voltage supplied to stator

E_1, E_R stator and rotor EMF

I_1, I_R stator and rotor currents

The induced rotor voltage and frequency in rotor winding depends upon the relative motion characterized by the slip s . The slip s is always between 0 and 1 ($0 \leq s \leq 1$) for induction machines operating in motoring mode. If the rotor is locked, then the largest relative motion occurs and maximum voltage is induced, when slip is equal to 1. Slip is equal to zero when the rotor runs at synchronous speed. The rotor runs at different speeds if the applied load is varied, and its induced voltage and frequency is proportional to the slip.

$$E_R = sE_{LR} \quad (1.21)$$

The resistance of the rotor is independent of slip, but the reactance changes due to the change in rotor frequency.

$$X_R = sX_{LR} \tag{1.22}$$

The new equivalent circuit is shown in Fig 1.10.

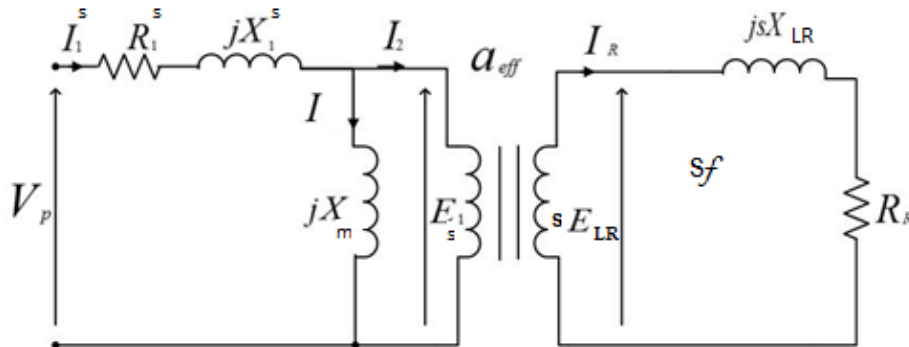


Fig 1.10: The Per Phase Equivalent Circuit of Induction Motor

From the secondary side the rotor winding current can be calculated as follows

$$I_R = sE_{LR} / (R_R + jsX_{LR}) \tag{1.23}$$

Equivalently, we have

$$I_R = E_{LR} / (R_R/s + jX_{LR}) \tag{1.24}$$

Considering the equivalent turns ratio $a_{eff} = n_s / n_r$, the per-phase equivalent circuit of induction motor referring rotor to the stator side is shown in Fig 1.11.

$$R_2 = a_{eff}^2 R_R \tag{1.25}$$

$$X_2 = a_{eff}^2 X_{LR} \tag{1.26}$$

$$I_2 = (1/a_{eff}) I_R \tag{1.27}$$

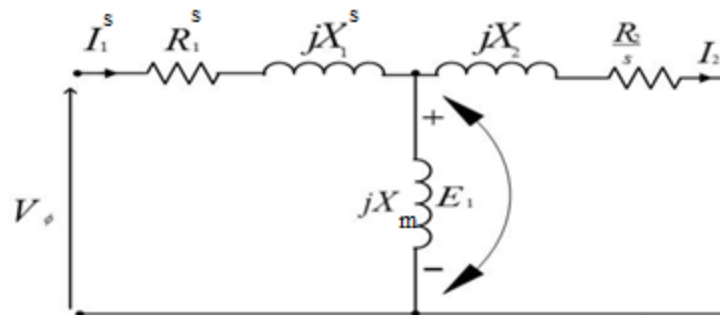


Fig 1.11: The Modified Per Phase Equivalent Circuit of Induction Motor

1.4 The System Equations in abc Reference Frame

The stator consists of a three-phase windings classified as the a_s , b_s , c_s having the same number of per phase effective turns n_s . Similarly, the rotor consists of three-phase windings a_r , b_r , c_r having the same number of turns per phase n_r . The voltage equations of the stator and rotor can be written using Kirchoff voltage law, where all three phases are represented in the matrix form as follows:

$$V_{abc}^s = r_s i_{abc}^s + \frac{d}{dt} \lambda_{abc}^s \quad (1.28)$$

$$V_{abc}^r = r_r i_{abc}^r + \frac{d}{dt} \lambda_{abc}^r \quad (1.29)$$

Where

$$V_{abc}^s = \begin{bmatrix} v_a^s \\ v_b^s \\ v_c^s \end{bmatrix} \quad V_{abc}^r = \begin{bmatrix} v_a^r \\ v_b^r \\ v_c^r \end{bmatrix}$$

$$i_{abc}^s = \begin{bmatrix} i_a^s \\ i_b^s \\ i_c^s \end{bmatrix} \quad i_{abc}^r = \begin{bmatrix} i_a^r \\ i_b^r \\ i_c^r \end{bmatrix}$$

$$\lambda_{abc}^s = \begin{bmatrix} \lambda_a^s \\ \lambda_b^s \\ \lambda_c^s \end{bmatrix} \quad \lambda_{abc}^r = \begin{bmatrix} \lambda_a^r \\ \lambda_b^r \\ \lambda_c^r \end{bmatrix}$$

The flux linkage equation is given as:

$$\lambda = Li \quad (1.30)$$

The time-varying magnetic flux is affected by both the stator and rotor currents. The coupling between the stator and rotor three phase windings leads to the flux linkage equations as

$$\lambda_{abc}^s = \lambda_{abc}^s(s) + \lambda_{abc}^s(r) \quad (1.31)$$

$$\lambda_{abc}^r = \lambda_{abc}^r(r) + \lambda_{abc}^r(s) \quad (1.32)$$

Where $\lambda_{abc}^s(s)$ is the total flux linkage of stator due to stator currents and $\lambda_{abc}^s(r)$ is the total flux linkage of stator due to the rotor currents. Similarly, the total flux linkage of rotor is equal to the summation of the flux linkages due to the rotor currents $\lambda_{abc}^r(r)$ and the flux

linkage due to the stator currents $\lambda_{abc}^r(s)$. The corresponding individual flux linkages are shown in the matrix form as follows:

$$\lambda_{abc}^s(s) = \begin{bmatrix} L_{as} & L_{abs} & L_{acs} \\ L_{abs} & L_{bs} & L_{bcs} \\ L_{acs} & L_{bcs} & L_{cs} \end{bmatrix} \begin{bmatrix} i_a^s \\ i_b^s \\ i_c^s \end{bmatrix} \quad (1.33)$$

$$\lambda_{abc}^s(r) = \begin{bmatrix} L_{as,ar} & L_{as,br} & L_{as,cr} \\ L_{bs,ar} & L_{bs,br} & L_{bs,cr} \\ L_{cs,ar} & L_{cs,br} & L_{cs,cr} \end{bmatrix} \begin{bmatrix} i_a^r \\ i_b^r \\ i_c^r \end{bmatrix} \quad (1.34)$$

$$\lambda_{abc}^r(r) = \begin{bmatrix} L_{ar} & L_{abr} & L_{acr} \\ L_{abr} & L_{br} & L_{bcr} \\ L_{acr} & L_{bcr} & L_{cr} \end{bmatrix} \begin{bmatrix} i_a^r \\ i_b^r \\ i_c^r \end{bmatrix} \quad (1.35)$$

$$\lambda_{abc}^r(s) = \begin{bmatrix} L_{ar,as} & L_{ar,bs} & L_{ar,cs} \\ L_{br,as} & L_{br,bs} & L_{br,cs} \\ L_{cr,as} & L_{cr,bs} & L_{cr,cs} \end{bmatrix} \begin{bmatrix} i_a^s \\ i_b^s \\ i_c^s \end{bmatrix} \quad (1.36)$$

1.5 Determination of Machine Inductances

Each winding has a self-inductance and a mutual inductance. The inductance due to change of current in its own winding is called self-inductance, and the inductance corresponding to the change of current in the other winding is called the mutual inductance. Now, let's calculate the total inductance of each winding in stator and rotor.

The total self-inductance of a coil is the summation of the leakage and magnetizing inductances. Considering the total self-inductance of stator phase a_s , we can express the total self inductance of phase a_s as:

$$L_{as} = L_{ls} + L_{am} \quad (1.37)$$

Similarly, for phase b_s and c_s of stator

$$L_{bs} = L_{ls} + L_{bm} \quad (1.38)$$

$$L_{cs} = L_{ls} + L_{cm} \quad (1.39)$$

Where L_{ls} is the self inductance and L_{ms} is the magnetizing inductance of stator.

The magnetizing inductance of all the phases of the stator is equal in magnitude and can be calculated as

$$L_{am} = L_{bm} = L_{cm} = L_{ms} = \mu_0 n_s^2 \frac{rl\pi}{4g} \quad (1.40)$$

The mutual inductance between stator three phase windings a_s , b_s and c_s can be calculated as:

$$L_{abs} = L_{bcs} = L_{cas} = -\mu_0 n_s^2 \frac{rl\pi}{8g} = -\frac{L_{ms}}{2} \quad (1.41)$$

The flux linkage of stator windings due to the currents flowing in stator can be written as:

$$\lambda_{abc}^s(s) = \begin{bmatrix} L_{ls} + L_{ms} & -\frac{L_{ms}}{2} & -\frac{L_{ms}}{2} \\ -\frac{L_{ms}}{2} & L_{ls} + L_{ms} & -\frac{L_{ms}}{2} \\ -\frac{L_{ms}}{2} & -\frac{L_{ms}}{2} & L_{ls} + L_{ms} \end{bmatrix} \begin{bmatrix} i_a^s \\ i_b^s \\ i_c^s \end{bmatrix} \quad (1.42)$$

Now, let's calculate the mutual inductance between rotor and stator windings. Consider that the rotor phase a_r is displaced by an angle θ_r from the stator phase a_s winding. Similarly, b_r and c_r are displaced from b_s and c_s by θ_r .

The corresponding mutual inductances can be calculated as:

$$L_{as,ar} = L_{bs,br} = L_{cs,cr} = \frac{n_r}{n_s} L_{ms} \cos(\theta_r) \quad (1.43)$$

The angle between the phase a_s and b_r phase is $(\theta_r + \frac{2\pi}{3})$. Similarly, the angle between the a_s and c_r phase is $(\theta_r - \frac{2\pi}{3})$.

$$L_{as,br} = L_{bs,cr} = L_{cs,ar} = \frac{n_r}{n_s} L_{ms} \cos(\theta_r + \frac{2\pi}{3}) \quad (1.44)$$

$$L_{as,cr} = L_{bs,ar} = L_{cs,br} = \frac{n_r}{n_s} L_{ms} \cos(\theta_r - \frac{2\pi}{3}) \quad (1.45)$$

The calculated flux linkages of the stator phases due to the rotor currents can be written in the matrix form as:

$$\lambda_{abc}^s(r) = \frac{n_r}{n_s} L_m \begin{bmatrix} \cos(\theta_r) & \cos(\theta_r + \frac{2\pi}{3}) & \cos(\theta_r - \frac{2\pi}{3}) \\ \cos(\theta_r - \frac{2\pi}{3}) & \cos(\theta_r) & \cos(\theta_r + \frac{2\pi}{3}) \\ \cos(\theta_r + \frac{2\pi}{3}) & \cos(\theta_r - \frac{2\pi}{3}) & \cos(\theta_r) \end{bmatrix} \begin{bmatrix} i_a^r \\ i_b^r \\ i_c^r \end{bmatrix} \quad (1.46)$$

The total flux linkage of the stator windings is:

$$\lambda_{abc}^s = \lambda_{abc}^s(s) + \lambda_{abc}^s(r)$$

The procedure for finding the rotor flux linkage is very similar to finding the stator flux linkage. The flux linkage due to the rotor currents is

$$\lambda_{abc}^r(\mathbf{r}) = \begin{bmatrix} L_{lr} + \left(\frac{n_r}{n_s}\right)^2 L_{ms} & -\frac{1}{2} \left(\frac{n_r}{n_s}\right)^2 L_{ms} & -\frac{1}{2} \left(\frac{n_r}{n_s}\right)^2 L_{ms} \\ -\frac{1}{2} \left(\frac{n_r}{n_s}\right)^2 L_{ms} & L_{lr} + \left(\frac{n_r}{n_s}\right)^2 L_{ms} & -\frac{1}{2} \left(\frac{n_r}{n_s}\right)^2 L_{ms} \\ -\frac{1}{2} \left(\frac{n_r}{n_s}\right)^2 L_{ms} & -\frac{1}{2} \left(\frac{n_r}{n_s}\right)^2 L_{ms} & L_{lr} + \left(\frac{n_r}{n_s}\right)^2 L_{ms} \end{bmatrix} \begin{bmatrix} i_a^r \\ i_b^r \\ i_c^r \end{bmatrix} \quad (1.47)$$

Where L_{lr} is the rotor leakage inductance

The rotor flux linkage due to stator currents is

$$\lambda_{abc}^r(\mathbf{s}) = \frac{n_r}{n_s} L_{ms} \begin{bmatrix} \cos(\theta_r) & \cos(\theta_r - \frac{2\pi}{3}) & \cos(\theta_r + \frac{2\pi}{3}) \\ \cos(\theta_r + \frac{2\pi}{3}) & \cos(\theta_r) & \cos(\theta_r - \frac{2\pi}{3}) \\ \cos(\theta_r - \frac{2\pi}{3}) & \cos(\theta_r + \frac{2\pi}{3}) & \cos(\theta_r) \end{bmatrix} \begin{bmatrix} i_a^s \\ i_b^s \\ i_c^s \end{bmatrix} \quad (1.48)$$

The summation of the two components leads to the total flux linkage of the rotor, i.e.

$$\lambda_{abc}^r = \lambda_{abc}^r(\mathbf{r}) + \lambda_{abc}^r(\mathbf{s})$$

1.6 Three phase to two phase transformation

1.6.1 Space vector

The time-varying inductances of stator and rotor cause difficulties in controlling the dynamic model of machine. In order to reduce the complexity of the machine, one can transfer the three coordinates into two coordinates by using the Park's transformation which was introduced by Robert H. Park in 1929. The conversion of three phase quantities into two dimensional rotating reference frames is carried out in two steps. The transformation from three coordinate system to the two coordinate stationary frame [(a,b,c) to (α, β)] is defined by Clarke's transformation. The transformation from the stationary coordinate system to the rotating coordinate frame [(α, β) to (d,q)] by rotational Park's transformation [15,16,17].

1.6.2 Clarke Transformation

The abc three phase quantities can be transferred into stationary $\alpha\beta$ two coordinate frame using Clarke's transformation and similarly its inverse is used to transform $\alpha\beta$ two coordinate vector to abc three coordinate frame. h represents any of the three vectors like current, voltage and flux. Now presenting the a, b, c coordinate frame in vector form as $\bar{h} = [h_a \quad h_b \quad h_c]^T$

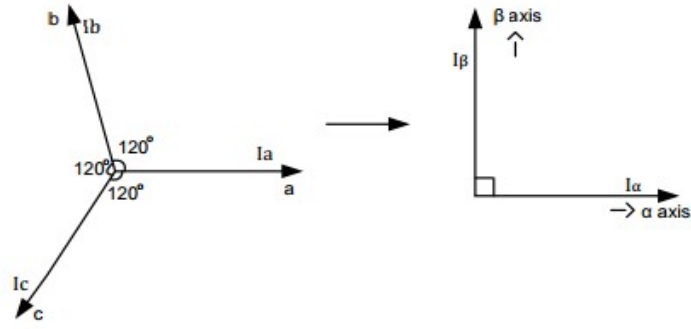


Fig 1.12: Clarke's Transformation

The Clarke's transformation is denoted as $\vec{h}^s = h_\alpha + jh_\beta$ and is given as follow

$$h_\alpha + jh_\beta = \frac{2}{3}[h_a + e^{j\frac{2\pi}{3}} h_b + e^{j\frac{4\pi}{3}} h_c] = \frac{2}{3}(h_a - \frac{1}{2}h_b - \frac{1}{2}h_c) + j\frac{2}{3}(\frac{\sqrt{3}}{2}h_b - \frac{\sqrt{3}}{2}h_c)$$

By separating real part and imaginary part, we have

$$h_\alpha = \frac{2}{3}(h_a - \frac{1}{2}h_b - \frac{1}{2}h_c) \tag{1.49}$$

$$h_\beta = \frac{2}{3}(\frac{\sqrt{3}}{2}h_b - \frac{\sqrt{3}}{2}h_c) \tag{1.50}$$

It is assumed that the axis “a” and the axis “α” are in the same direction. In order for the transformation to be invertible, a third variable, known as the zero-sequence component, is added.

$$\begin{bmatrix} h_\alpha \\ h_\beta \\ h_0 \end{bmatrix} = \frac{2}{3} \begin{bmatrix} 1 & -\frac{1}{2} & -\frac{1}{2} \\ 0 & \frac{\sqrt{3}}{2} & -\frac{\sqrt{3}}{2} \\ \frac{1}{\sqrt{2}} & -\frac{1}{\sqrt{2}} & -\frac{1}{\sqrt{2}} \end{bmatrix} \begin{bmatrix} f_a \\ f_b \\ f_c \end{bmatrix} \tag{1.51}$$

Notice that $h_0=0$ due to balance three phase condition ($h_a + h_b + h_c = 0$).

The Clarke's transformation and its inverse are shown in (1.52) and (1.53).

$$h_{\alpha\beta 0} = K h_{abc} \tag{1.52}$$

$$h_{abc} = K^{-1} h_{\alpha\beta 0} \tag{1.53}$$

Where K represents the transformation matrix and K^{-1} the inverse matrix.

$$K = \frac{2}{3} \begin{bmatrix} 1 & -\frac{1}{2} & -\frac{1}{2} \\ 0 & \frac{\sqrt{3}}{2} & -\frac{\sqrt{3}}{2} \\ \frac{1}{\sqrt{2}} & -\frac{1}{\sqrt{2}} & -\frac{1}{\sqrt{2}} \end{bmatrix}$$

$$K^{-1} = \frac{2}{3} \begin{bmatrix} 1 & 0 & 1 \\ -\frac{1}{2} & \frac{\sqrt{3}}{2} & 1 \\ -\frac{1}{2} & -\frac{\sqrt{3}}{2} & 1 \end{bmatrix}$$

Take the currents, for example:

$$\begin{bmatrix} i_\alpha \\ i_\beta \end{bmatrix} = \begin{bmatrix} \frac{2}{3} & -\frac{1}{3} & -\frac{1}{3} \\ 0 & \frac{\sqrt{3}}{3} & -\frac{\sqrt{3}}{3} \end{bmatrix} \begin{bmatrix} i_a \\ i_b \\ i_c \end{bmatrix}$$

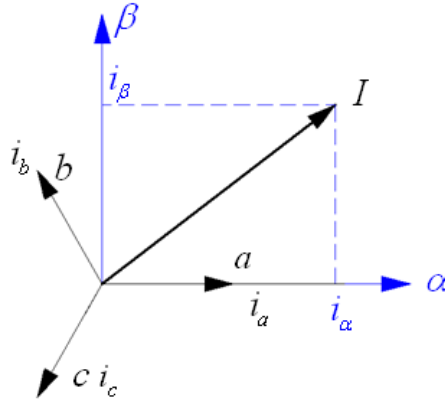


Fig 1.13: Clarke transformation of three-phase currents.

1.6.3 Park Transformation

The Park transformation transfers a stationary system into a rotational system. The rotational Park's transformation converts $\alpha\beta$ stationary coordinate (stationary system) system into dq rotating coordinate frame (rotational system). The term \bar{h}^e denotes the quantities in dq coordinate frame.

$$\bar{h}^e = e^{-j\theta_s} \bar{h}^s = h_d + jh_q \quad (1.54)$$

Where, \bar{h} denotes quantity in $\alpha\beta$ coordinate frame.

$$\begin{aligned} \bar{h}^e &= e^{-j\theta_s} [h_\alpha + jh_\beta] = (\cos \theta_s - j \sin \theta_s)(h_\alpha + jh_\beta) \\ &= (h_\alpha \cos \theta_s + h_\beta \sin \theta_s) - j(h_\alpha \sin \theta_s - h_\beta \cos \theta_s) = h_d + jh_q \end{aligned}$$

Now, by separating the real and imaginary part and rewriting them in matrix form, we have

$$h_d = h_\alpha \cos \theta_s + h_\beta \sin \theta_s \quad (1.55)$$

$$f_q = -f_\alpha \sin \theta_s + f_\beta \cos \theta_s \quad (1.56)$$

$$\begin{bmatrix} f_d \\ f_q \end{bmatrix} = \begin{bmatrix} \cos \theta_s & \sin \theta_s \\ -\sin \theta_s & \cos \theta_s \end{bmatrix} \begin{bmatrix} f_\alpha \\ f_\beta \end{bmatrix}$$

The Park's transformation and its inverse are shown in equations (1.57) and (1.58).

$$f_{dq} = Q f_{\alpha\beta} \quad (1.57)$$

$$f_{\alpha\beta} = Q^{-1} f_{dq} \quad (1.58)$$

Where, Q and Q^{-1} represents the forward and inverse calculations of rotational Park's transformation.

$$Q = \begin{bmatrix} \cos \theta_s & \sin \theta_s \\ -\sin \theta_s & \cos \theta_s \end{bmatrix}$$

$$Q^{-1} = \begin{bmatrix} \cos \theta_s & -\sin \theta_s \\ \sin \theta_s & \cos \theta_s \end{bmatrix}$$

Take the currents, for example:

$$\begin{bmatrix} i_d \\ i_q \end{bmatrix} = \begin{bmatrix} \cos \theta & \sin \theta \\ -\sin \theta & \cos \theta \end{bmatrix} \begin{bmatrix} i_\alpha \\ i_\beta \end{bmatrix}$$

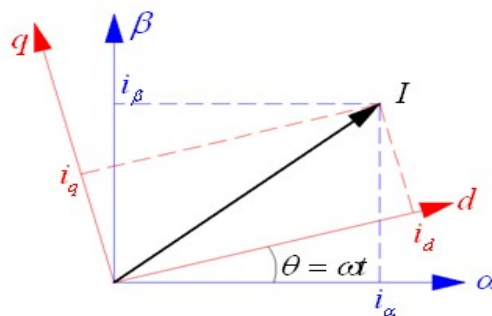


Fig 1.14: Park transformation of two-phase currents.

The total transformation from abc into dq coordinate frame is shown in Fig 1.15.

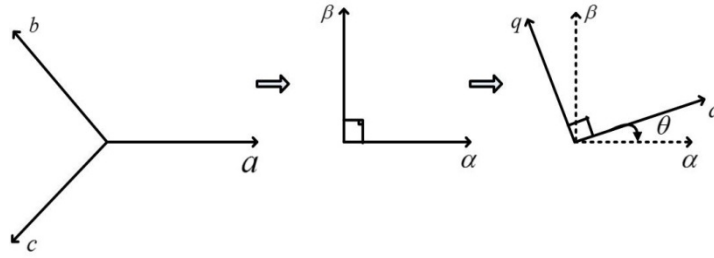


Fig 1.15: The total Transformation from abc to dq coordinates.

The total Park's transformation from abc to dq coordinate frame obtained by combining (3.52) and (3.57).

$$\begin{bmatrix} h_d \\ h_q \\ h_0 \end{bmatrix} = \frac{2}{3} \begin{bmatrix} \cos \theta_s & \sin \theta_s & 0 \\ -\sin \theta_s & \cos \theta_s & 0 \\ 0 & 0 & 1 \end{bmatrix} \begin{bmatrix} 1 & -\frac{1}{2} & -\frac{1}{2} \\ 0 & \frac{\sqrt{3}}{2} & -\frac{\sqrt{3}}{2} \\ \frac{1}{\sqrt{2}} & -\frac{1}{\sqrt{2}} & -\frac{1}{\sqrt{2}} \end{bmatrix} \begin{bmatrix} h_a \\ h_b \\ h_c \end{bmatrix}$$

$$T(\theta_s) = \frac{2}{3} \begin{bmatrix} \cos \theta_s & \cos \left(\theta_s - \frac{2\pi}{3} \right) & \cos \left(\theta_s + \frac{2\pi}{3} \right) \\ -\sin \theta_s & -\sin \left(\theta_s - \frac{2\pi}{3} \right) & -\sin \left(\theta_s + \frac{2\pi}{3} \right) \\ \frac{1}{\sqrt{2}} & \frac{1}{\sqrt{2}} & \frac{1}{\sqrt{2}} \end{bmatrix} \quad (1.59)$$

The total transformation matrix is calculated and is represented by T (θ).

The important property $T^{-1}(\theta_s) = 3/2 T^T(\theta_s)$ can be proved based on (1.59).

1.7 Dynamic Model of Induction Motor

1.7.1 Flux equations

The complexity caused by the time-varying parameters (flux linkage calculated with (2.31) and (2.32)) is reduced using Clarke's and Park's transformation. Assuming the turns ratio a_{eff} equals to 1 ($n_s=n_r$).

From (2.42) and (2.46), the stator flux linkage can be written as

$$\lambda_{abc}^s = \lambda_{abc}^s(s) + \lambda_{abc}^s(r) = L_{abc}^s i_{abc}^s + M(\theta_r) i_{abc}^r \quad (1.60)$$

Where

$$L_{abc}^s = \begin{bmatrix} L_{ls} + L_{ms} & -\frac{L_{ms}}{2} & -\frac{L_{ms}}{2} \\ -\frac{L_{ms}}{2} & L_{ls} + L_{ms} & -\frac{L_{ms}}{2} \\ -\frac{L_{ms}}{2} & -\frac{L_{ms}}{2} & L_{ls} + L_{ms} \end{bmatrix}$$

$$M(\theta_r) = L_{ms} \begin{bmatrix} \cos(\theta_r) & \cos(\theta_r + \frac{2\pi}{3}) & \cos(\theta_r - \frac{2\pi}{3}) \\ \cos(\theta_r - \frac{2\pi}{3}) & \cos(\theta_r) & \cos(\theta_r + \frac{2\pi}{3}) \\ \cos(\theta_r + \frac{2\pi}{3}) & \cos(\theta_r - \frac{2\pi}{3}) & \cos(\theta_r) \end{bmatrix}$$

1.7.1.1 Converting stator and rotor flux linkages into $\alpha\beta$ coordinate frame

The rotor flux linkage equations are similar to the stator equations except that the angle for mutual inductance is negative. The rotor flux linkage can be written as

$$\lambda_{abc}^r = \lambda_{abc}^r(\mathbf{r}) + \lambda_{abc}^r(\mathbf{s}) = L_{abc}^r \mathbf{i}_{abc}^r + M(-\theta_r) \mathbf{i}_{abc}^s \quad (1.61)$$

Where

$$L_{abc}^r = \begin{bmatrix} L_{lr} + L_{ms} & -\frac{1}{2}L_{ms} & -\frac{1}{2}L_{ms} \\ -\frac{1}{2}L_{ms} & L_{lr} + L_{ms} & -\frac{1}{2}L_{ms} \\ -\frac{1}{2}L_{ms} & -\frac{1}{2}L_{ms} & L_{lr} + L_{ms} \end{bmatrix}$$

$$M(-\theta_r) = \frac{n_r}{n_s} L_{ms} \begin{bmatrix} \cos(\theta_r) & \cos(\theta_r - \frac{2\pi}{3}) & \cos(\theta_r + \frac{2\pi}{3}) \\ \cos(\theta_r + \frac{2\pi}{3}) & \cos(\theta_r) & \cos(\theta_r - \frac{2\pi}{3}) \\ \cos(\theta_r - \frac{2\pi}{3}) & \cos(\theta_r + \frac{2\pi}{3}) & \cos(\theta_r) \end{bmatrix}$$

Firstly, convert all the flux linkages into the $\alpha\beta$ stationary coordinate frame using Clarke's transformation for both stator and rotor. We divide (1.60) into two parts and apply Clarke's transformation to them separately. The first is self inductance $L_{abc}^s \mathbf{i}_{abc}^s$, and the second part is mutual inductance $M(\theta_r) \mathbf{i}_{abc}^r$.

Converting first part $L_{abc}^s \mathbf{i}_{abc}^s$ into $\alpha\beta$ coordinate frame

$$\lambda_{abc}^s(\mathbf{s}) = L_{abc}^s \mathbf{i}_{abc}^s$$

Based on Clarke's transformation, λ_{abc}^s can be written as

$$\lambda_{\alpha\beta}^s(\mathbf{s}) = \frac{2}{3} [\lambda_a^s + e^{j\frac{2\pi}{3}} \lambda_b^s + e^{j\frac{4\pi}{3}} \lambda_c^s] \quad (1.62)$$

By replacing λ_{abc}^s with the self inductance L_{abc}^s and \mathbf{i}_{abc}^s we get

$$\begin{aligned}\lambda_{\alpha\beta}^s(s) &= \frac{2}{3}[(L_{ls} + L_{ms})i_a^s - \frac{1}{2}L_{ms}i_b^s - \frac{1}{2}L_{ms}i_c^s] \\ &+ \frac{2}{3}e^{j\frac{2\pi}{3}} [-\frac{1}{2}L_{ms}i_a^s + (L_{ls} + L_{ms})i_b^s - \frac{1}{2}L_{ms}i_c^s] \\ &+ \frac{2}{3}e^{j\frac{4\pi}{3}} [-\frac{1}{2}L_{ms}i_a^s - \frac{1}{2}L_{ms}i_b^s + (L_{ls} + L_{ms})i_c^s]\end{aligned}\quad (1.63)$$

By replacing L_{ms} with $\frac{3}{2}L_{ms} - \frac{1}{2}L_{ms}$ and rearranging the terms we have

$$\begin{aligned}\lambda_{\alpha\beta}^s(s) &= \frac{2}{3}[\frac{3}{2}L_{ms} + L_{ls})(i_a^s + e^{j\frac{2\pi}{3}}i_b^s + e^{j\frac{4\pi}{3}}i_c^s)] \\ &+ \frac{2}{3}(-\frac{1}{2}L_{ms}i_a^s - \frac{1}{2}L_{ms}i_b^s - \frac{1}{2}L_{ms}i_c^s) \\ &+ \frac{2}{3}e^{j\frac{2\pi}{3}}(-\frac{1}{2}L_{ms}i_a^s - \frac{1}{2}L_{ms}i_b^s - \frac{1}{2}L_{ms}i_c^s) \\ &+ \frac{2}{3}e^{j\frac{4\pi}{3}}(-\frac{1}{2}L_{ms}i_a^s - \frac{1}{2}L_{ms}i_b^s - \frac{1}{2}L_{ms}i_c^s)\end{aligned}$$

Substituting $i_a + i_b + i_c = 0$ and $\frac{2}{3}(i_a^s + e^{j\frac{2\pi}{3}}i_b^s + e^{j\frac{4\pi}{3}}i_c^s) = i_{\alpha\beta}^s$ we have

$$\lambda_{\alpha\beta}^s(s) = (\frac{3}{2}L_{ms} + L_{ls})i_{\alpha\beta}^s \quad (1.64)$$

Denote $L_s = (\frac{3}{2}L_{ms} + L_{ls})$ then (2.64) becomes

$$\lambda_{\alpha\beta}^s(s) = L_s i_{\alpha\beta}^s \quad (1.65)$$

Converting the second part $M(\theta_r) i_{abc}^r$ into $\alpha\beta$ coordinate frame

$$\lambda_{abc}^s(r) = M(\theta_r) i_{abc}^r$$

Substituting the mutual inductance $M(\theta_r)$ and i_{abc}^r , we get

$$\begin{aligned}\lambda_{\alpha\beta}^s(r) &= \frac{2}{3}[L_{ms} \cos(\theta_r) i_a^r + L_{ms} \cos(\theta_r + \frac{2\pi}{3}) i_b^r + L_{ms} \cos(\theta_r - \frac{2\pi}{3}) i_c^r] \\ &+ \frac{2}{3}e^{j\frac{2\pi}{3}} [L_{ms} \cos(\theta_r - \frac{2\pi}{3}) i_a^r + L_{ms} \cos(\theta_r) i_b^r + L_{ms} \cos(\theta_r + \frac{2\pi}{3}) i_c^r] \\ &+ \frac{2}{3}e^{j\frac{4\pi}{3}} [L_{ms} \cos(\theta_r + \frac{2\pi}{3}) i_a^r + L_{ms} \cos(\theta_r - \frac{2\pi}{3}) i_b^r + L_{ms} \cos(\theta_r) i_c^r]\end{aligned}\quad (1.66)$$

Based on trigonometric function $\frac{e^{ja} + e^{-ja}}{2} = \cos a$ we have

$$\cos(\theta_r - \frac{2\pi}{3}) = \frac{1}{2} (e^{j(\theta_r - \frac{2\pi}{3})} + e^{-j(\theta_r - \frac{2\pi}{3})})$$

This reduces (2.66) to

$$\begin{aligned} \lambda_{\alpha\beta}^s(r) &= \frac{1}{2} L_{ms} \frac{2}{3} [3 e^{j\theta_r} i_a^r + 3e^{j(\theta_r + \frac{2\pi}{3})} i_b^r + 3 e^{j(\theta_r - \frac{2\pi}{3})} i_c^r] \\ &= L_{ms} e^{j\theta_r} (i_a^r + e^{j\frac{2\pi}{3}} i_b^r + e^{j\frac{4\pi}{3}} i_c^r) \end{aligned} \quad (1.67)$$

Substituting $\frac{2}{3} (i_a^r + e^{j\frac{2\pi}{3}} i_b^r + e^{j\frac{4\pi}{3}} i_c^r) = i_{\alpha\beta}^r$ into (2.67) we obtain

$$\lambda_{\alpha\beta}^s(r) = L_m e^{j\theta_r} i_{\alpha\beta}^r \quad (1.68)$$

$$\text{Denote } L_m = \frac{3}{2} L_{ms} \quad (1.69)$$

The combination of the first and the second part leads to the total flux linkage of stator in the $\alpha\beta$ coordinate frame.

Similar procedure can be applied to determine the rotor flux linkage. The total stator and rotor flux linkages in $\alpha\beta$ coordinate frame are summarized in (1.70) and (1.71).

$$\lambda_{\alpha\beta}^s = L_s i_{\alpha\beta}^s + L_m e^{j\theta_r} i_{\alpha\beta}^r \quad (1.70)$$

$$\lambda_{\alpha\beta}^r = L_r i_{\alpha\beta}^r + L_m e^{-j\theta_r} i_{\alpha\beta}^s \quad (1.71)$$

1.7.1.2 Converting stator flux linkages into dq coordinate frame

Rotating Park's transformation is used to convert stationary coordinate frame into rotating coordinate frame, Where $\bar{h}^e = e^{-j\theta_s} \bar{h}^s = h_d + jh_q$

Now applying this condition to the (1.70), we have

$$\lambda_{dq}^s = e^{-j\theta_s} \lambda_{\alpha\beta}^s \quad (1.72)$$

Substituting (1.70) into(1.72), we have

$$\lambda_{dq}^s = \lambda_{dq}^s(s) + \lambda_{dq}^s(r) = L_s i_{dq}^s + L_m e^{j\theta_r} e^{-j\theta_s} i_{\alpha\beta}^r$$

Based on Park's transformation, $e^{-j(\theta_s - \theta_r)} i_{\alpha\beta}^r = i_{dq}^r$ the following flux equations are reached.

$$\lambda_{dq}^s = L_s i_{dq}^s + L_m i_{dq}^r \quad (1.73)$$

we have $i_{dq}^s = i_d^s + j i_q^s$

Now by separating the real and imaginary parts in (2.73) we obtain

$$\lambda_d^s = L_s i_d^s + L_m i_d^r \quad (1.74)$$

$$\lambda_q^s = L_s i_q^s + L_m i_q^r \quad (1.75)$$

Denote, $L_s = (\frac{3}{2} L_{ms} + L_{ls})$ and $L_m = \frac{3}{2} L_{ms}$.

1.7.1.3 Converting rotor flux linkages into dq coordinate frame,

Denote θ_s as the angle of stator magnetic field, with $\theta_s = \omega_s t + \theta_0$. Denote θ_r as the rotor angle, with $\theta_r = \omega_r t + \theta_{r0}$.

Therefore, the transformation angle $\theta_s - \theta_r$ is used in rotating Park's transformation of rotor voltage. (1.71) becomes

$$\lambda_{dq}^r = e^{-j(\theta_s - \theta_r)} \lambda_{\alpha\beta}^r \quad (1.76)$$

Substituting (1.71) into (1.76), we have

$$\lambda_{dq}^r = \lambda_{dq}^r(\Gamma) + \lambda_{dq}^r(s) = L_r i_{dq}^r + L_m e^{-j\theta_r} e^{-j(\theta_s - \theta_r)} i_{\alpha\beta}^s$$

based on Park's transformation, $e^{-j\theta_s} i_{\alpha\beta}^s = i_{dq}^s$ the following flux equations are reached.

$$\lambda_{dq}^r = L_r i_{dq}^r + L_m i_{dq}^s \quad (1.77)$$

we have $i_{dq}^s = i_d^s + j i_q^s$

Now by separating the real and imaginary parts in (1.77), we obtain

$$\lambda_d^r = L_r i_d^r + L_m i_d^s \quad (1.78)$$

$$\lambda_q^r = L_r i_q^r + L_m i_q^s \quad (1.79)$$

Denote, $L_r = (\frac{3}{2} L_{mr} + L_{lr})$ and $L_m = \frac{3}{2} L_{ms}$.

1.7.2 Voltage Equations

The voltage across the stator and rotor is equal to the summation of voltage drop across their resistance and the derivation of the time varying flux linkage.

$$v_{abc}^s = r_s i_{abc}^s + \frac{d}{dt} \lambda_{abc}^s \quad (1.80)$$

$$\mathbf{v}_{abc}^r = r_r \mathbf{i}_{abc}^r + \frac{d}{dt} \lambda_{abc}^r \quad (1.81)$$

Converting (1.80) and (1.81) into $\alpha\beta$ stationary coordinate frame using Clarke's transformation, we have:

$$\mathbf{v}_{\alpha\beta}^s = r_s \mathbf{i}_{\alpha\beta}^s + \frac{d}{dt} \lambda_{\alpha\beta}^s \quad (2.82)$$

$$\mathbf{v}_{\alpha\beta}^r = r_r \mathbf{i}_{\alpha\beta}^r + \frac{d}{dt} \lambda_{\alpha\beta}^r \quad (2.83)$$

1.7.2.1 The conversion of stator voltage into rotating coordinate frame

Rotating Park's transformation is used to convert stationary coordinate frame into rotating coordinate frame, where $\bar{h}^e = e^{-j\theta_s} \bar{h}^s = h_d + jh_q$

Now applying this condition to the (1.82), we have

$$\mathbf{v}_{dq}^s = e^{-j\theta_s} \mathbf{v}_{\alpha\beta}^s = r_s e^{-j\theta_s} \mathbf{i}_{\alpha\beta}^s + e^{-j\theta_s} \frac{d}{dt} \lambda_{\alpha\beta}^s \quad (1.84)$$

since $e^{-j\theta_s} \mathbf{i}_{\alpha\beta}^s = \mathbf{i}_{dq}^s$, and $e^{j\theta_s} e^{-j\theta_s} \lambda_{\alpha\beta}^s = \lambda_{\alpha\beta}^s$ we have

$$\mathbf{v}_{dq}^s = r_s \mathbf{i}_{dq}^s + e^{-j\theta_s} \left(\frac{d}{dt} e^{j\theta_s} e^{-j\theta_s} \lambda_{\alpha\beta}^s \right) \quad (1.85)$$

based on rotating Park's transformation ($e^{-j\theta_s} \lambda_{\alpha\beta}^s = \lambda_{dq}^s$) and replace $\frac{d}{dt} \theta_s = \omega_s$ in (1.85) we obtain

$$\mathbf{v}_{dq}^s = r_s \mathbf{i}_{dq}^s + e^{-j\theta_s} \left(e^{j\theta_s} j\omega_s \lambda_{dq}^s + e^{j\theta_s} \frac{d}{dt} \lambda_{dq}^s \right)$$

$$\mathbf{v}_{dq}^s = r_s \mathbf{i}_{dq}^s + j\omega_s \lambda_{dq}^s + \frac{d}{dt} \lambda_{dq}^s \quad (1.86)$$

we have

$$\mathbf{v}_{dq}^s = \mathbf{v}_d^s + j\mathbf{v}_q^s \quad (1.87)$$

$$\mathbf{i}_{dq}^s = \mathbf{i}_d^s + j\mathbf{i}_q^s \quad (1.88)$$

$$\lambda_{dq}^s = \lambda_d^s + j\lambda_q^s \quad (1.89)$$

Now by separating the real and imaginary parts in (1.86), we obtain

$$\mathbf{v}_d^s = r_s \mathbf{i}_d^s - \omega_s \lambda_q^s + \frac{d}{dt} \lambda_d^s \quad (1.90)$$

$$v_q^s = r_s i_q^s + \omega_s \lambda_d^s + \frac{d}{dt} \lambda_q^s \quad (1.91)$$

1.7.2.2 The conversion of rotor voltage into dq rotating coordinate frame:

Denote θ_s as the angle of stator magnetic field, with $\theta_s = \omega_s t + \theta_0$. Denote θ_r as the rotor angle, with $\theta_r = \omega_r t + \theta_{r0}$.

Therefore, the transformation angle $\theta_s - \theta_r$ is used in rotating Park's transformation of rotor voltage. (2.83) becomes

$$V_{dq}^r = r_r i_{dq}^r + e^{-j(\theta_s - \theta_r)} \left(\frac{d}{dt} e^{j(\theta_s - \theta_r)} e^{-j(\theta_s - \theta_r)} \lambda_{\alpha\beta}^r \right)$$

$$V_{dq}^r = r_r i_{dq}^r + j(\omega_s - \omega_r) \lambda_{dq}^r + \frac{d}{dt} \lambda_{dq}^r \quad (1.92)$$

By separating the real and imaginary parts similar to stator voltage equations, the following equations are obtained

$$V_d^r = r_r i_d^r - (\omega_s - \omega_r) \lambda_q^r + \frac{d}{dt} \lambda_d^r \quad (1.93)$$

$$V_q^r = r_r i_q^r + (\omega_s - \omega_r) \lambda_d^r + \frac{d}{dt} \lambda_q^r \quad (1.94)$$

Since there is no supply to the rotor, (2.93) and (2.94) become

$$0 = r_r i_d^r - (\omega_s - \omega_r) \lambda_q^r + \frac{d}{dt} \lambda_d^r \quad (1.95)$$

$$0 = r_r i_q^r + (\omega_s - \omega_r) \lambda_d^r + \frac{d}{dt} \lambda_q^r \quad (1.96)$$

Substituting (1.74)(1.75)(1.78)(1.79) into (1.90)(1.91)(1.95)(1.96) we have

$$v_d^s = r_s i_d^s - \omega_s \lambda_q^s + \frac{d}{dt} \lambda_d^s = r_s i_d^s - \omega_s (L_s i_q^s + L_m i_q^r) + \frac{d}{dt} (L_s i_d^s + L_m i_d^r)$$

$$v_q^s = r_s i_q^s + \omega_s \lambda_d^s + \frac{d}{dt} \lambda_q^s = r_s i_q^s + \omega_s (L_s i_d^s + L_m i_d^r) + \frac{d}{dt} (L_s i_q^s + L_m i_q^r)$$

$$0 = r_r i_d^r - (\omega_s - \omega_r) \lambda_q^r + \frac{d}{dt} \lambda_d^r$$

$$= r_r i_d^r - (\omega_s - \omega_r) (L_r i_q^r + L_m i_q^s) + \frac{d}{dt} (L_r i_d^r + L_m i_d^s)$$

$$0 = r_r i_q^r + (\omega_s - \omega_r) \lambda_d^r + \frac{d}{dt} \lambda_q^r$$

$$= r_r i_q^r + (\omega_s - \omega_r) (L_r i_d^r + L_m i_d^s) + \frac{d}{dt} (L_r i_q^r + L_m i_q^s)$$

Denote $\frac{d}{dt} = p$ (the differential operator) and $(\omega_s - \omega_r) = \omega_{sl}$ we get

$$\begin{bmatrix} v_d^s \\ v_q^s \\ 0 \\ 0 \end{bmatrix} = \begin{bmatrix} r_s + pL_s & -\omega_s L_s & pL_m & -\omega_s L_m \\ \omega_s L_s & r_s + pL_s & \omega_s L_m & pL_m \\ pL_m & -\omega_{sl} L_m & r_r + pL_r & -\omega_{sl} L_r \\ \omega_{sl} L_m & pL_m & \omega_{sl} L_r & r_r + pL_r \end{bmatrix} \begin{bmatrix} i_d^s \\ i_q^s \\ i_d^r \\ i_q^r \end{bmatrix} \quad (1.97)$$

1.8 Power and Torque

The torque of machine is generated by electrical to mechanical power conversion. It can be obtained by taking derivative of the electric power with respect to the angular speed.

$$T_e = \frac{dP_e}{d\omega_r} = \frac{P}{2} \frac{dP_e}{d\omega_s} \quad (1.98)$$

Where ω_s is the electrical speed, ω_r is the mechanical speed P is the number of poles and P_e is the electric power.

The power of the rotor is zero, since there is no voltage in the rotor. The power applied to the stator is the total power input.

$$P_e = (v_{abc}^s)^T i_{abc}^s \quad (1.99)$$

Based on total Park's transformation $v_{abc}^s = T^{-1} v_{dq0}^s$ and $i_{abc}^s = T^{-1} i_{dq0}^s$, (1.99) can be expressed as

$$P_e = (T^{-1} v_{dq0}^s)^T T^{-1} i_{dq0}^s$$

$$T^{-1} = \frac{3}{2} T^T$$

$$P_e = \frac{3}{2} (T^T v_{dq0}^s)^T T^{-1} i_{dq0}^s$$

$$P_e = \frac{3}{2} (v_{dq0}^s)^T T T^{-1} i_{dq0}^s$$

$$P_e = \frac{3}{2} (v_{dq0}^s)^T i_{dq0}^s \quad (1.100)$$

Since $T T^{-1} = 1$ now substitute $(v_{dq0}^s)^T = [v_d^s \quad v_q^s \quad 0]$ and $i_{dq0}^s = \begin{bmatrix} i_d^s \\ i_q^s \\ 0 \end{bmatrix}$ in (1.100) we have

$$P_e = \frac{3}{2} (v_d^s i_d^s + v_q^s i_q^s) \quad (1.101)$$

Now substituting (1.97) in (1.101) we get

$$P_e = \frac{3}{2} [(r_s + pL_s)i_d^s - \omega_s L_s i_q^s + pL_m i_d^r - \omega_s L_m i_q^r] i_d^s + \frac{3}{2} [\omega_s L_s i_d^s + (r_s + pL_s)i_q^s + \omega_s L_m i_d^r + pL_m i_q^r] i_q^s \quad (1.102)$$

The torque of the machine can be obtained as

$$T_e = \frac{dP_e}{d\omega_r} = \frac{P}{2} \frac{dP_e}{d\omega_s} = \frac{P}{2} \frac{3}{2} L_m (i_q^s i_d^r - i_d^s i_q^r) \quad (1.103)$$

The torque equation (2.103) can be also written as follows

$$\begin{aligned} T_e &= \frac{P}{2} \frac{3}{2} L_m \operatorname{Im}((i_d^s + j i_q^s) (i_d^r - j i_q^r)) \\ &= \frac{P}{2} \frac{3}{2} L_m \operatorname{Im}((i_{dq}^s i_{dq}^{r*}) = \frac{P}{2} \frac{3}{2} L_m \operatorname{Im}(\frac{1}{L_r} (i_{dq}^s \lambda_{dq}^{r*})) \\ &= \frac{P}{2} \frac{3}{2} \frac{L_m}{L_r} \operatorname{Im}(i_{dq}^s \lambda_{dq}^{r*}) \\ T_e &= \frac{P}{2} \frac{3}{2} \frac{L_m}{L_r} (\lambda_d^r i_q^s - \lambda_q^r i_d^s) \end{aligned} \quad (1.104)$$

Also the system motion equation is given by

$$T_e = T_L + J \frac{d\omega}{dt} \quad (1.105)$$

Where T_L is the load torque, ω is the electric rotor speed, p is the poles numbers and J is rotor's moment of inertia.

1.9 Simulation

In this section the different graphs of the current, torque and speed are presented from the simulation of the induction motor using Matlab/Simulink. The motor is fed by a three phase voltage of 200V. The load torque is varied from 0 to 1 Nm at $t=1s$.

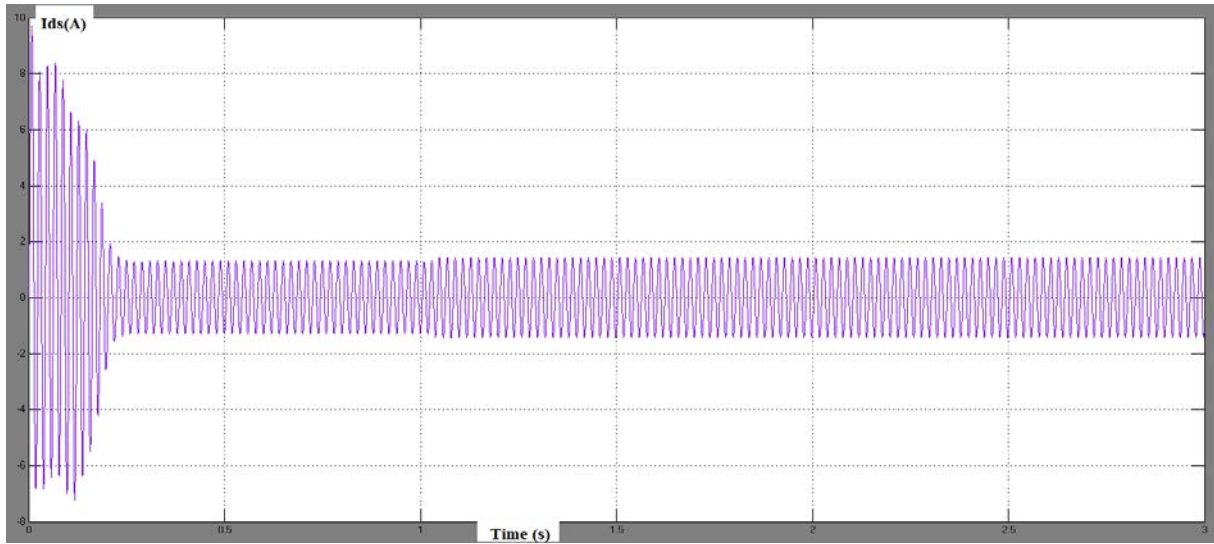


Fig 1.16: The stator current I_{ds} .

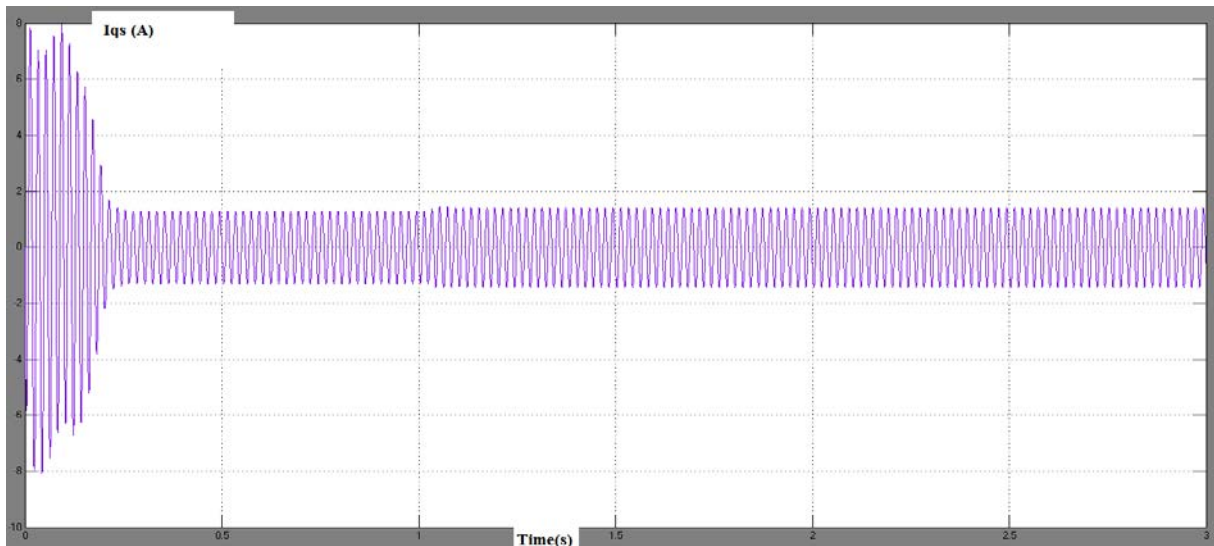


Fig 1.17: The stator current I_{qs}

During the starting the motor needs a high current in a short time to reach the target speed, after that the current is kept at a value around of 1.25 A. When the load torque is varied from 0 to 1Nm the current increases to 1.5A.

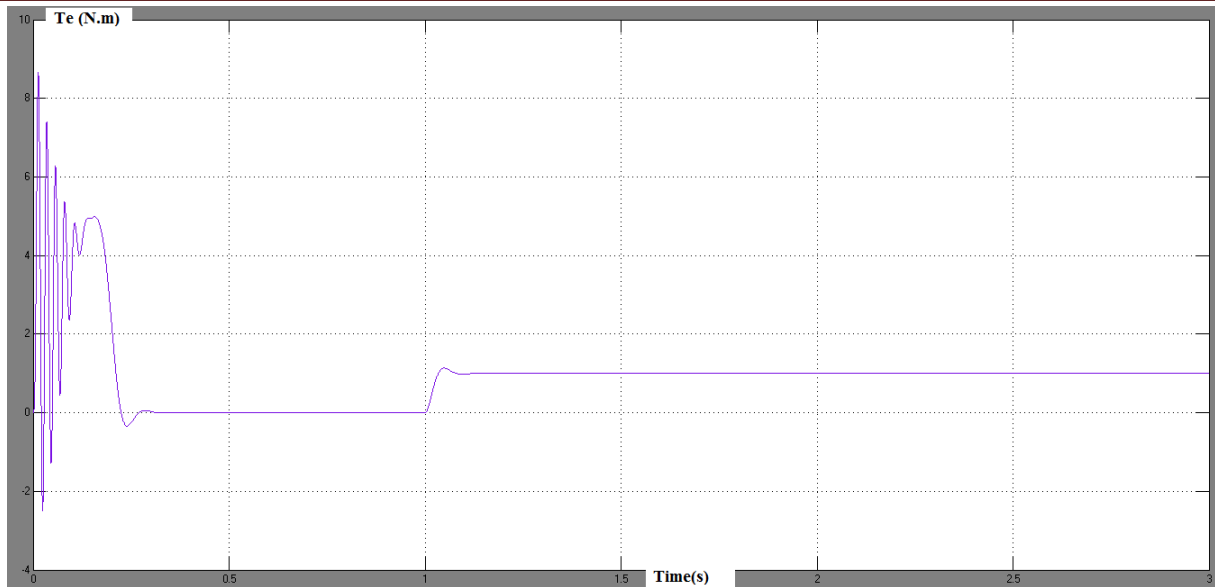


Fig 1.18: The torque (T_e).

At first a large torque is generated to accelerate the motor, after reaching the target speed the torque decreases to the value 0 Nm.

At $t=1$ s the torque follows the load torque value $T_l=1$ N.m.

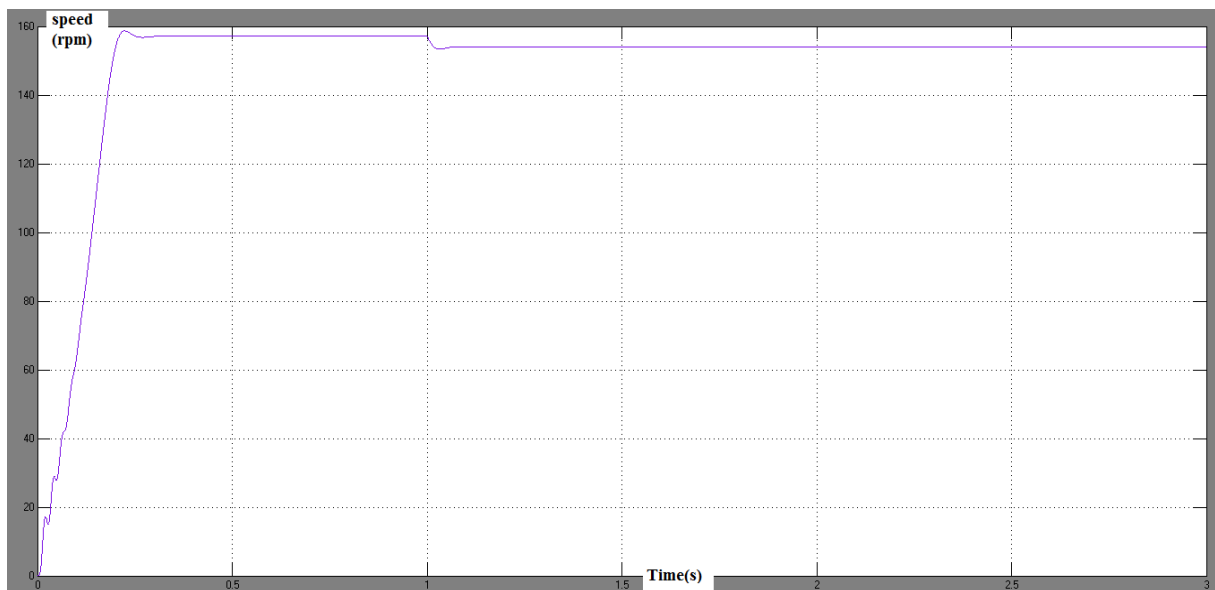


Fig 1.19: The speed.

When the load torque is varied at $t= 1$ s the speed decreases from 157rpm to 150rpm.

It is important to implement a control algorithm to drives the motor and get the desired target speed.

1.10 Conclusion

The dynamic model of induction motor was derived in this chapter. The concept of rotating magnetic field was explained and the equivalent circuit of induction motor was illustrated. Park's and Clarke's transformations are used to convert abc quantities frame to dq frame. The dynamic model of induction motor in dq coordinates frame was presented and finally the simulation of the induction motor was discussed.

CHAPTER 2**SPACE VECTOR PULSE WIDTH MODULATION****2.1 Inverters**

Inverters are converters used to convert a DC voltage to an AC voltage of required magnitude and frequency. They can give a fixed or variable output voltage for a fixed or variable frequency. The output can be varied by changing the input supply or by varying the states of the inverter. The states can be changed using pulse width modulation control of the inverter.

The inverters are mainly used in industrial applications, such as variable speed AC motor drives, transportation, uninterrupted power supplies, etc. For high power applications, the harmonics can be reduced by using high-speed semiconductor devices such as IGBT or IGCT.

The inverters can be classified into two types: current source inverters and voltage source inverters.

2.1.1 Current Source Inverter (CSI)

In current source inverter, the output current is constant and independent of the load applied to the inverter. The CSI operation can be achieved by keeping a series of inductor on the input side. The inductor provides constant input dc current source. The example of a three-phase current source inverter is shown in Fig 2.1

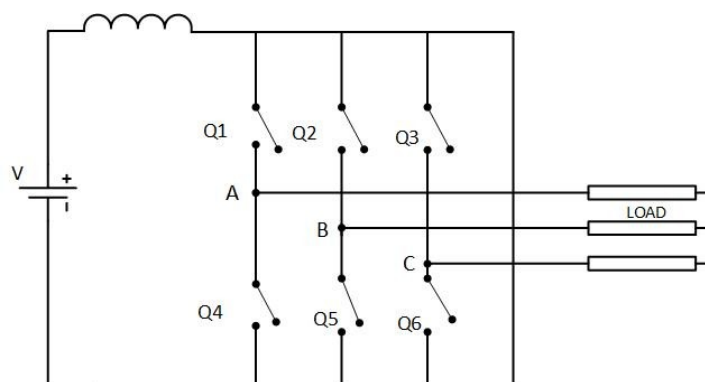


Fig 2.1: Current Source Inverter

2.1.2 Voltage Source Inverter (VSI)

VSI converts fixed DC voltage to a variable AC voltage. Depending upon the type of applications one can use single or three-phase inverters. The three-phase inverter can be constructed by using three single phases half bridge inverter in parallel. The other way to get three phase output is by using six semiconductor switches such as MOSFET, IGBT, IGCT, etc.

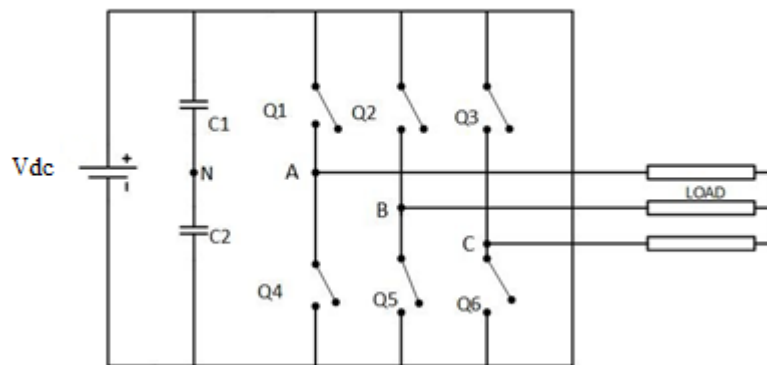


Fig 2.2: Three phases Voltage Source Inverter

The Fig 2.2 shows a simple circuit of the three phases VSI consisting of six switches and two capacitors. The capacitors are placed to provide a neutral point N and each capacitor keeps half of the voltage V_{dc} . The inverter may be connected to a Y or delta connected load.

In order to control the output voltage, we need to change the states by using PWM control. The two main PWM controls which are widely used in the industry are sinusoidal PWM and space vector PWM.

2.1.3 120° conduction mode

In 120° conduction mode, each switch operates for 120° conduction cycle. The pair in each leg are turned on for a time interval of 120° .

The operation of switches of one cycle is shown in Fig 2.3.

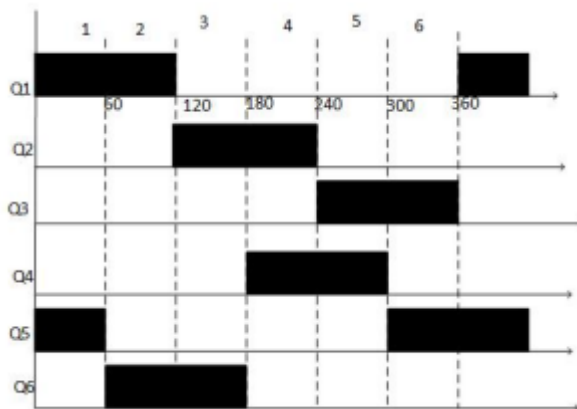


Fig 2.3: Operation of switches over a cycle.

It requires six states over one cycle and each state conducts for 60° . In every state, only two switches are conducting, depending upon the on and off states of switches the respective voltages are determined using the following Fig 2.4.

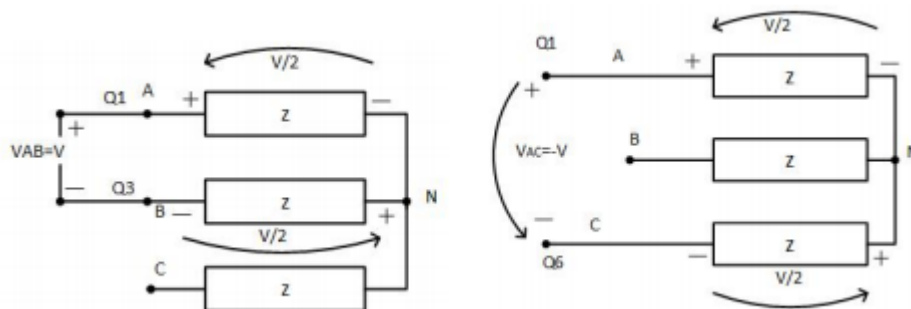


Fig 2.4: Voltage state.

2.2 PWM

2.2.1 Principle of Sinusoidal Pulse Width Modulation (SPWM)

Fig 2.5 shows circuit model of a single-phase inverter with a center-tapped grounded DC bus, and Fig.2.6 illustrates principle of pulse width modulation.

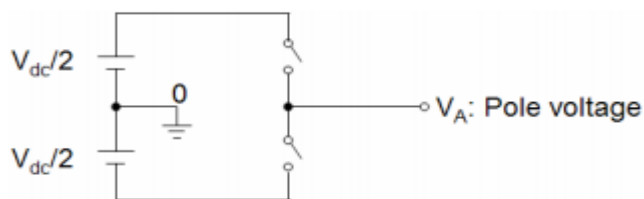


Fig 2.5: Circuit model of a single-phase inverter.

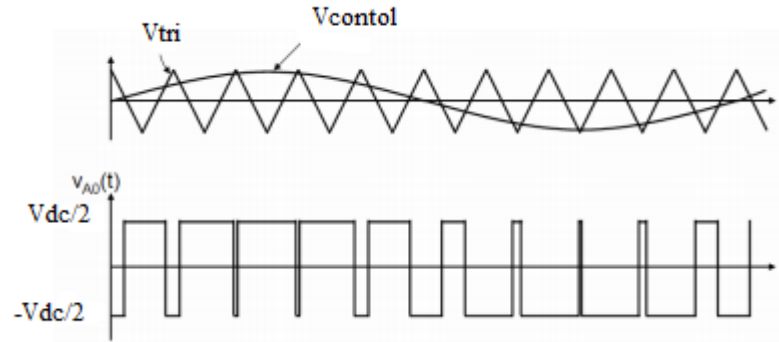


Fig 2.6: Sinusoidal Pulse Width Modulation

As depicted in Fig 2.4, the inverter output voltage is determined in the following:

When $V_{control} > V_{tri}$ $V_{A0} = V_{dc}/2$

When $V_{control} < V_{tri}$ $V_{A0} = -V_{dc}/2$

Also, the inverter output voltage has the following features:

- PWM frequency is the same as the frequency of V_{tri} .
- Amplitude is controlled by the peak value of $V_{control}$.
- Fundamental frequency is controlled by the frequency of $V_{control}$.

Modulation index (m) is defined as:

$$m = \frac{V_{control}}{V_{tri}} \quad (2.1)$$

2.2.2 Space Vector PWM

The output of three-phase voltage source inverter can be shaped using the Space Vector PWM technique. When top switches are on, i.e., S1, S3 or S5 is 1, the corresponding lower switches S4, S6 or S7 are off. The output voltages are determined by selecting the on and off modes of the three upper switches and therefore, the total possible number of combinations are 2^3 .

The relation between the phase voltage and line to line voltages to the switching states of the two level inverter are given as follows:

$$\begin{bmatrix} V_{ab} \\ V_{bc} \\ V_{ca} \end{bmatrix} = V_{dc} \begin{bmatrix} 1 & -1 & 0 \\ 0 & 1 & -1 \\ -1 & 0 & 1 \end{bmatrix} \begin{bmatrix} a \\ b \\ c \end{bmatrix} \quad (2.2)$$

$$\begin{bmatrix} V_a \\ V_b \\ V_c \end{bmatrix} = \frac{1}{3} V_{dc} \begin{bmatrix} 2 & -1 & -1 \\ -1 & 2 & -1 \\ -1 & -1 & 2 \end{bmatrix} \begin{bmatrix} a \\ b \\ c \end{bmatrix} \quad (2.3)$$

Based on the on and off states of upper switches, we can know the lower switches on and off-states, because they act complimentary to the upper switches. The output line to line and phase voltage are summarized in Table 2. 1.

Table 2.1: Switching vectors, phase voltages and output line to line voltages [18].

Voltage vectors	switching vectors			Line to neutral voltage			Line to line voltage		
	S1	S3	S5	V _{an}	v _{bn}	v _{cn}	V _{ab}	v _{bc}	V _{ca}
V0	0	0	0	0	0	0	0	0	0
V1	1	0	0	2/3	-1/3	-1/3	1	0	-1
V2	1	1	0	1/3	1/3	-2/3	0	1	-1
V3	0	1	0	-1/3	2/3	-1/3	-1	1	0
V4	0	1	1	2/3	1/3	1/3	-1	0	1
V5	0	0	1	-1/3	-1/3	2/3	0	-1	1
V6	1	0	1	1/3	-2/3	1/3	1	-1	0
V7	1	1	1	0	0	0	0	0	0

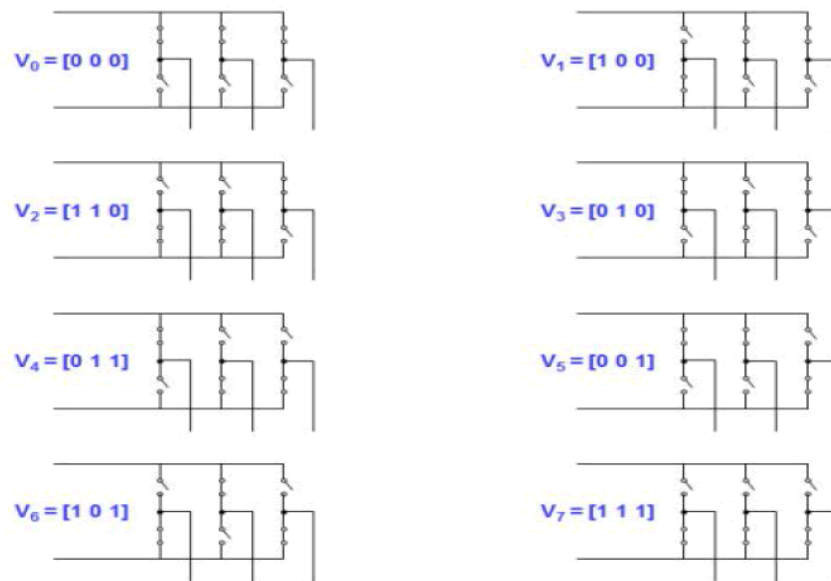


Fig 2.7: The eight inverter voltage vectors (V_0 to V_7).

2.3 Implementation of Space Vector PWM

The output voltages of inverter are balanced three phase voltages. The three phase balanced voltages from the inverter output differ from each other by 120° . The three phase voltages in the a, b and c coordinate frame are transformed to the stationary two coordinate frame using Clark's transformation.

The voltage equations in the three-phase are transferred to the $\alpha\beta$ coordinate frame as shown in the Fig 2.8.

$$v_{\alpha\beta 0} = h_0 v_{abc} \quad (2.4)$$

We can neglect the zero components in the two stationary coordinate frames, because the sum of three phase balanced voltages is equal to zero.

$$V_a + V_b + V_c = 0 \quad (2.5)$$

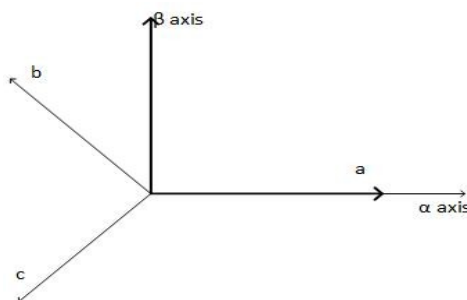


Fig 2.8: Clarke's Transformation

After the transformation into $\alpha\beta$ coordinate frame, from total eight combinations of turn off and turn on of switches, we get six non-zero vectors and two zero vectors. The six non-zero vectors supply power to the load and the zero vectors do not supply power to the load. The eight vectors are considered to be the space vectors and form the six vertices of a hexagon. The same transformation can be applied to get the reference voltage vector V_{ref} in $\alpha\beta$ plane. Now obtain the reference voltage from those eight space vectors. The eight space vectors are considered to be stationary vectors and the only vector which rotates in space is V_{ref} with an angular velocity $\omega = 2\pi f$, where f is the inverter frequency.

V_{ref_alpha} , V_{ref_beta} and angle (α) can be determined as follows:

$$\begin{bmatrix} v_\alpha \\ v_\beta \end{bmatrix} = \frac{2}{3} \begin{bmatrix} 1 & -\frac{1}{2} & -\frac{1}{2} \\ 0 & \frac{\sqrt{3}}{2} & -\frac{\sqrt{3}}{2} \end{bmatrix} \begin{bmatrix} v_a \\ v_b \\ v_c \end{bmatrix} \quad (2.6)$$

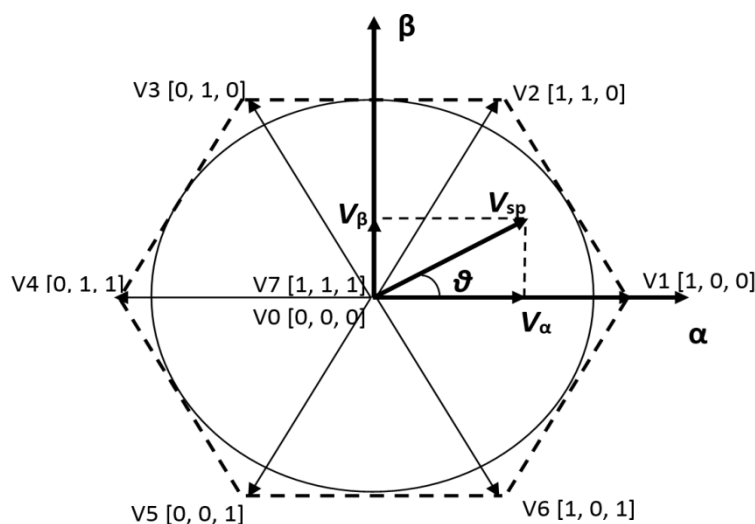


Fig 2.9: Hexagon Representation of Space Vectors.

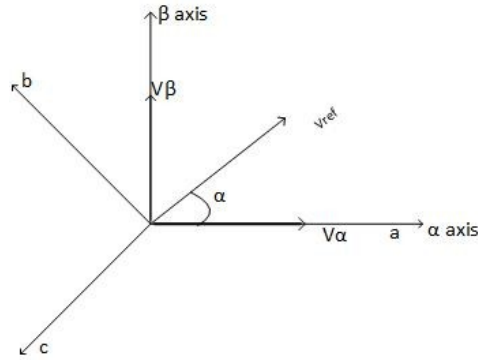


Fig 2.10: The V_{ref} in $\alpha \beta$ axis.

$$|V_{ref}| = \sqrt{v_{\alpha}^2 + v_{\beta}^2} \tag{2.7}$$

$$\alpha^{\circ} = \tan^{-1} \frac{v_{\alpha}}{v_{\beta}} = \omega t = 2\pi f t \tag{2.8}$$

Where f : is the fundamental frequency of the desired output voltage.

- Determine time duration of T_1 , T_2 and T_0 [19]:

Considering V_{ref} is in Sector 1, and it can be synthesized by vectors adjacent to it in that sector. The time duration of the V_{ref} is based on the following principle: The product of reference voltage and its sampling time period is equal to the sum of voltages multiplied by their time interval of space vectors in chosen sector.

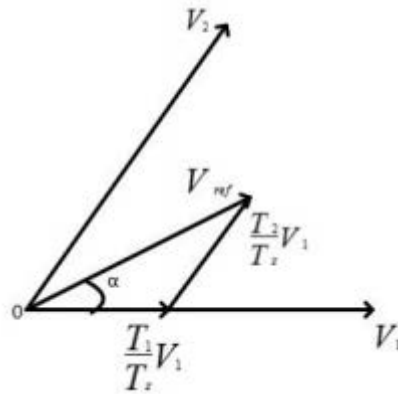


Fig 2.11: The reference voltage in sector 1.

In the Fig 2.12, we show the corresponding space vectors and respective time duration.

- Switching time duration in sector 1:

$$\int_{T_0}^{T_z} \bar{V}_{ref} dt = \int_{T_0}^{T_1} V_1 dt + \int_{T_1}^{T_1+T_2} \bar{V}_2 dt + \int_{T_1+T_2}^{T_z} \bar{V}_0 dt \quad (2.9)$$

$$T_z = T_1 + T_2 + T_0 \quad (2.10)$$

Where T_1 , T_2 and T_0 are the switching times of V_1 , V_2 and V_0 respectively.

T_z is switching period ($2T_z = T_s = \frac{1}{f_s}$). T_s and f_s are the sampling time and frequency.

From above equation, we obtain

$$T_z \bar{V}_{ref} = T_1 \bar{V}_1 + T_2 \bar{V}_2 + T_0 \bar{V}_0 \quad (2.11)$$

However, \bar{V}_0 applies a zero voltage to the output load, so the equation becomes

$$T_z \bar{V}_{ref} = T_1 \bar{V}_1 + T_2 \bar{V}_2 \quad (2.12)$$

Now, substituting the value of \bar{V}_1 and \bar{V}_2 from Tab1

$$T_z |\bar{V}_{ref}| \begin{bmatrix} \cos a \\ \sin a \end{bmatrix} = T_1 \frac{2}{3} V_{dc} \begin{bmatrix} 1 \\ 2 \end{bmatrix} + T_2 \frac{2}{3} V_{dc} \begin{bmatrix} \cos \frac{\pi}{3} \\ \sin \frac{\pi}{3} \end{bmatrix} \quad (2.13)$$

$$T_2 = T_z \frac{3}{2} \frac{|\bar{V}_{ref}|}{V_{dc}} \frac{\sin a}{\sin \frac{\pi}{3}}$$

$$T_2 = T_z a \frac{\sin a}{\sin \frac{\pi}{3}} \quad (2.14)$$

$$T_1 = T_z \frac{3}{2} \frac{|\bar{V}_{ref}|}{V_{dc}} \frac{\sin(\frac{\pi}{3}-a)}{\sin \frac{\pi}{3}}$$

$$T_1 = T_z a \frac{\sin(\frac{\pi}{3}-a)}{\sin \frac{\pi}{3}} \quad (2.15)$$

The angle between any two adjacent sides of hexagon is 60° , therefore

($0^\circ \leq a \leq 60^\circ$) in sector one, and a is the modulation index, $a = \frac{3}{2} \frac{|\bar{V}_{ref}|}{V_{dc}}$.

Switching time duration in arbitrary sector

The time duration in the other sectors can be calculated by substituting

$\alpha = \alpha - (n-1) \frac{\pi}{3}$ Where n is the sector number which is from 1 to 6.

$$\begin{aligned} T_1 &= T_z \frac{3}{2} \frac{|\bar{V}_{ref}|}{V_{dc}} \frac{\sin\left(\frac{\pi}{3} - (\alpha - (n-1)\frac{\pi}{3})\right)}{\sin\frac{\pi}{3}} \\ &= \frac{\sqrt{3} T_z |\bar{V}_{ref}|}{V_{dc}} \sin\left(\frac{n}{3}\pi - \alpha\right) \end{aligned}$$

Then
$$T_1 = \frac{\sqrt{3} T_z |\bar{V}_{ref}|}{V_{dc}} \left\{ \sin\left(n \frac{\pi}{3}\right) \cos(\alpha) - \cos\left(n \frac{\pi}{3}\right) \sin(\alpha) \right\} \quad (2.16)$$

$$\begin{aligned} T_2 &= T_z \frac{3}{2} \frac{|\bar{V}_{ref}|}{V_{dc}} \frac{\sin\left(\alpha - (n-1)\frac{\pi}{3}\right)}{\sin\frac{\pi}{3}} \\ &= \frac{\sqrt{3} T_z |\bar{V}_{ref}|}{V_{dc}} \sin\left(\alpha + (n-1)\frac{\pi}{3}\right) \end{aligned}$$

$$T_2 = \frac{\sqrt{3} T_z |\bar{V}_{ref}|}{V_{dc}} \left\{ \cos\left((n-1)\frac{\pi}{3}\right) \sin(\alpha) + \cos\left((n-1)\frac{\pi}{3}\right) \cos(\alpha) \right\} \quad (2.17)$$

$$T_0 = T_z - (T_1 + T_2) \quad (2.18)$$

- To find sector number:

To get sector number, n, first of all, we use angle α from the step 1 considering one cycle ($0, 2\pi$), we divide angle by 2π and take the remaining angle for one cycle. In the hexagon, each sector is multiple of $\pi/3$, so we divide new angle by $\pi/3$ and round that remainder to a less integer. The sector number can find by adding one to the integer.

For example, let $\alpha = 450^\circ$

$$\text{remain} = \text{rem}\left(\frac{450^\circ}{360^\circ}\right)$$

$$= 90^\circ$$

$$n = 1 + \text{fix}\left(\frac{90^\circ}{60^\circ}\right) = 1 + \text{fix}(1.5)$$

$$= 1 + 1 = 2$$

Therefore sector number is 2.

Table 2.2: Calculation of Switching Time at each Sector [19].

Sector	Upper Group Switches (S ₁ ,S ₃ ,S ₅)	Lower Group Switches (S ₄ ,S ₆ ,S ₂)
1	$S_1 = T_1 + T_2 + T_0/2$ $S_3 = T_2 + T_0/2$ $S_5 = T_0/2$	$S_4 = T_0/2$ $S_6 = T_1 + T_0/2$ $S_2 = T_1 + T_2 + T_0/2$
2	$S_1 = T_1 + T_0/2$ $S_3 = T_1 + T_2 + T_0/2$ $S_5 = T_0/2$	$S_4 = T_2 + T_0/2$ $S_6 = T_0/2$ $S_2 = T_1 + T_2 + T_0/2$
3	$S_1 = T_0/2$ $S_3 = T_1 + T_2 + T_0/2$ $S_5 = T_2 + T_0/2$	$S_4 = T_1 + T_2 + T_0/2$ $S_6 = T_0/2$ $S_2 = T_1 + T_0/2$
4	$S_1 = T_0/2$ $S_3 = T_1 + T_0/2$ $S_5 = T_1 + T_2 + T_0/2$	$S_4 = T_1 + T_2 + T_0/2$ $S_6 = T_2 + T_0/2$ $S_2 = T_0/2$
5	$S_1 = T_2 + T_0/2$ $S_3 = T_0/2$ $S_5 = T_1 + T_2 + T_0/2$	$S_4 = T_1 + T_0/2$ $S_6 = T_1 + T_2 + T_0/2$ $S_2 = T_0/2$
6	$S_1 = T_1 + T_2 + T_0/2$ $S_3 = T_0/2$ $S_5 = T_1 + T_0/2$	$S_4 = T_0/2$ $S_6 = T_1 + T_2 + T_0/2$ $S_2 = T_2 + T_0/2$

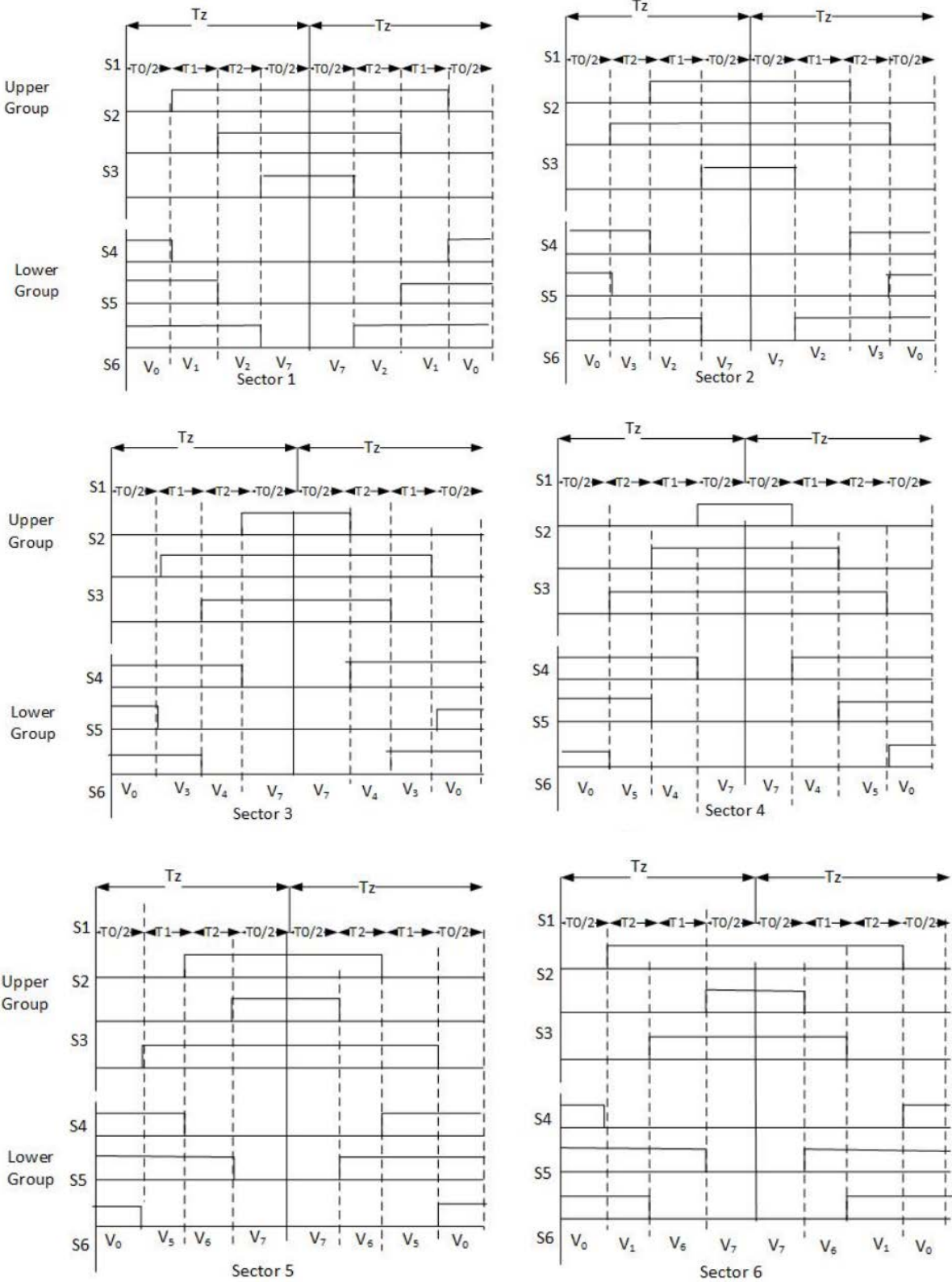


Fig 2.12: The Switching Pattern of SVPWM at each Sector.

2.4 SVPWM Simulation

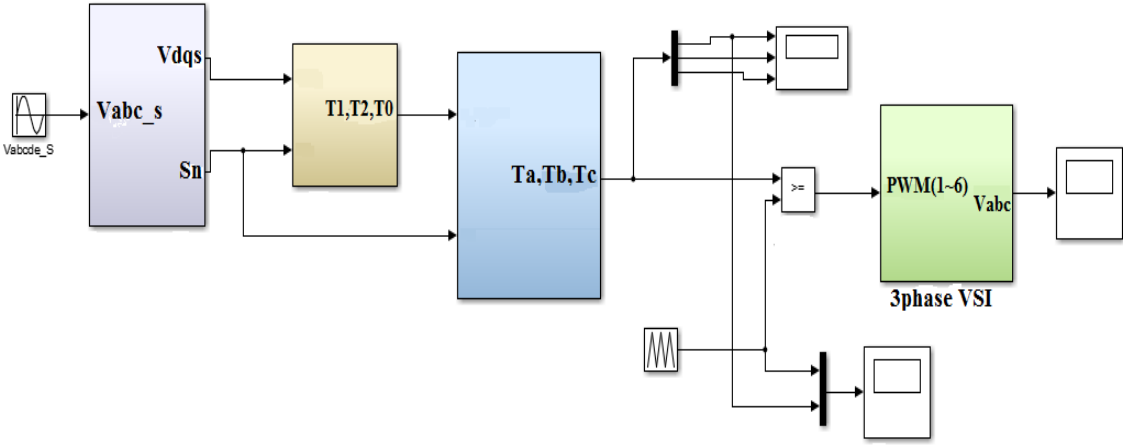


Fig 2.13: SVPWM simulation model.

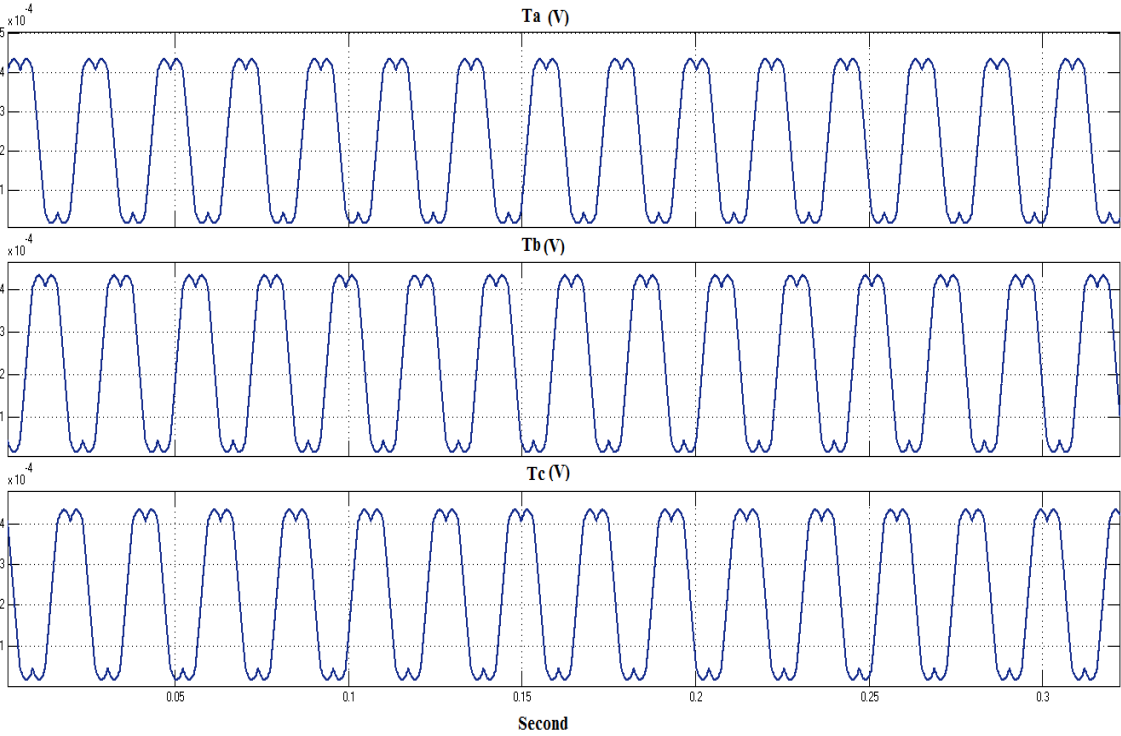


Fig 2.14: SVPWM duty cycle (T_a , T_b , T_c).

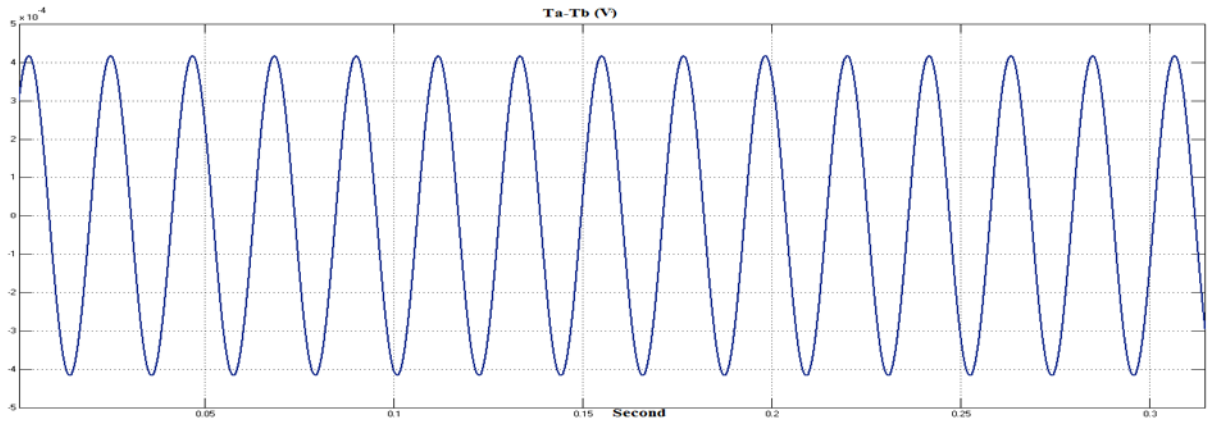


Fig 2.15: SVPWM duty cycle (T_a-T_b).

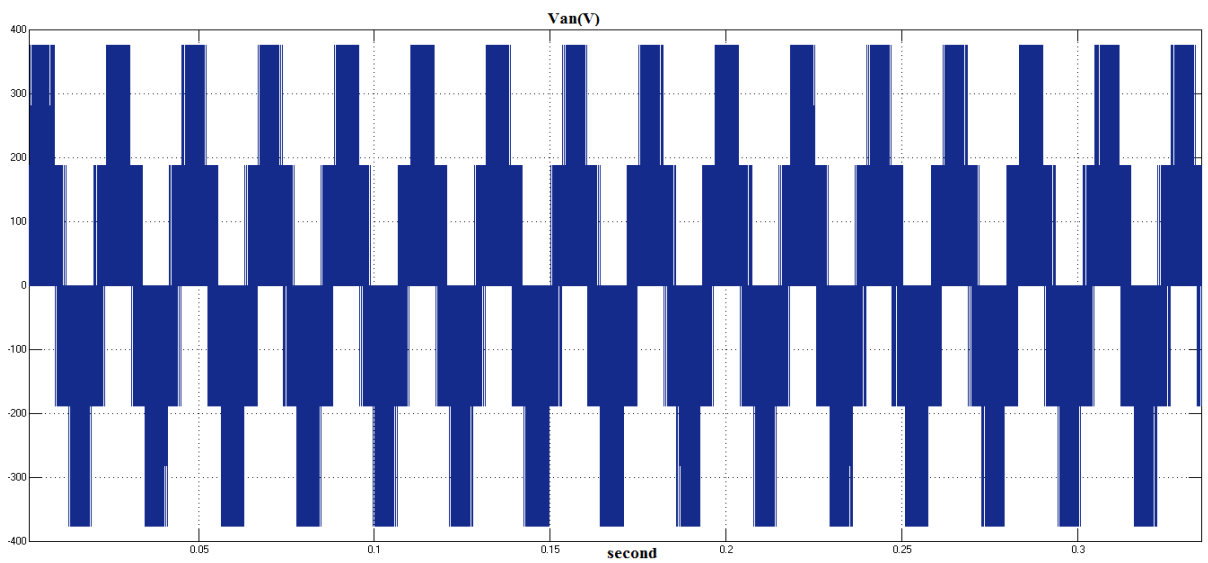


Fig 2.16: The output line to neutral voltage (V_{an}).

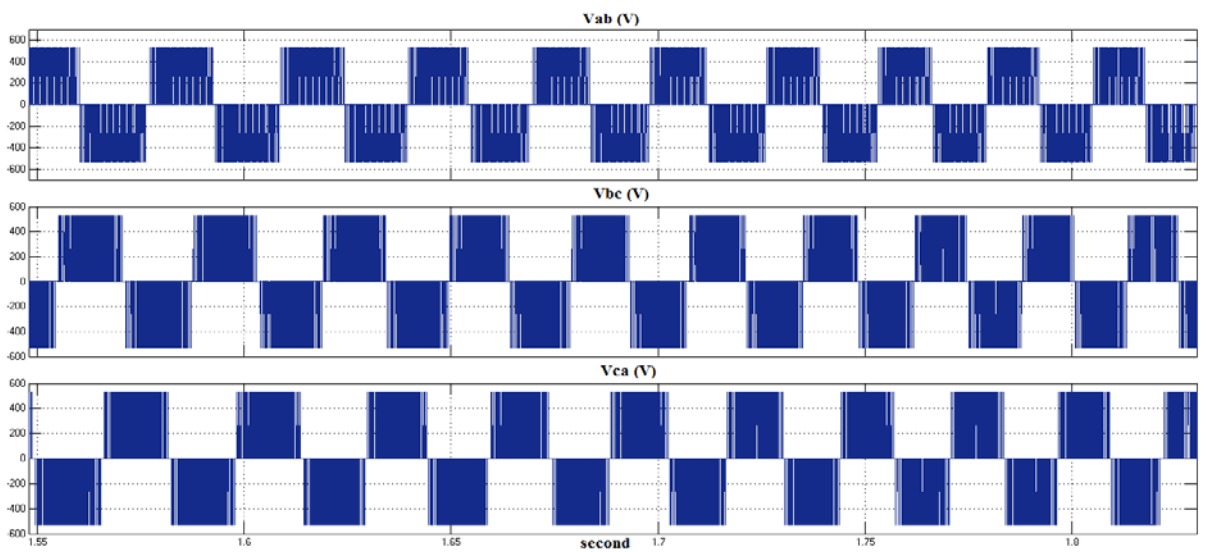


Fig2.17: The output line to line voltage (V_{ab} , V_{bc} , V_{ca}).

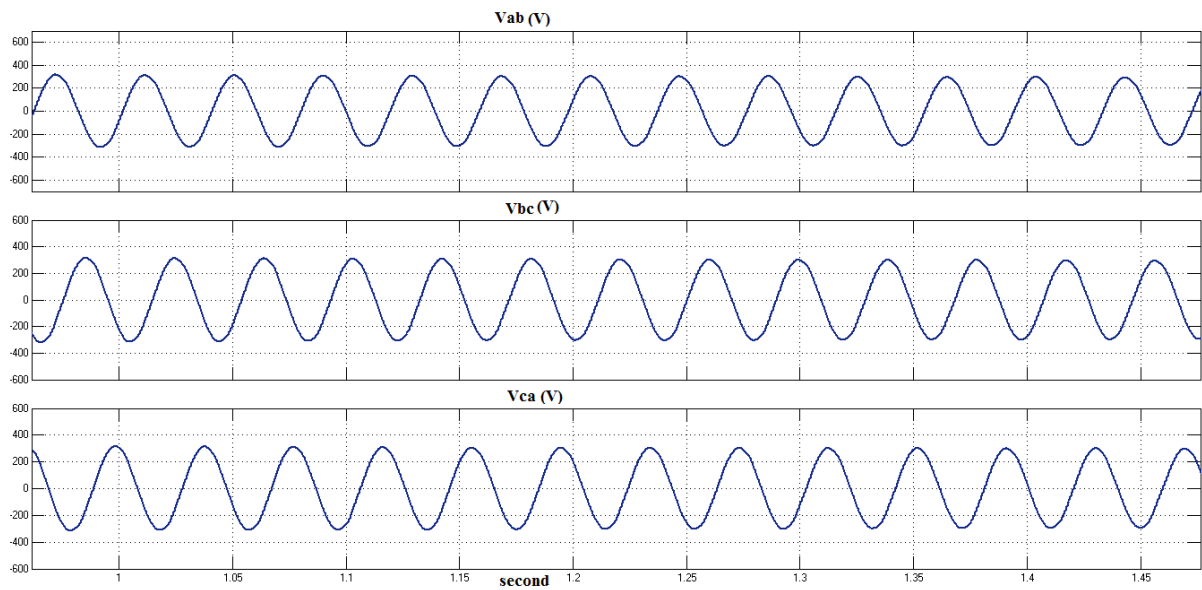


Fig 2.18: The filtered output line to line voltage (V_{ab} , V_{bc} , V_{ca}).

2.5 Summary

In this chapter the operation and characteristics of inverters were explained. The conduction modes of 120° voltage source inverters (VSI) were used in simulation model. The concept and design of Space Vector PWM were explained in this chapter. The Space Vector PWM was simulated using Matlab/Simulink. The results show that the SVPWM method produces very low harmonic distortion in the output waveform.

CHAPTER 3**FIELD ORIENTED CONTROL****3.1 INTRODUCTION**

The DC motors have been widely used in variable speed control applications. In DC drives, the torque and flux are decoupled and can be controlled by the armature and field current. However, DC machines have many disadvantages, such as sparks, commutator and brushes wear out, difficulty to maintain, etc. The field oriented control of induction motor was first developed by Hasse in 1969 and Blaschke in 1972. The development in power electronics devices and microprocessors make the AC machines speed control available and overcome the disadvantages of DC machines like high cost, commutator and brushes problems. Initially, the speed control of induction machine is performed by changing the voltage and frequency and keeping the V/f ratio constant. These types of controlling methods are called the scalar control methods. The high performance of field oriented control drives outperforms the scalar control method due to the following advantages [20]:

- Full torque control capability at low speed.
- Better dynamic behavior.
- Higher efficiency.
- Operating point in a wide range of speed.
- Decoupled torque and flux control.
- Four quadrant operation.

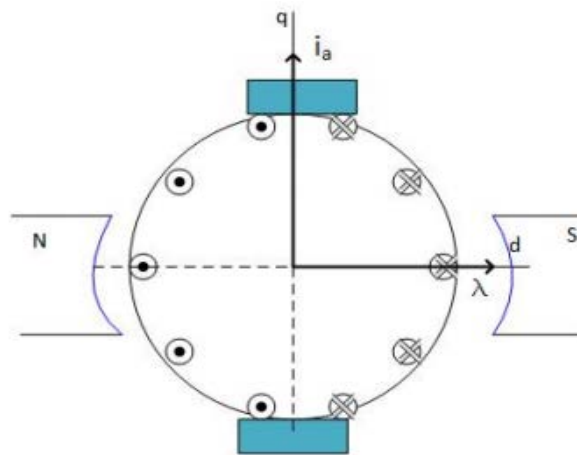


Fig 3.1: A simple representation of DC motor

As we apply the concept of DC motor control to the AC machines, in DC motor the torque is proportional to the cross product of current i_a and flux λ_f . The current and flux are along the two axis of coordinate system, which means they are always perpendicular to each other and produces maximum torque all the time. The torque equation of DC motor which can be used as reference for field oriented control is

$$\tau_m = K_T \lambda_f i_a \quad (3.1)$$

Where K_T is torque constant.

3.1.1 MODEL OF FIELD ORIENTED CONTROL [21]

The DC machine control approach to AC Drives is not easier, because the orientation of stator and rotor fluxes are not held orthogonal and vary with the operating conditions [20].

To obtain like DC machine control one need to align stator currents with respect to the rotor flux to get independently controlled torque and flux. This type of control is achieved by:

- Converting AC motor dynamics into dq synchronous frame under certain conditions.
- Aligning the flux of the machine to the reference frame.

Depending upon the alignment of flux, the system categorized into two different schemes:

- Stator field oriented control “the reference frame is aligned to the stator field”
- Rotor field oriented control “the reference frame is aligned to the rotor field”

However, calculation of the rotor flux is carried in two different ways. If it is measured directly by using sensors, then it is called direct Field Oriented Control (DFOC). If the measurement is from slip that is calculated from the dynamic model of induction motor, then it is called indirect Field Oriented Control (IFOC). The simplicity of implementation and the more reliability makes IFOC widely used in industries.

In DFOC the rotor flux is measured from Hall Effect sensors. Therefore, the rotor angle can be calculated from the rotor flux by the equation:

$$\theta = \tan^{-1} \frac{\lambda_{dr}^s}{\lambda_{qr}^s} \quad (3.2)$$

The installation of flux sensors is difficult due to limitations of air gap space, armature reaction, noise, etc. Due to these limitations the rotor flux is calculated indirectly from stator currents that are measured using current sensors.

In IFOC we have two approaches of measuring rotor flux angle. The first one is by calculating the rotor flux equations indirectly by using the stator flux and currents .and the second is from slip information ω_{sl} .

How do we precede with the rotor flux equations from the stator currents and fluxes?

The current sensors are used to measure the stator currents, and fluxes can be obtained using equations (3.3) and (3.4).

$$\lambda_d^s = \int_0^t (v_d^s - r_s i_d^s) dt \quad (3.3)$$

$$\lambda_q^s = \int_0^t (v_q^s - r_s i_q^s) dt \quad (3.4)$$

By converting the equations of the stator flux and rotor flux in synchronous rotating frame into $\alpha\beta$ stationary coordinate frame by multiplying with $e^{j\theta}$, we obtain:

$$\lambda_\alpha^s = L_s i_\alpha^s + L_m i_\alpha^r \quad (3.5)$$

$$\lambda_\beta^s = L_s i_\beta^s + L_m i_\beta^r \quad (3.6)$$

$$\lambda_\alpha^r = L_r i_\alpha^r + L_m i_\alpha^s \quad (3.7)$$

$$\lambda_\beta^r = L_r i_\beta^r + L_m i_\beta^s \quad (3.8)$$

Now we substitute the i_α^r , i_β^r taken from (3.5) and (3.6) in (3.7) and (3.8) we get

$$\lambda_\alpha^r = \frac{L_r (\lambda_\alpha^s + L_s i_\alpha^s)}{L_m} + L_m i_\alpha^s = \frac{(L_m^2 - L_s L_r) i_\alpha^s + L_r \lambda_\alpha^s}{L_m}$$

$$\lambda_\beta^r = \frac{L_r (\lambda_\beta^s + L_s i_\beta^s)}{L_m} + L_m i_\beta^s = \frac{(L_m^2 - L_s L_r) i_\beta^s + L_r \lambda_\beta^s}{L_m}$$

$$\sigma = 1 - \frac{L_m}{L_s L_r} \quad (3.9)$$

After rearranging the terms and substituting terms, the two equations can be written as:

$$\lambda_\alpha^r = \frac{L_r}{L_m} (\lambda_\alpha^s + \sigma L_s i_\alpha^s) \quad (3.10)$$

$$\lambda_{\beta}^r = \frac{L_r}{L_m} (\lambda_{\beta}^s + \sigma L_s i_{\beta}^s) \quad (3.11)$$

Now, substituting the stator currents measured from sensors and fluxes from (3.3) and (3.4) in the above equations, we get rotor flux equations. From (3.10) and (3.11), the rotor flux angle can be obtained. However, this method is not suitable when a DC offset is present.

The second method for calculating rotor flux angle, which is from slip information.

From (1.95) and (1.96), we know

$$0 = r_r i_d^r + p \lambda_d^r - (\omega - \omega_r) \lambda_q^r$$

$$0 = r_r i_q^r + p \lambda_q^r + (\omega - \omega_r) \lambda_d^r$$

Now applying $\lambda_q^r = 0$ and $p \lambda_q^r = 0$, the rotor equations become:

$$0 = r_r i_d^r + p \lambda_d^r \quad (3.12)$$

$$0 = r_r i_q^r + (\omega - \omega_r) \lambda_d^r \quad (3.13)$$

From (1.78) we know λ_d^r and substituting that in (3.12) we get:

$$0 = r_r i_d^r + p(L_r i_d^r + L_m i_d^s)$$

$$0 = (r_r + pL_r) i_d^r + pL_m i_d^s \quad (3.14)$$

$$i_d^r = \frac{-pL_m i_d^s}{(r_r + pL_r)} \quad (3.15)$$

Again by substituting i_d^r in the (1.78) i.e λ_d^r becomes

$$\lambda_d^r = L_r \frac{-pL_m i_d^s}{(r_r + pL_r)} + L_m i_d^s$$

$$= [L_m - \frac{L_r L_m i_d^s}{(r_r + pL_r)} p] i_d^s$$

After canceling the respective terms the rotor flux along the direct axis, λ_d^r can be written as

$$\lambda_d^r = \frac{L_m}{(1+pT_r)} i_d^s \quad (3.16)$$

Where T_r is the rotor time constant

$$T_r = \frac{L_r}{r_r} \quad (3.17)$$

In the steady state

$$\lambda_d^r = L_m i_d^s \quad (3.18)$$

Since $\lambda_d^r = 0$, (1.79) can be written as $i_q^r = -\frac{L_m i_q^s}{L_r}$, substituting this equation in (3.13) we obtain the slip speed information.

$$\text{Slip_speed} = \omega_{sl} = \omega_s - \omega_r = \frac{r_r L_m}{L_r \lambda_d^r} i_q^s \quad (3.19)$$

Now, adding obtained slip speed to the rotor shaft speed, we get synchronous speed of the machine. The rotor flux angle can be measured by integrating the synchronous speed which is shown in (3.20)

$$\theta = \int_0^t \omega_e dt = \int_0^t (\omega_{sl} + \omega_r) dt \quad (3.20)$$

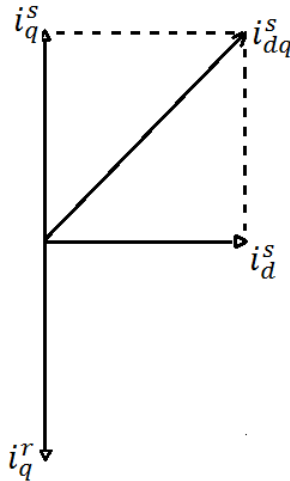


Fig 3.2: The vector representation of rotor field oriented scheme

From $\lambda_d^r = \frac{L_m}{(1+pT_r)} i_d^s$, we find that i_d^s is used to generate rotor flux.

Comparing the equations (1.78) and (3.18), we obtain $i_d^r = 0$.

From (3.19) i_q^s is proportional to the slip.

From $i_q^r = -\frac{L_m i_q^s}{L_r}$, we find i_q^r nullifies flux caused by i_q^s .

The $\lambda_q^r = 0$ reduces the torque equation (1.103) to follow the equation, which is similar to the DC machine

$$T_e = \frac{3}{2} \frac{P}{2} \frac{L_m}{L_r} (\lambda_d^r i_q^s) \quad (3.21)$$

Based on the field oriented control method, we have the flux along the direct axis and current along the quadrature axis, which is similar to the DC machine. Based on (3.18) and (3.19), the rotor flux along the direct axis is proportional to the i_d^s and the current i_q^s along the quadrature axis is proportional to slip. The two currents i_d^s, i_q^s are used for the control of Induction machine.

3.1.2 FOC ALGORITHM

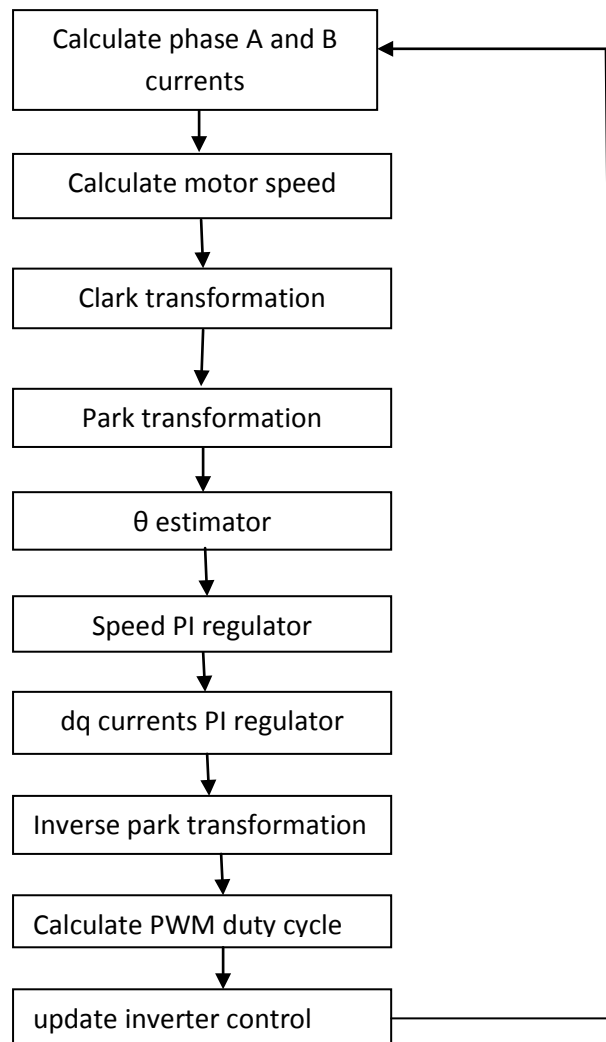


Fig 3.3: The flow chart of the FOC algorithm

The Basic Scheme for Field Oriented Control of Induction Motor

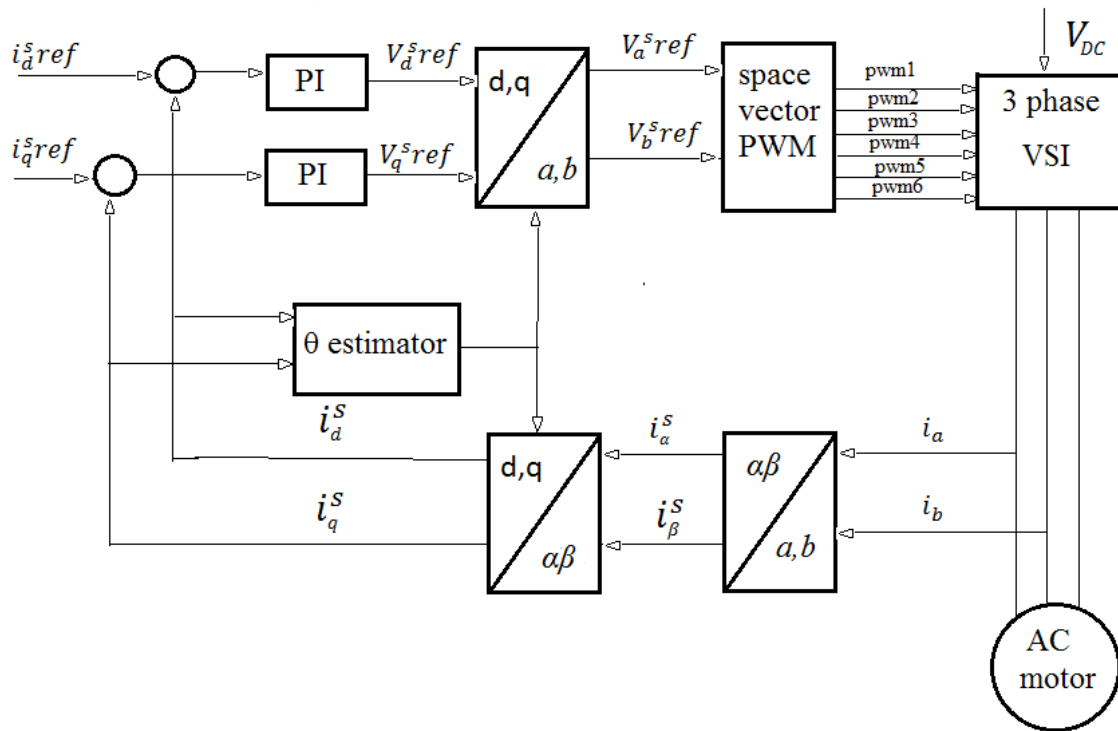


Fig 3.4: The basic scheme of field oriented control

Fig 3.4, explains the basic scheme of speed control with FOC. Firstly, it measures the two input currents of the motor. These input currents are converted to stationary coordinate frame using Clarke's transformation module. The currents in the stationary frame are converted to rotating frame using Park's transformation module. These currents are compared to the reference currents and the resulting error is passed through the current controllers. The output of current controllers, which are in dq coordinate frame, are converted into $\alpha\beta$ coordinate frame using inverse rotating Park's transformation module. These are input to the Space Vector PWM module. The output of Space Vector PWM module operates the gating signal of the three phase inverter. The Clarke and Park Transformation modules require the rotor flux position which is the key factor in controlling the machine. The calculation of rotor flux position is mentioned in direct and indirect rotor field oriented scheme.

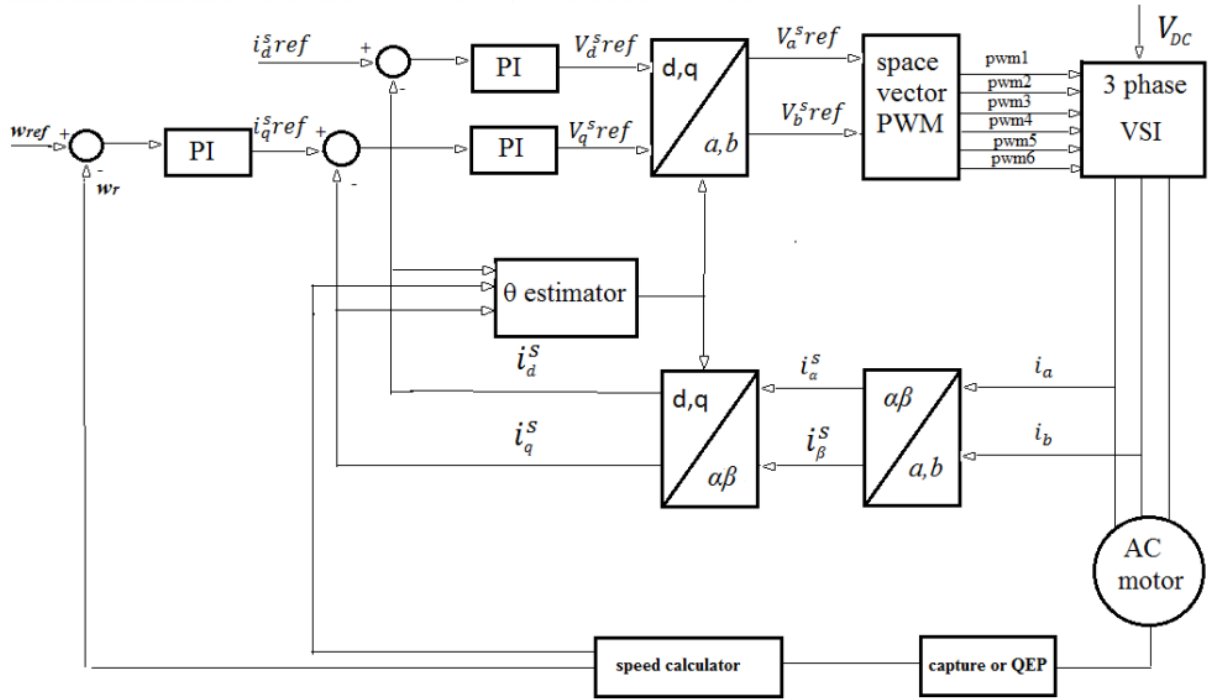


Fig 3.5: Block diagram of indirect rotor field oriented control

3.2 ROTOR FIELD ORIENTED SCHEME

From (1.78) and (1.79) we get

$$i_d^r = \frac{1}{L_r} (\lambda_d^r - L_m i_d^s) \quad (3.22)$$

$$i_q^r = \frac{1}{L_r} (\lambda_q^r - L_m i_q^s) \quad (3.23)$$

Substituting (3.22) and (3.23) into the system model (1.97)

$$v_d^s = (r_s + p\sigma L_s) i_d^s + \frac{L_m}{L_r} p \lambda_d^r - \omega \left[\frac{L_m}{L_r} \lambda_q^r + L_s \sigma i_q^s \right] \quad (3.24)$$

$$v_q^s = (r_s + p\sigma L_s) i_q^s + \frac{L_m}{L_r} p \lambda_q^r - \omega \left[\frac{L_m}{L_r} \lambda_d^r + L_s \sigma i_d^s \right] \quad (3.25)$$

Where

$$\sigma = \left(1 - \frac{L_m}{L_s L_r} \right)$$

The field oriented control can be achieved by aligning the rotor flux along the direct axis, i.e. $\lambda_q^r = 0$, and $p \lambda_q^r = 0$. Therefore, (3.24) and (3.25) are reduced to

$$v_d^s = (r_s + p\sigma L_s)i_d^s + \frac{L_m}{L_r}p\lambda_d^r - \omega_e[L_s\sigma i_q^s] \quad (3.26)$$

$$v_q^s = (r_s + p\sigma L_s)i_q^s - \omega_e\left[\frac{L_m}{L_r}\lambda_d^r + L_s\sigma i_d^s\right] \quad (3.27)$$

The torque equation (1.104) reduced to

$$T_e = \frac{3}{2} \frac{P}{2} \frac{L_m}{L_r} (\lambda_d^r i_q^s) \quad (3.28)$$

Applying the Laplace transformation for above two voltage equations and considering the steady state condition $p\lambda_q^r = 0$

$$i_d^s = \frac{\frac{1}{L_s\sigma}}{s + \frac{r_s}{L_s\sigma}} v_d^s + \frac{\frac{\omega_e}{r_s}}{s + \frac{r_s}{L_s\sigma}} i_q^s \quad (3.29)$$

$$i_q^s = \frac{\frac{1}{L_s\sigma}}{s + \frac{r_s}{L_s\sigma}} v_q^s - \frac{\frac{\omega_e}{r_s}}{s + \frac{r_s}{L_s\sigma}} i_d^s - \frac{\frac{L_m}{L_r L_m \sigma}}{s + \frac{r_s}{L_s\sigma}} \omega_e \lambda_d^r \quad (3.30)$$

Neglecting the r_s term and considering $p\lambda_q^r = 0$ for the steady state condition, we reach the following conditions:

$$L_s\sigma \frac{d}{dt} i_d^s = v_d^s + \omega_e L_s\sigma i_q^s \quad (3.31)$$

$$L_s\sigma \frac{d}{dt} i_q^s = v_q^s - \omega_e L_s\sigma i_d^s - \omega_e \frac{L_m}{L_r} \lambda_d^r \quad (3.32)$$

From (3.26) and (3.27) we find $\omega_e L_s\sigma i_q^s$ and $-\omega_e L_s\sigma i_d^s$, are cross-coupling current terms of d-axis and q-axis. In order to decouple the coupling terms, the feed-forward control is used.

Equate right hand side of equations (3.31) and (3.32) with u_d^* and u_q^* , we have

$$u_d^* = u_d^s + \omega_e L_s\sigma i_q^s \quad (3.33)$$

$$u_q^* = u_q^s - \omega_e L_s\sigma i_d^s - \omega_e \frac{L_m}{L_r} \lambda_d^r \quad (3.34)$$

By applying the Laplace transformation, we have the plant transfer function $G_i(s)$ for the current control as

$$G_i(s) = \frac{i_d^s}{u_d^*} = \frac{1}{L_s \sigma s} \quad (3.35)$$

$$G_i(s) = \frac{i_q^s}{u_q^*} = \frac{1}{L_s \sigma s} \quad (3.36)$$

Where $\sigma = (1 - \frac{L_m}{L_s L_r})$

3.2.1 PI CURRENT CONTROLLER DESIGN

Let's consider the PI controller given below

$$R_i(s) = k_p (1 + \frac{1}{s T_i}) \quad (3.37)$$

Where $T_i = \frac{k_p}{k_i}$

We design the current controller based on frequency response method using the phase and gain margin. Let us choose the crossover frequency, $\omega_c = \frac{2\pi f_s}{10}$, where f_s is the switching frequency of the inverter and phase margin $PM = 60^\circ$, i.e.

$$|G_{i,o}(j\omega_c)| = 1 \quad (3.38)$$

$$\arg(G_{i,o}(j\omega_c)) = -\frac{2\pi}{3} \quad (3.39)$$

The transfer function of the plant to be controlled is (3.31) for direct and (3.32) for quadrature axis current control respectively. The overall schematic for current control loop is shown in Fig 3.6.

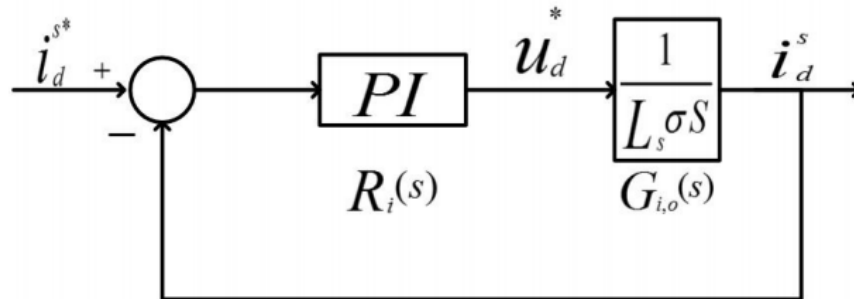


Fig 3.6: The block diagram of the direct axis current control

$$G_{i,o} = R_i(s)G_i(s) = \frac{K_p^i}{L_s\sigma T_i^i} \frac{1}{s^2} (1 + sT_i^i)$$

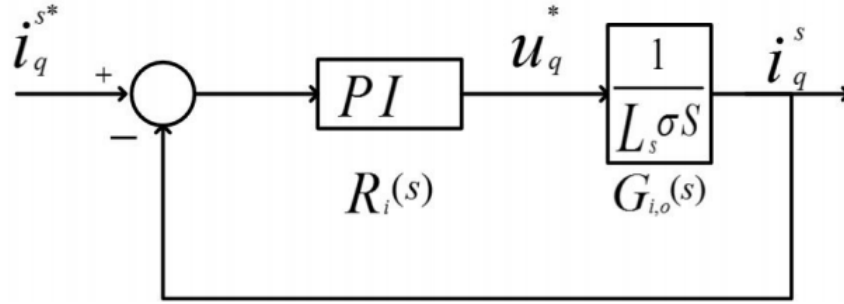


Fig 3.7: The block diagram of the quadrature axis current control

Where K_p^i and T_i^i are the corresponding K_p and T_i parameters for current PI Controller.

Applying the phase margin condition (3.39) of $G_{i,o}$ we have

$$\begin{aligned} \arg(G_{i,o}(j\omega_c)) &= \tan^{-1} \frac{\omega_c T_i^i}{1} - \pi \\ &= \tan^{-1}(\omega_c T_i^i) - \pi = -\frac{2\pi}{3} \end{aligned} \quad (3.40)$$

Therefore, the T_i^i value can be obtained from

Applying the magnitude condition (3.39) of $G_{i,o}$ and substituting T_i^i value, we get K_p^i .

$$\begin{aligned} G_{i,o}(j\omega) &= \frac{K_p^i}{L_s\sigma T_i^i} \frac{1}{\omega_c^2} \sqrt{1 + (\omega_c T_i^i)^2} = 1 \\ K_p^i &= \frac{L_s\sigma T_i^i \omega_c^2}{\sqrt{1 + (\omega_c T_i^i)^2}} \end{aligned} \quad (3.41)$$

Therefore, based on the calculated T_i^i and K_p^i values, we obtain K_i^i from

$$K_i^i = \frac{K_p^i}{T_i^i} \quad (3.42)$$

The closed loop transfer function can be obtained based on the open loop transfer function $G_{i,o}$, as follows

$$G_{i,c} = \frac{G_{i,o}}{1+G_{i,o}} = \frac{1+sT_i^i}{1+sT_i^i+s^2\frac{T_i^i\sigma L_s}{K_p^i}} \quad (3.43)$$

3.2.2 PI SPEED CONTROLLER DESIGN

In this section, we design the K_p^ω and K_i^ω values for the speed controller using symmetrical optimum method which guarantees the maximum phase margin. First, notice the equation (3.43) is a second-order system, we need to approximate it by simplified first-order transfer function. That significantly simplifies the speed controller design as follows [22].

$$G_{i,c}(s) = G_{i,sim}(s) = \frac{1}{1+\frac{s}{\omega_g}} \quad (3.44)$$

Where $\omega_g = \frac{1}{T_g}$

Since the magnitude of closed loop transfer function decreases by 20 dB/decade for high frequencies, the cut-off frequency of low pass filter can be determined easily. First the frequency ω_1 , is chosen as ten times the switching frequency:

$$\omega_1 = 10 \cdot f_s \cdot 2\pi \quad (3.45)$$

Then, the cutoff frequency ω_g of the simplified transfer function can be obtained by interpolating the Bode plot:

$$-20 \cdot \log\left(\frac{\omega_1}{\omega_g}\right) = |G_{i,c}(j\omega_1)| \quad (3.46)$$

Therefore, ω_g can be calculated from

$$\omega_g = 10^{\left[\log(\omega_1) - \frac{|G_{i,c}(j\omega_1)|}{20}\right]} \quad (3.47)$$

Therefore, the simplified transfer function (3.44) can be determined with the cutoff frequency ω_g . Based on (3.28), and the load equation

$$T_e - T_L = J \dot{\omega}_m \quad (3.48)$$

The open loop transfer function for speed control is given as follows

$$G_{\omega}(s) = G_{i,sim}(s) \frac{3}{2} \frac{P}{L_r} \frac{L_m}{L_r} \lambda_d^r \frac{1}{sJ} \quad (3.49)$$

Where P is the number of poles.

Now introducing the PI speed controller into the system, the open loop transfer function of the overall plant is shown below :

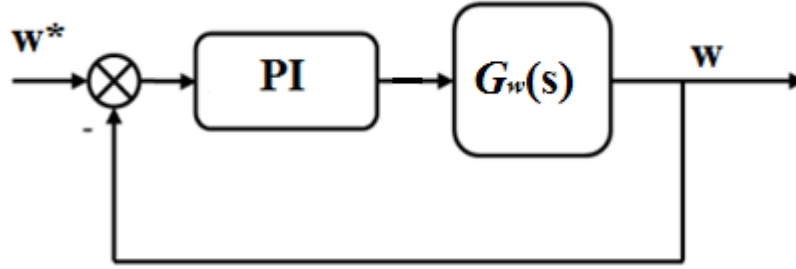


Fig 3.8: The block diagram of the speed control

$$\begin{aligned}
 G_{\omega,o}(s) &= R_{\omega}(s)G_{\omega}(s) \\
 &= K_p^{\omega} \left(1 + \frac{1}{sT_i^{\omega}}\right) \frac{1}{1 + \frac{s}{\omega_g}} \frac{3}{2} \frac{P}{L_r} \frac{L_m}{L_r} \lambda_d^r \frac{1}{sJ} \\
 &= K_p^{\omega} \left(1 + \frac{1}{sT_i^{\omega}}\right) \left(\frac{1}{s + \frac{s^2}{\omega_g}}\right) \frac{3PL_m\lambda_d^r}{4L_rJ} \\
 &= K_p^{\omega} \frac{3PL_m\lambda_d^r}{4L_rJ} \frac{1+sT_i^{\omega}}{sT_i^{\omega}(s+\frac{s^2}{\omega_g})} \quad (3.50)
 \end{aligned}$$

The symmetrical optimum method is used for determining the parameters of the PI speed controller. The method can produce the balance phase and magnitude characteristic of the open loop transfer function, by placing the crossover frequency precisely at the location where we can obtain the maximum phase margin. The slope of -20 dB/decade produced by PI controller becomes -40 dB/decade after the cutoff frequency ω_g of current control loop low-filter.

We introduce the factor α that relates the cross-over frequency ω_c and PI speed controller cutoff frequency ω_w with the first-order system cutoff frequency ω_g , where

$$\omega_c = \frac{1}{\alpha} \omega_g, \omega_w = \frac{1}{\alpha^2} \omega_g$$

On logarithmic scale ω_c is exactly the middle point between ω_w and ω_g . Applying these two conditions to the open loop transfer function, we have:

$$|(G_{w,o}(j\omega_c))| = \left| G_{w,o} \left(\frac{j\omega_g}{\alpha} \right) \right| = 1 \quad (3.51)$$

$$\arg(G_{w,o}(j\omega_c)) = \arg\left(G_{w,o} \left(\frac{j\omega_g}{\alpha} \right)\right) = -\frac{2\pi}{3} \quad (3.52)$$

Firstly, α is solved from the phase margin condition, i.e.

$$\begin{aligned} \arg(G_{w,o}(j\omega_c)) &= \arg(1 + j\omega_c T_i^w) - \arg(1 + j\omega_c T_g) - \pi \\ &= \tan^{-1}(\omega_c T_i^w) - \tan^{-1}(\omega_c T_g) - \pi \end{aligned} \quad (3.53)$$

Since $\omega_c = \frac{1}{\alpha} \omega_g = \frac{1}{\alpha T_g}$ and $T_i^w = \alpha^2 T_g$ we get,

$$\tan^{-1}(\alpha) - \tan^{-1}\left(\frac{1}{\alpha}\right) = \frac{\pi}{3} \quad (3.54)$$

Based on trigonometric rules, we can obtain the value of α . The controller parameter K_p^w can be determined by substituting α in the magnitude condition (3.51).

$$\left| G_{w,o} \left(\frac{j\omega_g}{\alpha} \right) \right| = \left| G_{w,o} \left(\frac{1}{j\alpha T_g} \right) \right| = K_p^\omega \frac{3PL_m \lambda_d^r}{4L_r J} T_g \sqrt{\frac{1 + \alpha^2}{1 + \frac{1}{\alpha^2}}} = 1$$

$$K_p^\omega = \frac{1}{\frac{3PL_m \lambda_d^r}{4L_r J} T_g \sqrt{\frac{1 + \alpha^2}{1 + \frac{1}{\alpha^2}}}} \quad (3.55)$$

Therefore, based on the calculated T_i^ω and K_p^ω value, we can obtain K_i^ω from

$$K_i^\omega = \frac{K_p^\omega}{T_i^\omega} \quad (3.56)$$

3.3 Simulation

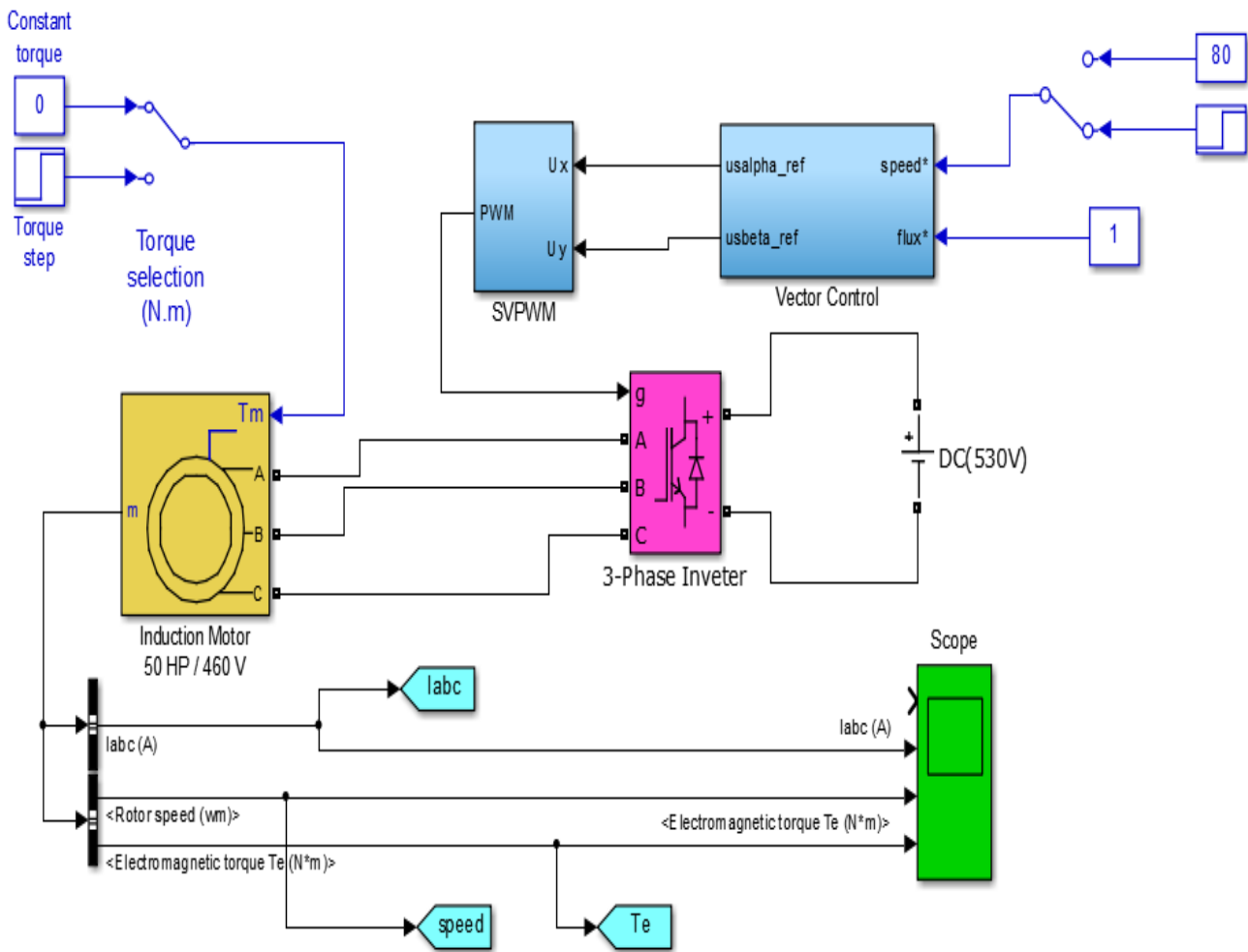


Fig 3.9: FOC Simulink Model

The proposed control system has been simulated using Matlab/Simulink, a sensorless induction motor drive simulation was setup.

The FOC model contains four main sub-blocks (Induction motor, 3-phase Inverter, SVPWM and vector control).

In order to generate the regulated voltage the reference values such as speed and flux are injected in the vector control sub block, also the actual speed and current values are used from the motor outputs.

In the SVPWM sub-block the regulated voltages are used to generate the six pwm to control the inverter.

The inverter drives the motor with the controlled abc voltage to reach the desired speed.

Scenario 1

The speed reference is set at 80 (rad/sec), at $t=1.5$ s the speed reference is set to 160 (rad/sec) and the load torque is set to 0 (no load).

The results are shown in Fig 3.10:

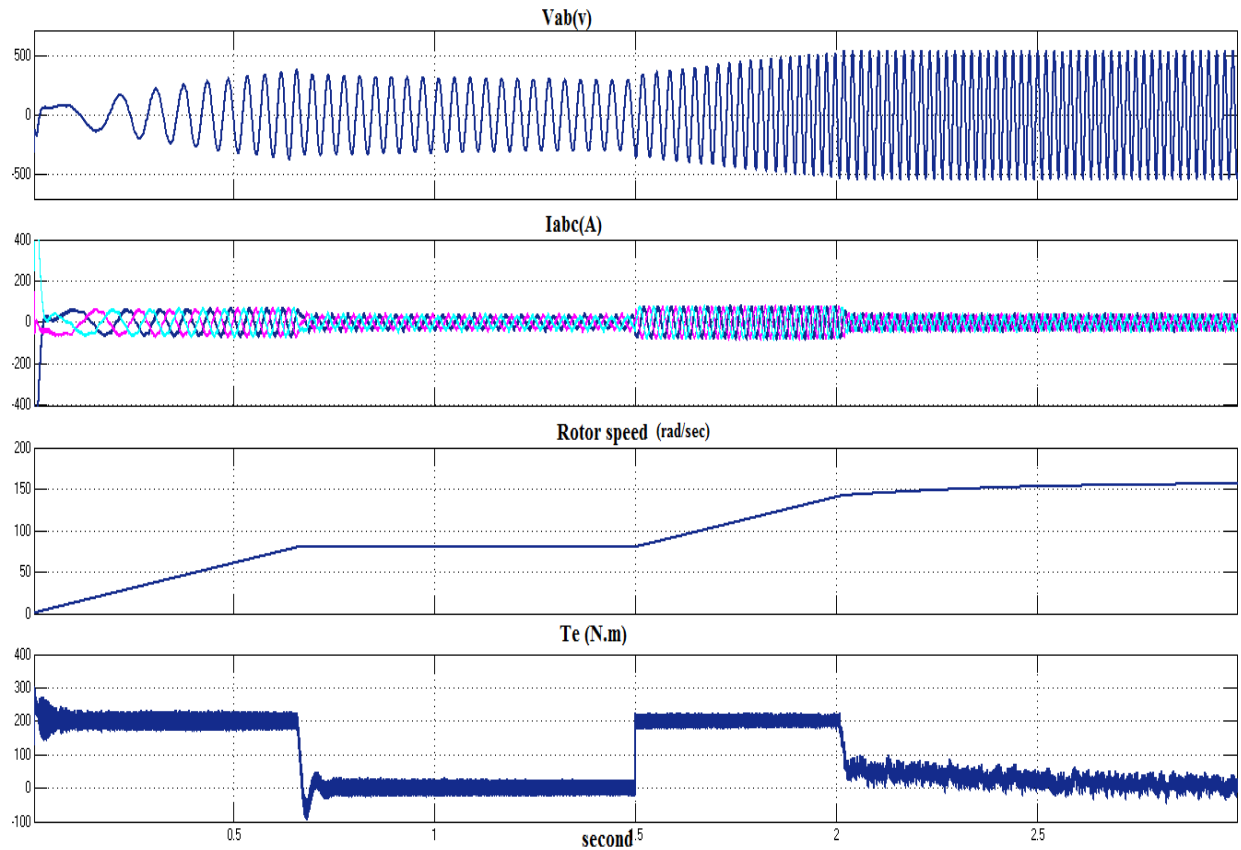


Fig 3.10: Test results for scenario 1.

First, it is important to analyze the starting performance. During this starting period, the electric motor needs to produce a relatively high torque in a very short time to accelerate itself. The investigation here is focused on speed response time and fluctuations.

For the torque responses, at first, a large torque is generated to start the motor. After reaching the target speed, the torque output follows the command closely.

Since the FOC is aimed for controlling the decoupled currents I_{qs} and I_{ds} of the system, so generally speaking, the currents are well regulated. It can be seen that, at the starting stage, three phase currents are constrained within -50 to +50 Amps. After that, the magnitude of the current is kept around 20 Amps.

A ramp signal is used to simulate the vehicle starting speed behavior, after the motor speed has reached the target value of 80 rad/sec, it was kept as a constant. At $t=1.5$ s, the speed is increased from 80 to 160 rad/sec.

Scenario 2

The speed reference is set at 80 rad/sec. The torque load is set to 0 (no load) at $t=1$ s the torque load is set to 50 N.m.

The results are shown in Fig 3.11:

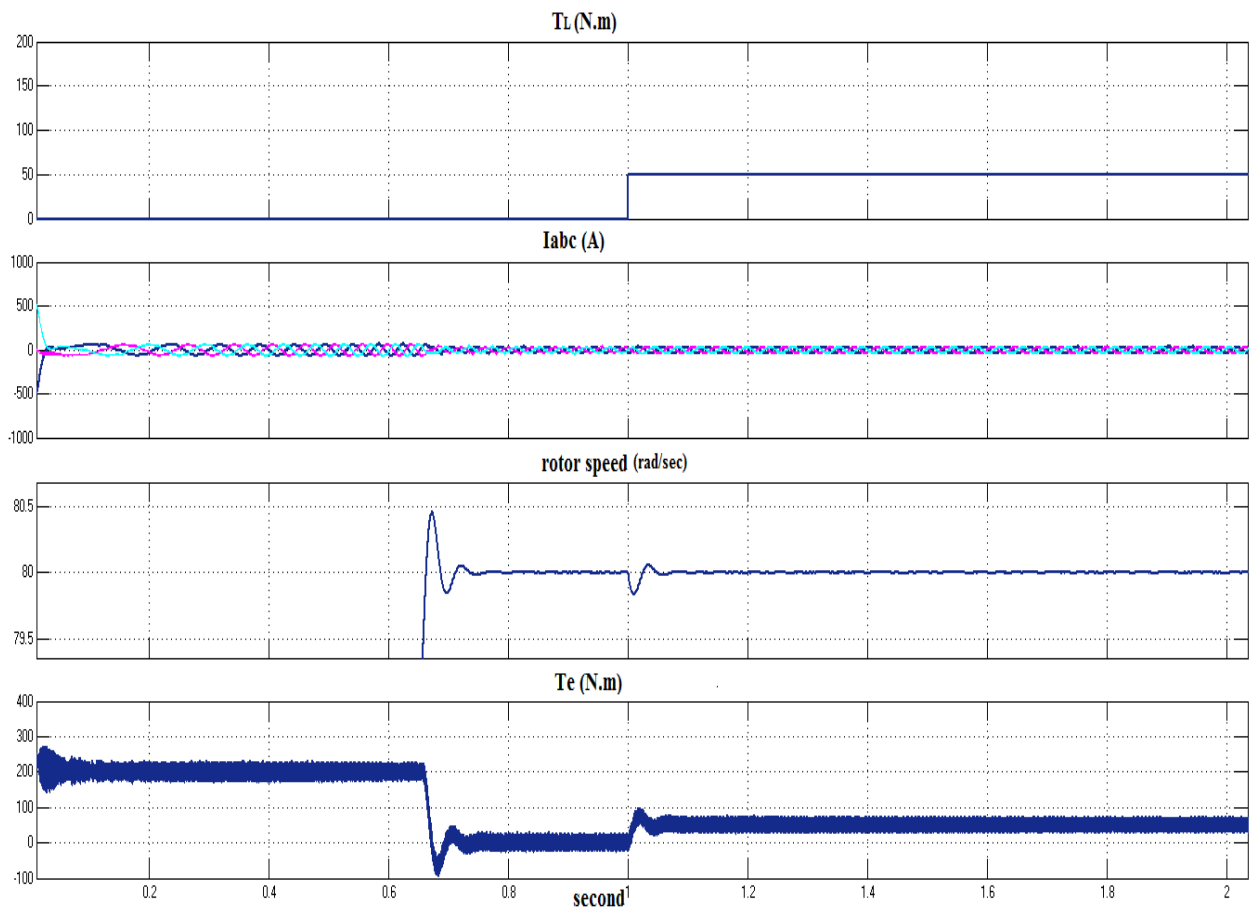


Fig 3.11: Test results for scenario 2

When the vehicle is running at a constant speed, the load on the motor can vary abruptly because of the change of the road conditions. In this scenario, the speed is kept constant all the time and load torque is varied.

For the torque responses, at first, a large torque is generated to start the motor. After reaching the target speed, the torque output follows the command closely during the constant speed

period. The load was changed at $t=1$ s from 0 Nm to 50 Nm, it can be seen that the load torque is suddenly changed, there is a small speed dip, but it is restored quickly.

From the zoomed pictures of speed response, we can see that at the time $t = 1$ s, the speed response of FOC follows the command very closely and the overshoot is almost 0.

From the zoomed picture of torque response, it can be seen clearly that the torque fluctuations of FOC are restrained within +20 and -20 (Nm).

Scenario 3

The speed reference is set at 80 rad/sec, at $t=1.5$ s the speed reference is set to 160 rad/sec.

The torque load is set to 0 (no load) at $t=1$ s the torque load is set to 50 N.m.

In this scenario we mixed the two previous scenarios. The results are shown in Fig 3.12:

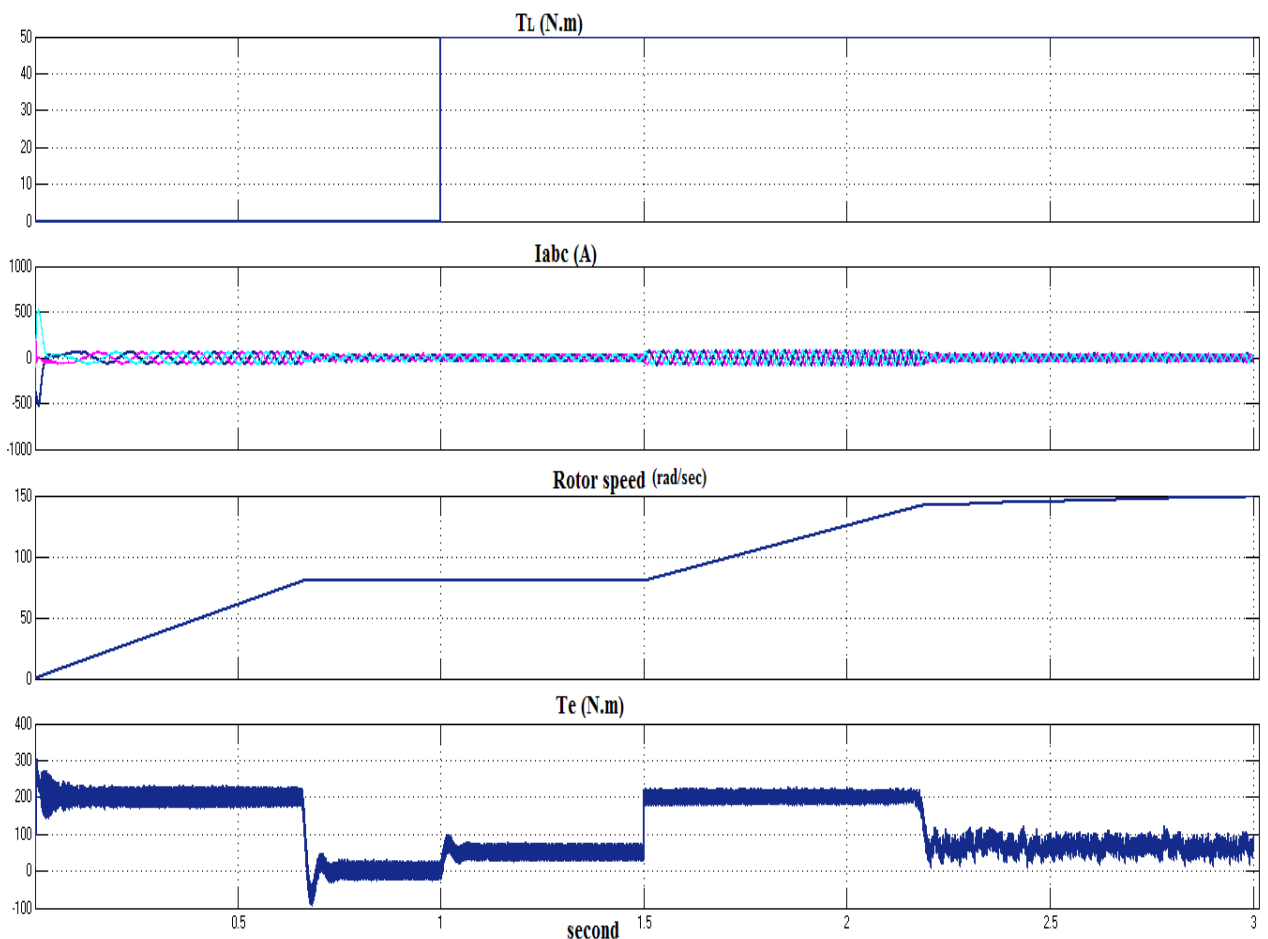


Fig 3.12: Test results for scenario 3.

3.4 Conclusion

In this chapter the concept and the model of field oriented control were presented. The feed-forward control method is designed for decoupling the torque and flux. The effectiveness of the proposed control scheme of induction motor control was demonstrated by computer simulations. The simulation results show the robustness and effectiveness of the designed controllers.

CHAPTER 4

DSP PROGRAMMING

4.1 Introduction

In order to complete this project successfully, we have two approaches that can be implemented similarly on the target hardware. Fig 4.1 shows the diagram representing the various steps involved in both the approaches. As seen from the figure, both the approaches produce the same result.

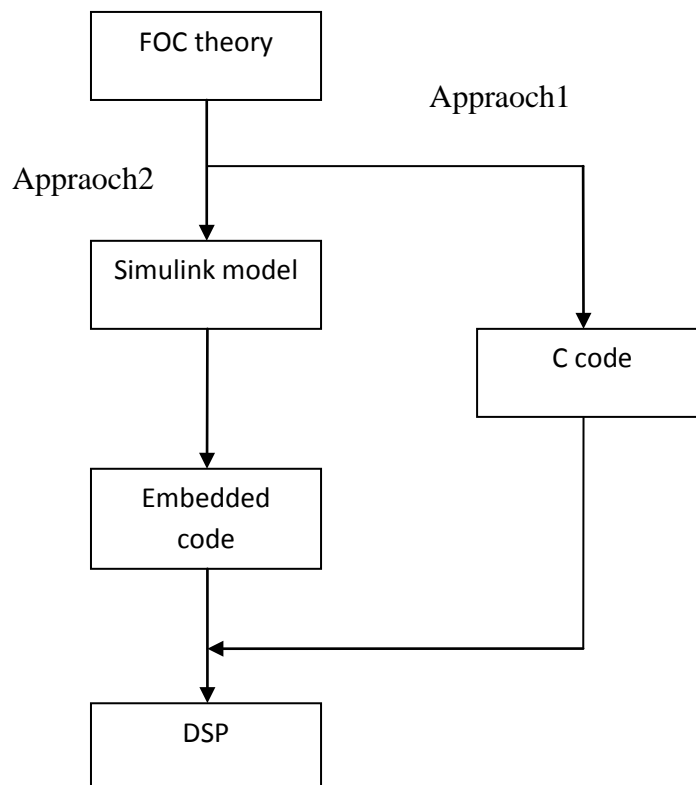


Fig 4.1: Illustration of two different approaches that can be used in the DSP project

4.1.1 Approach1

The Embedded Processors can be programmed using various languages. However, the most common language used to program embedded processors is C language. Fig. 4.2 shows that C language is used by more than a four-to-one margin over its nearest competitor, Assembly language.

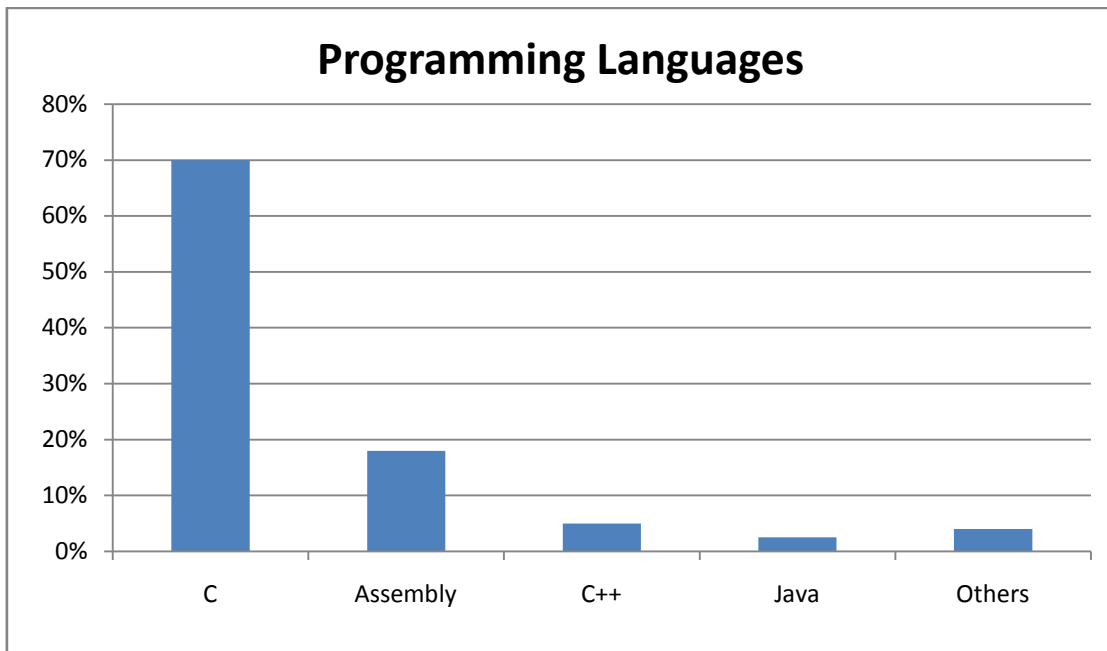


Fig 4.2: Programming Languages used in Embedded Designs

The reason that C language is used widely in programming embedded machines is that it is a medium level language, in contrast to other high level languages like JAVA or low languages like Assembly. C, with its medium level of complexity is understandable to humans, executes at a reasonably fast speed and usually allows programmers to exercise enough control over the working of the embedded processor. This balance between intelligibility and fundamental control make C language the prime choice for embedded processor programming. Sometimes, when additional control or an extremely fast execution speed is needed for a specific instruction, a few lines of Assembly language may be combined with the main C program [25]

4.1.2 Approach2

Simulink provides an interactive graphical environment and a customizable set of block libraries that let us design, simulate, implement, and test a variety of time-varying systems, including communications, controls, signal processing, video processing and image processing. Simulink offers the quickest way of developing your model in contrast to text-based programming language like C. Also, Simulink has integrated solvers.

In our project approach1 (C language) is used.

4.2 DSP Programming and CCS

In this section, an introduction to the DSP F28335 is briefly discussed which is followed by the modules description and also its features.

The PWM module plays an important role in this project because it is used to output the three-phase signals to the inverter, decide the control loop period and synchronize the ADC. This is the reason why more details are given to PWM module in this document.

The Code Composer Studio (CCS) is the Integrated Development Environment (IDE) for TI's microcontrollers. It has many extensive examples and example codes that might help any new user for a quick start of developing code [26].

4.2.1 Description of the F28335 DSP and Used Hardware.

The F28335 DSP consists of a 32-bit CPU and a single-precision 32-bit floating-point unit (FPU), which enables the floating-point computation to be performed in the hardware. Also the CPU of the F28335 has 8-stage pipeline structure, which makes the CPU able to execute eight instructions simultaneously on one system clock period. The 150MHz system clock is provided by an internal oscillator and a phase-locked loop (PLL) circuit. The oscillator generates 30MHz clock signal, which is increased to 150 MHz by the PLL circuit. The F28335 has independent logical memory spaces and separated memory buses for the program and the data as seen in Fig. 4.3. The memory bus consists of a program read bus, a data read bus and data write bus. The physical memory of the F28335 consists of 34Kx16 single-access random access memory (SARAM), a 256K x16 Flash, an 8K x 16 read-only memory (ROM), a 1K x 16 one-time programmable memory (OTP) and the registers. The ROM has been preprogrammed by the DSP manufacturer. The program existing in the ROM has a standard programming procedure for DSP booting as well as some optimized codes for the mathematical functions. The registers control the behavior of the DSP and each peripheral module. For the F28335, reading from or writing to registers applies the bit-field address structures. F28335 also has the feature of direct memory access (DMA). With the DMA bus, the data can be passed from one part of the DSP to the other part without the interaction of the CPU, which increases the data transmission speed. Since it is designed mainly for control applications like ours, the F28335 has plenty of peripheral circuits. For instance, in our project, the motor vector control uses ADC module, the PWM module, the encoder and other modules. Also there are different communications modules that could be achieved with the

F28335, which are controller area network (CAN) module, the serial communication interface (SCI) module, the serial peripheral interface (SPI), the multichannel buffered serial port (McBSP) module and the inter-integrated circuit (I2C) module. F28335, also, supports 96 interrupts. These interrupts are governed by the peripheral interrupt expansion (PIE) block, which helps in enabling or disabling the interrupts, decide the interrupt priorities and inform the CPU of the occurrence of a new interrupt. The F28335 has the joint test action group (JTAG) interface, which helps us in real-time debugging. With the help of this JTAG, anyone can look and modify the contents of the memory and the registers without stopping the processor [23].

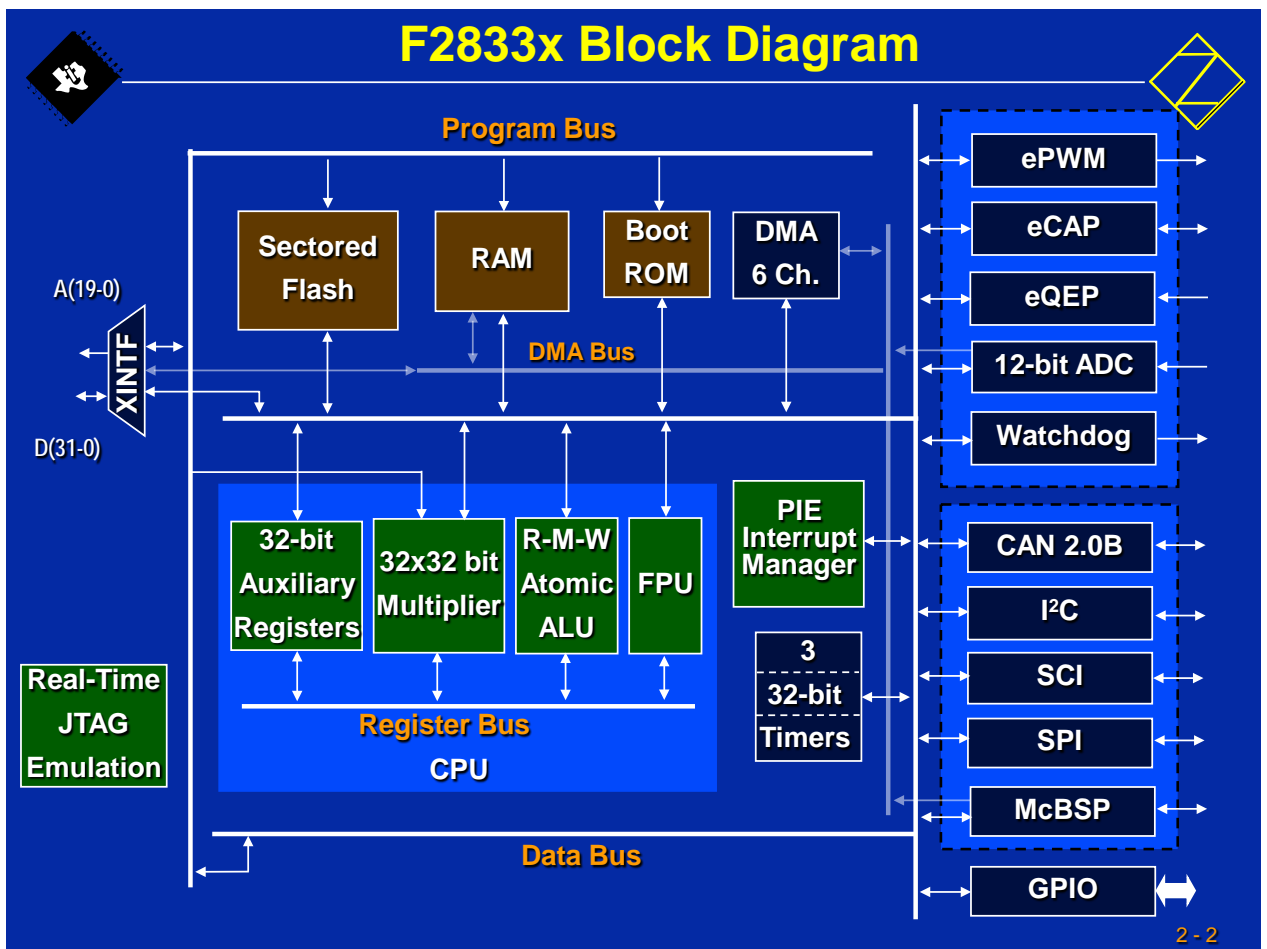


Fig 4.3: Block Diagram of F28335

4.2.2 FOC Implementation:

The F28335 DSP is used to read the feedback speed and the current signals, to implement the speed control algorithm, and to generate the gate signals based on the control algorithm for the inverter.



Fig 4.4: The used F28335 modules

The used modules of the F28335 are illustrated in Fig 4.4. The input channels related to the Analog-to-Digital Converter (ADC) are selected to read the two-phase currents (It is sufficient to take the measurements of two current phases because the three phase currents are balanced [$i_a(t) + i_b(t) + i_c(t) = 0$]). The QEP sensor is used to measure the feedback speed. The output pins PWM1 to PWM6 control the inverter.

The design of induction motor vector control is shown in Fig 4.5.

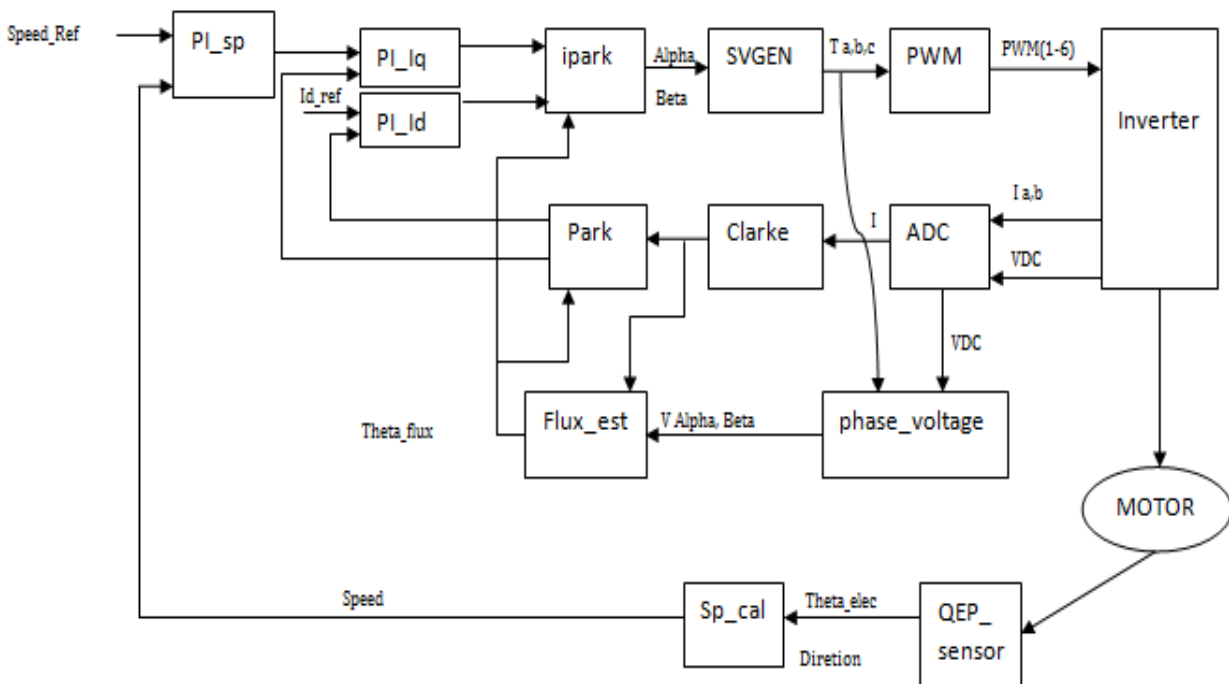


Fig 4.5: Design of vector control pwm for induction motor

The program, as shown in fig 4.6, starts with variables declarations, initializations, configuration of the used hardware in the DSP and the offset measurement.

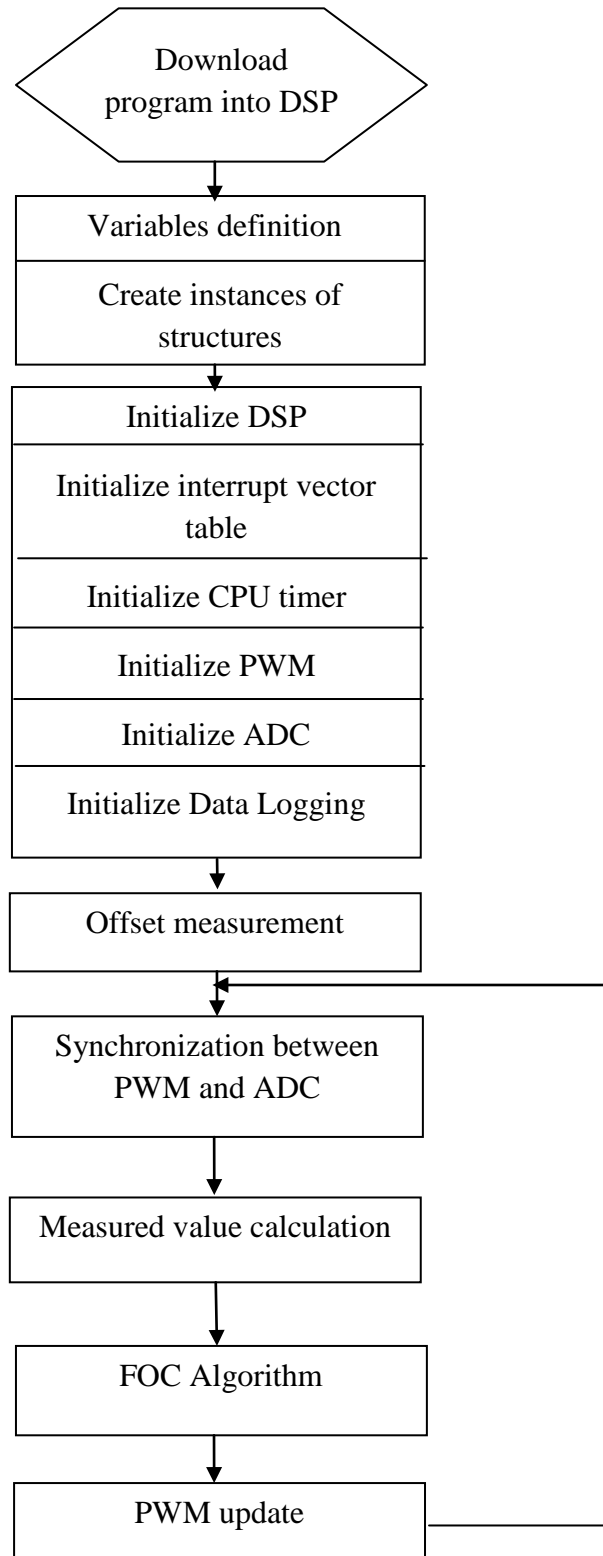


Fig 4.6: Flow chart of the DSPF28335 program

After the DSP is configured, the PWM sequence is started and the program enters in a loop. In this project, the control strategy is designed such that, the control loop is synchronized with the PWM carrier wave. Every start of PWM period will trigger an ADC sequence. The ADC sequence consists of eight channels, which are used to measure phase currents. At the end of ADC sequence, the program jumps into measuring the current and speed values, where the offset compensation is added. Following the measurement calculations, the vector control algorithm is executed. Finally, the PWM duty cycles are updated with the new calculated values and the program then waits for the next trigger from the PWM. The following paragraphs explains the different modules used in our project.

ADC Module

ADC module consists of 16 analog input channels, which are connected to an analog multiplexer (MUX). A channel to be sampled can be selected by sending its corresponding 4-bit address to the MUX. The relations between the channels and the 4-bit addresses are listed in Table 4.1. From Fig 4.7, we can observe that the analog MUX consists of two 8-to-1 multiplexers, MUX1 and MUX2. The outputs from the two multiplexers are connected to two sample-and-hold (S/H) circuits, S/H-A and S/H-B, respectively. The two S/H circuits allow the possibility of sampling two analog signals simultaneously. After the S/H circuit has done the sampling, the analog-to-digital converter begins to transfer the analog signal held on the S/H circuit into a 12-bit binary number. The entire functioning of the ADC is governed by the ADC control registers. There are sequencer blocks in the ADC, Sequencer1 and Sequencer2. These two sequencers are then merged into a cascaded sequencer, where maximum sixteen channels can be selected. These two sequencers are placed in an appropriate order and in each sequencer maximum of eight channels can be selected.

In order to start an ADC sequence a start-of-conversion (SOC) signal is needed. For sequencer1 and sequencer2 or cascaded sequencer, the SOC signal could be given by the PWM module or the bit S/W, which can be set or reset in the software. Sequencer1 and the cascaded sequencer could also be triggered by an external signal through a general-purpose input/output (GPIO) pin. The ADC clock frequency decides the time to take for one conversion. The ADC clock is obtained by prescaling the system clock. This is done in default if you set the DSP as F28335. The total prescaling factor is equal to the product of the prescaling factors of the high-speed prescaler, the ADC clock prescaler and the extra

prescaler. The conversion results will be written into the result registers, through a result selection MUX. For each sequence, the result selection MUX will send the first conversion result to Result Reg0, the second one to Result Reg1 and so on, until this sequence is finished. Whenever the complex conversions occur like analog-to-digital conversions are needed in two different moments during one control, the dual-sequence mode can be applied. In this project, all the analog signals are sampled at the same moment and they are less than eight signals.

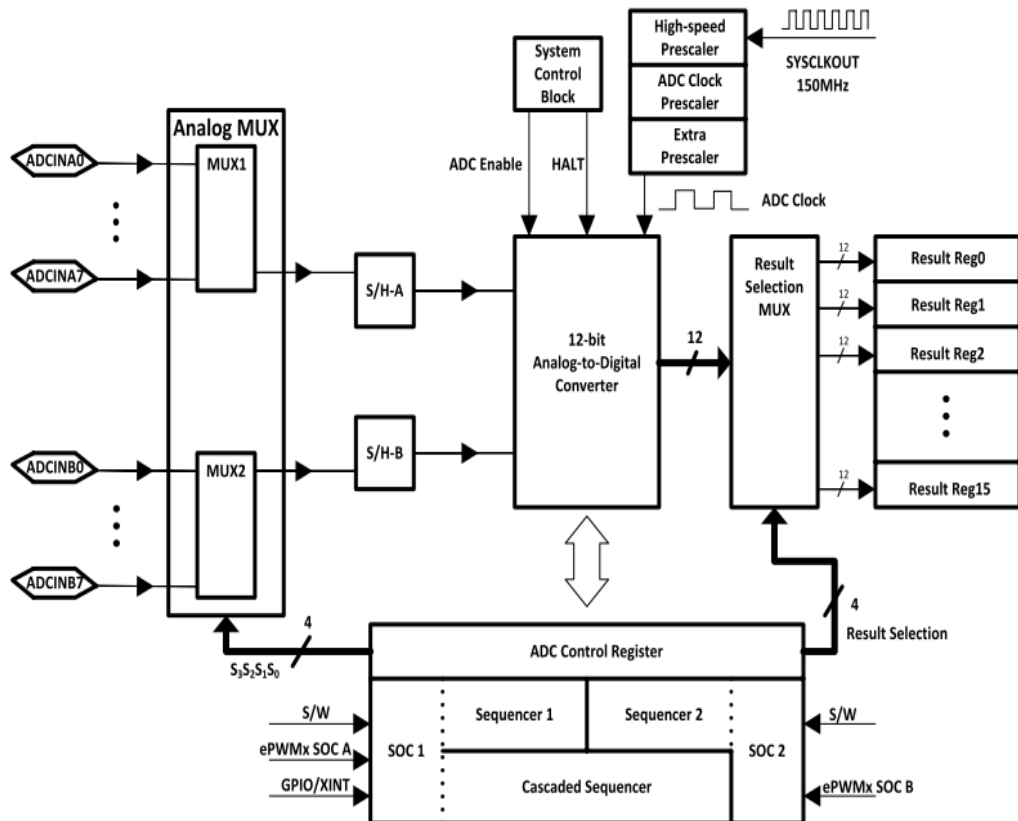


Fig 4.7: Block diagram of ADC module.

Table 4.1: ADC input channels and corresponding addresses.

Input channel	Address $S_3 S_2 S_1 S_0$	Input channel	Address $S_3 S_2 S_1 S_0$
ADCINA0	0000b	ADCINB0	1000b
ADCINA1	0001b	ADCINB1	1001b
ADCINA2	0010b	ADCINB2	1010b
ADCINA3	0011b	ADCINB3	1011b
ADCINA4	0100b	ADCINB4	1100b
ADCINA5	0101b	ADCINB5	1101b
ADCINA6	0110b	ADCINB6	1110b
ADCINA7	0111b	ADCINB7	1111b

Due to this, one sequence of conversion per control loop is enough. Sometimes it is required that all the analog signals are sampled at exactly when the PWM carrier wave reaches its peak. But since there are only two S/H circuits, in the practical implementation, the two phase currents phase A and phase B are sampled firstly and then the other parameters are sampled. The sampling mode of the ADC module should be simultaneous. The ADC clock frequency is better to be high, from the point of conversion speed. But too high ADC clock frequency might cause some non-linearity to the conversion results [27]. So 12.5MHz, the highest ADC clock frequency is recommended and is being set in this project. Another issue that might be noticed is the width of the sampling window, which is defined as the number of clocks that the S/H circuit spends on sampling the signal. For the signals that change very slowly, a wider sampling window might work perfectly bringing the advantage of removing the noise by averaging the input signal. But in this project, since the currents change very fast, wide sampling does not work; instead smallest sampling window of one ADC clock is applied. Then the ADC module should work in start/stop mode, which means that the conversion is started by the SOC signal and stops when the sequence is finished, waiting for the next SOC signal. The SOC signal is triggered by the PWM module. Finally, an interrupt service routine has to be generated by the ADC, once the sequence is finished. The vector control algorithm will be executed in the Interrupt Service Routines (ISR). The block diagram based on the ADC module configurations is shown in Fig 4.8.

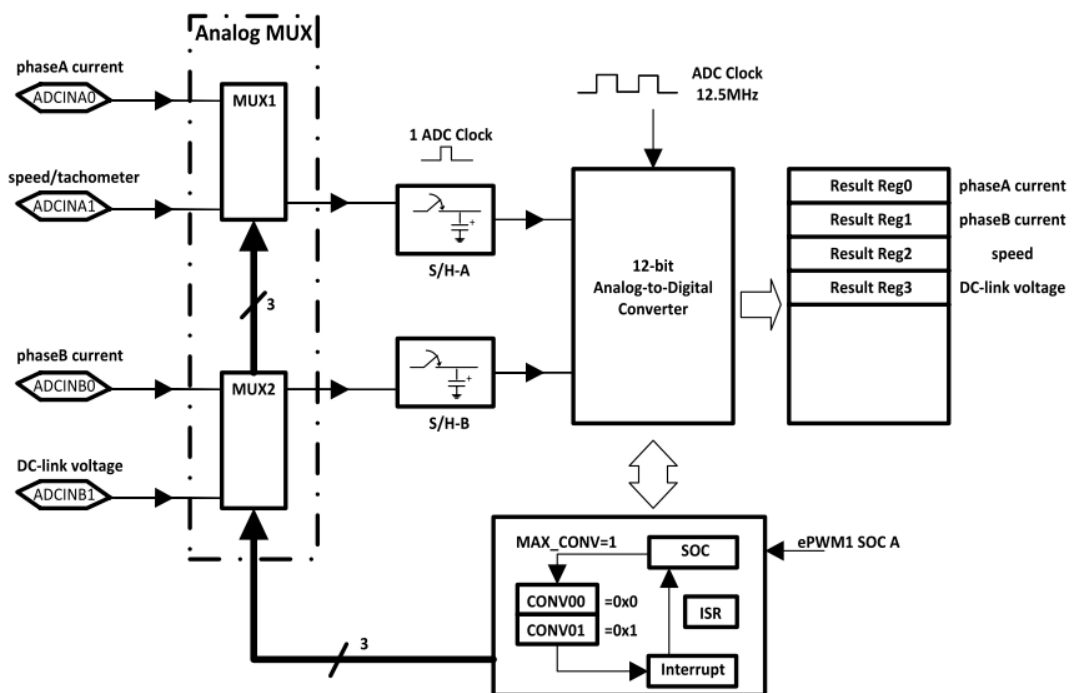


Fig 4.8: ADC module configuration.

PWM module

There are six independent enhanced PWM (ePWM) modules in the F28335 DSP. The enhanced PWM means that it can generate complex PWM waveform with the least CPU resources occupied [28]. Each of the ePWM modules has two output channels: ePWMxA and ePWMxB belonging to the ePWMx module. Each ePWM module contains seven submodules, which can realize different functions in the generation of PWM waveforms. They are time-base (TB) submodule, counter-compare (CC) submodule, action-qualifier (AQ) submodule, dead-band (DB) submodule, PWM- chopper (PC) submodule, trip zone (TZ) submodule and event-trigger (ET) submodule. The Fig 4.9 shows the complete structure of a single ePWM module with each submodule. In this project, not all but some of them are used for various accomplishments. The following sections will briefly describe the ePWM modules individually to get a clear idea on how the ePWM operates.

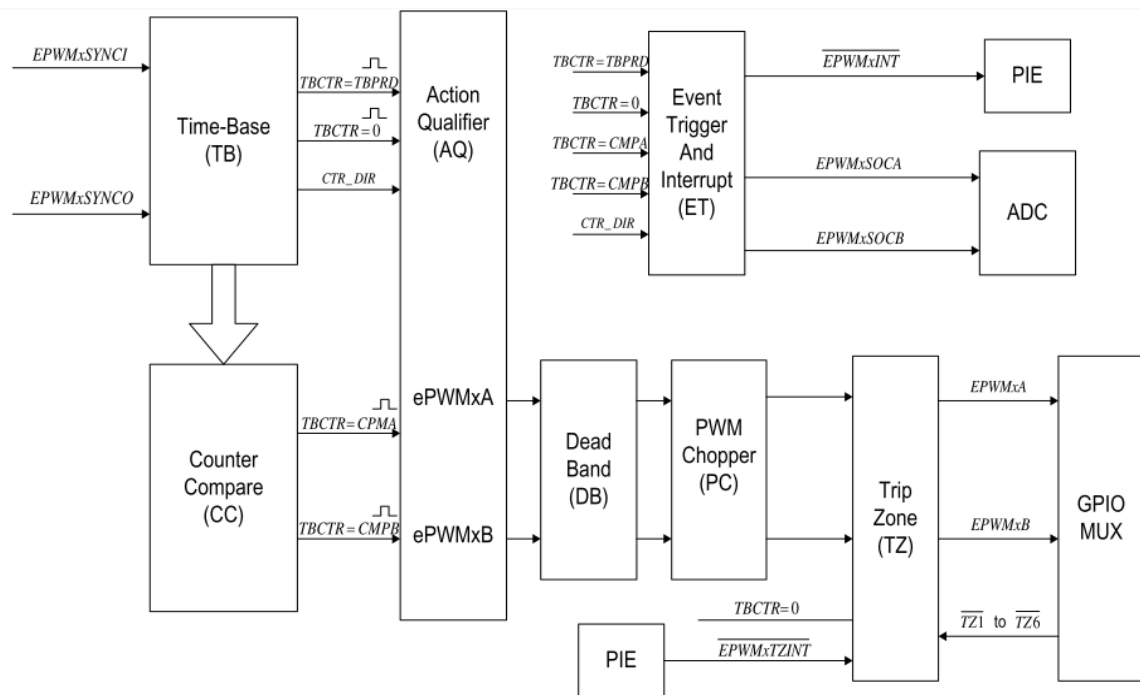


Fig 4.9: The sub-modules of each ePWM module

Time-base sub-module

The function of time-base module is to take charge of the event timing for its own ePWM module. The structure and block diagram of the time-base sub-module containing registers is shown in Fig 4.10. The main function of the time-base sub-module is to find the PWM time-base block relative to the system clock. The PWM time-base clock is to regulate the timing of all the events in the PWM module. The system clock period is defined as

$T_{SY_SCLKOUT}$ and the time-base clock is defined as T_{TBCLK} . The time-base clock period can be scaled to many times the system clock period as:

$$T_{TBCLK} = T_{SY_SCLKOUT} \times CLKDIV \times HSP\ CLKDIV \quad (4.1)$$

Where $CLKDIV$ and $HSP\ CLKDIV$ are bits in the time-base control register (TBCTL) help to set the time-base clock pre-scale.

The time-base sub-module is also used to specify the period of the time-base counter (TBCTR) depending in which mode it is operating. There are three modes of operation for the time-base sub-module, which can be selected in time-base control register (TBCTL), namely up-count mode, down-count mode and up-down mode. In the first mode and the second mode, TBCTR always keep incrementing or decrementing all the time giving a saw tooth carrier wave. But the third one i.e. up-down mode, the TBCTR increments in the first half of the PWM period and then decrements the second half part of the PWM period giving a triangular carrier wave. The main difference of the up-down mode is that in one period the counter changes in a symmetrical fashion, where the corresponding movement to the PWM carrier peak time is easily found. The peak time of the PWM carrier wave has to be known for signal sampling and that is the reason why up-down count mode is used in this project. To obtain the desired PWM frequency, the value in time-base period register (TBPRD) is supposed to be determined. For up-down-count mode, the relation between time-base period and PWM frequency can be written as:

$$T_{PWM} = 2 \times T_{BPRD} \times T_{TBCLK} \quad (4.2)$$

$$f_{PWM} = 1/(T_{PWM}) \quad (4.3)$$

Where T_{PWM} is PWM period and T_{TBCLK} is time-base clock period. From the above relations, the value in the time-base period register can be determined as follows

$$T_{BPRD} = \frac{f_{SY_SCLKOUT}}{2 * f_{PWM} * CLKDIV * HSPCLKDIV} \quad (4.4)$$

Therefore the only parameters that are known to compute T_{BPRD} are DSP system clock frequency and the desired PWM frequency. The parameters that have been used in this project for the configuration of DSP are PWM frequency of 10 kHz and the system clock frequency of the DSP F28335 is 150MHz. The values for $CLKDIV$ and $HSPCLKDIV$, used in this project are respectively 1 and 1 for convenience. From the above equation, the value set in the time-base period register can be calculated directly as shown below.

$$T_{BPRD} = \frac{150M}{2*10K*1*1} = 7500 \quad (4.5)$$

Besides, synchronization between different ePWM modules can also be realized in the time-base submodules. The three-phase PWM is used to produce a three-phase alternating voltage; hence the synchronization between the three-phase PWM signals is very important. Each ePWM module has two signals for synchronization between different ePWM modules. One is synchronization input EPWMxSYNCI and second is synchronization output EPWMxSYNCO. The Fig 4.11 shows time-base counter synchronization scheme for F28335. It can be seen that the PWM modules are connected in series with the synchronization output EPWMxSYNCO of the previous one fed onto the synchronization input EPWMxSYNCI of the next one. Only the input synchronization for the first ePWM module is taken from an external pin. For each ePWM module, once a pulse from the synchronization input is detected, the value in the time-base phase register (TBPHS) will be loaded into time-base counter (TBCTR), where time-base phase register (TBPHS) will be loaded into time-base register (TBPHS) is used to store the time-base counter (TBCTR) phase value of the ePWM module with respect to the time-base of its synchronization input signal. As we know that the inverter output are three phase voltages which are leading or lagging each other by 120, this is not going to show up in the project i.e. the three PWM signals have the same phase at any moment. The ePWM module ePWM1, ePWM2 and ePWM3 are selected for the three-phase PWM generation. Hence the time-base phase register (TBPHS) for the ePWM modules are assigned the value of 0. It means that there is no phase shift between the output signal ePWM1A, ePWM2A and ePWM3A. To synchronize between different ePWM modules, the synchronization output select bit (SYNCOSEL) in the time base control register (TBCTL) is supposed to be configured. ePWM1 is defined as the master phase to generate a synchronization output EPWM1SYNCO pulse each time its time-base counter (TBCTR) equals zero, while ePWM2 is defined as a slave phase whose synchronization input EPWM2SYNCI signal is enabled. Meanwhile, ePWM2s synchronization output EPWM2SYNCO signal is set equal to its synchronization input EPWM2SYNCi signal to drive it into ePWM3 unit. Except ePWM1, the other modules ePWM2 and ePWM3 have to load the time-base counter (TBCTR) with the time-base phase register (TBPHS) when synchronization input EPWMxSYNCI pulse appears.

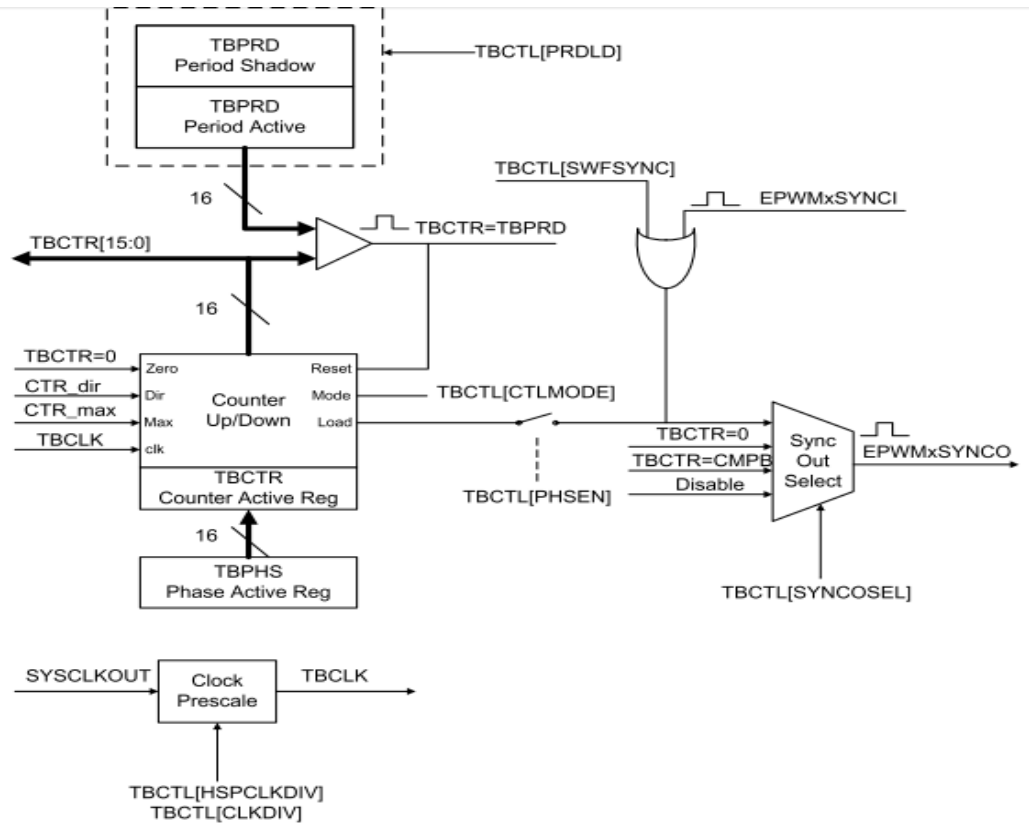


Fig 4.10: Time-base submodule structure in each ePWM module.

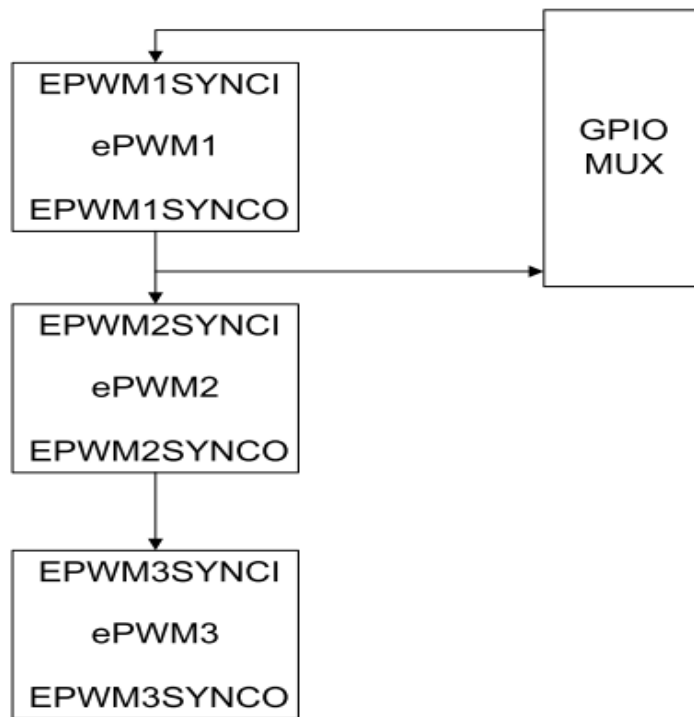


Fig 4.11: Time base counter synchronization scheme for F28335

Counter-compare sub-module

More practically approaching the things, the PWM waveform generation is mainly achieved by the comparison between a counter (TBCTR) value (carrier wave) and a set-point (reference wave) which is stored in counter-compare register. Fig 4.12 shows the way to generate a PWM waveform. In the PWM waveform generation process, the counter-compare submodule (CC) takes the part of event generation. In counter-compare submodule, there are two counter-compare registers: counter-compare A register (CMPA) and the counter-compare B register (CMPB) to store the values which are used to compare values against time-base counter (TBCTR) submodule continuously. The time-base counter (TBCTR) is treated as the input while the generated event $TBCTR = CMPA$ or $TBCTR = CMPB$ is the expected output. The Fig 4.12 shows the way it is done.

In this project whenever the carrier wave hits the counter-compare (CMPA) value on the rise, the ePWMxA is set to on and whenever the carrier ePWMxA hits the counter-compare (CMPA) value on the down-count, ePWMxA is set to off. This process is explained in action qualifier submodule.

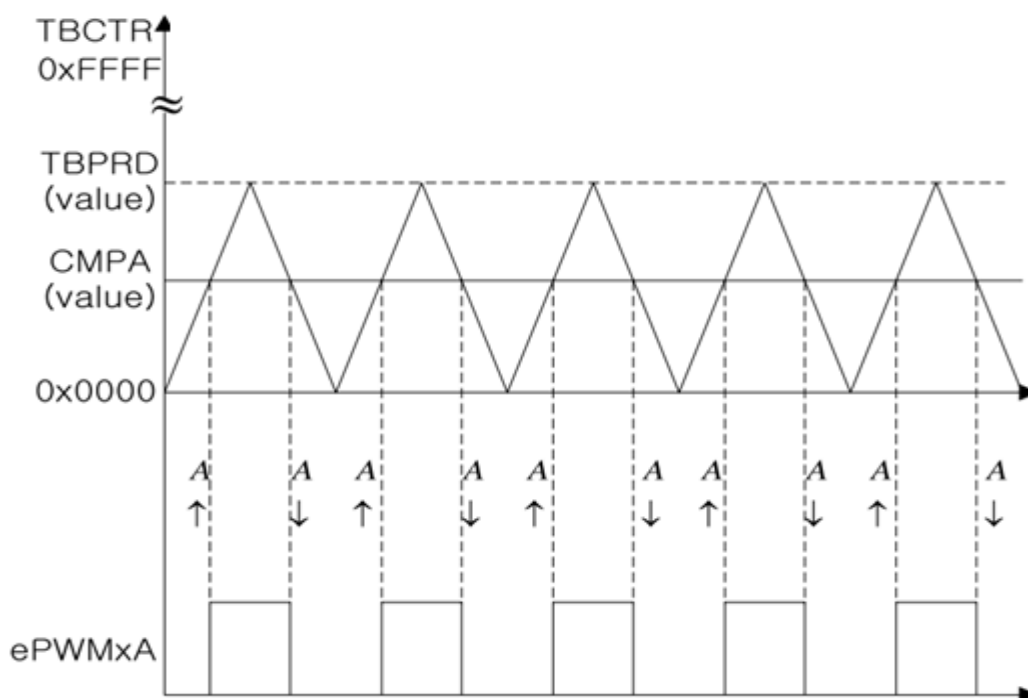


Fig 4.12: Counter-compare event, up-down counter mode

Action Qualifier sub-module

The action qualifier sub-module takes action whenever the generated events from the previous sub-modules are available. The previous sub-modules that have to generate events are time-base sub-module and counter-compare sub-module and hence these two sub-module events are the inputs to the action qualifier sub-module. The first one generates event $TBCTR = 0$ and $TBCTR = TBPRD$ while the second one produces $TBCTR = CMPA$ and $TBCTR = CMPB$. Having time-base counter (TBCTR) state incrementing or decrementing, the four events are expanded into eight event combinations. When a specified event takes place out of the eight events, there are four possible actions to be triggered whether to set it high, to low, to toggle and to do nothing, which can determine the shape of the PWM waveform. The action qualifier output control register (AQCTLA) is used to define the actions that should be taken if specified events occur. The conditions that are selected in this project to be configured such that when $TBCTR = CMPA$ and TBCTR is decrementing, ePWMxA is set to high; while TBCTR is incrementing, ePWMxA is cleared low. The arrows in the figure show the direction of time-base counter.

Dead band sub-module

Now we have the ePWMxA signal generated by the action qualifier sub-module. We also require a complimentary signal which is required to feed both the upper and lower IGBTs in the same leg of the inverter. The dead band sub-module can be used to take the ePWMxA as the signal source and then to produce the two mutually complimentary PWM outputs as ePWMxA and ePWMxB. The structure of dead-band sub-module is shown in Fig 4.13. The function of dead band sub-module depends on the six switches present in it. Different combinations of the switches generate different modes for signal pairs. Since there are six switches, many combinations can be produced. But in this project, we don't use many of them. The reason behind inserting the dead band into the ideal PWM waveform is to avoid the two IGBTs on the same bridge leg of the inverter turned on simultaneously. Therefore operating mode Active High Complementary (AHC) is selected as the desired one for a pair of power switches in one phase of a 3-phase motor control system, which can be achieved by setting the states of the switches in Fig 4.13, which can be configured in dead band control register (DBCTL). In Fig 4.13, a rising edges delay block and a falling edges delay block are used to insert a rising edge delay or a falling edge delay into the original PWM output. With the switch S4 and S5 set to 0, ePWMxA is chosen as the input source for both output A and

B. By setting switch S2 to 0 and S1 to 1, a rising edge delay is inserted into the original ePWMxA signal; by setting switch S3 and S0 to 1, ePWMxA signal is reversed with a falling edge delay added, which is output as ePWMxB signal. The generated PWM signal in Active High Complimentary mode is shown in Fig 4.14. It can be observed that there is an extremely short period of each PWM period, when both outputs of the ePWMx module are cleared, which avoids the mutually complimentary PWM signals are set high at the same time.

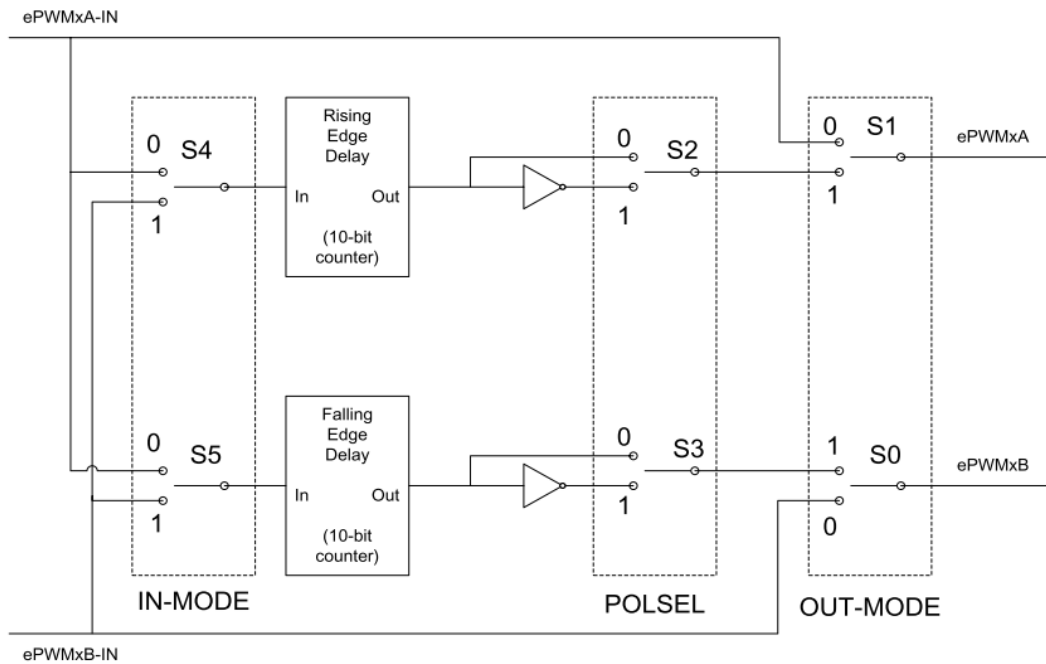


Fig 4.13: Block diagram of Dead band sub-module

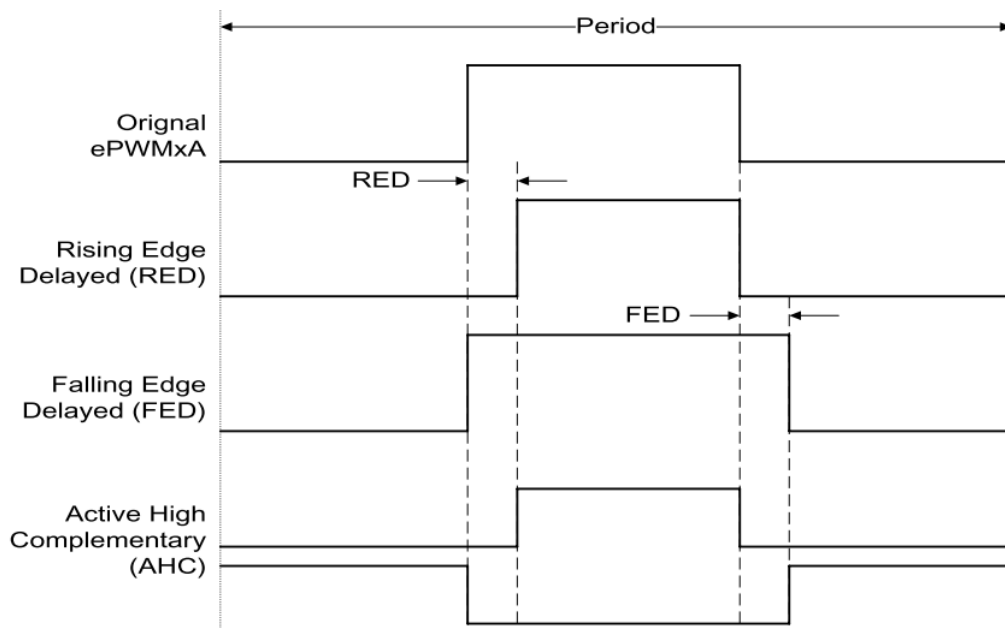


Fig 4.14: Waveform of PWM with dead band inserted

Event Trigger sub-module

The occurrence of events of ADC and PWM should be such that the PWM output should trigger the ADC start of conversion. But sometimes in a sampling period, the ADC start of conversion is executed first, and then the sampled data is used to calculate the PWM output. This shouldn't happen which might return in wrong results. Therefore ADC and PWM signals should be synchronized to function in the same pace. The event trigger sub-module in ePWM is to issue interrupt request or ADC conversion after receiving event inputs. In order to avoid aliasing from current ripple, the carrier wave peaks are always chosen as the sampling time instants. Both $TBCTR = 0$ and $TBCTR = TBPRD$ can meet this requirement and sampling. In this project, $TBCTR = 0$ is defined as the event that triggers ADC start of conversion by EPWMxSOCA pulse.

Duty cycle calculation

The most important part of the PWM generation is the duty cycle. The value entered in the counter-compare register corresponds to the duty cycle of the PWM period. So the counter-compare event register (CMPA) needs to be updated once in each PWM period to generate the PWM wave with varying duty cycle. The relation between the values set in CMPA register and PWM duty cycle can be written as:

$$CMP A = T BPRD \times (1 - T) \quad (4.6)$$

All the submodule roles are introduced in previous sections. The specific output value of the inverter should be equal to the digital signal given by the DSP, at any point of time. For instance, let us take an extreme situation case, phase A. The output voltage for phase A is controlled by switch S1 and S4 and the PWM signals imposed on S1 and S4 are mutually complimentary. The V_{dc} is defined as the DC link voltage for the inverter. During a sampling period of the PWM, the switch S1 is turned on and switch S4 is turned off for the same period. It also can be said in this way that, the duty cycle of the PWM wave fed to switch S1 is 100 percent, the output voltage of phase A should be $+V_{dc}/2$; on the other side, if the switch stays off and switch S4 is turned on for the whole cycle, the duty cycle for switch S1 is 0 percent, the output voltage of phase A turns to be $-V_{dc}/2$. And if both the switches are on for one half of the cycle period, the average voltage of phase A is supposed to be 0. From the principle of PWM, as the carrier wave of the modulation is triangular wave, from the basic geometrical knowledge it can be found that the relation between the output phase voltage

from the inverter and the corresponding PWM duty cycle is linear. In general, if the PWM duty cycle stands at any one point in the range from 0 to 1, the output voltage for phase A can be written as:

$$V_a = \frac{V_{dc}}{2} * T_a + \left(\frac{-V_{dc}}{2}\right) * (1 - T_a) \quad (4.7)$$

Where T_a is denoted as the duty cycle for the upper IGBT of the bridge leg connected to phase A. From the above relation, the duty cycle can be written as

$$T_a = \frac{V_a + \frac{V_{dc}}{2}}{V_{dc}} \quad (4.8)$$

The complimentary PWM waveform ePWMxB for the lower IGBT on the bridge leg can be generated by reversing ePWMxA in the dead band submodule. Hence only one counter-compare register (CMPA) is required for the generation of one pair of PWM outputs on the same bridge leg. From the above relations, the value set in CMPA can be easily calculated. This process applies to other two phases. As a result, the duty cycles for three phases can be derived as

$$CMPA_a = TBPRT_a \left(0.5 - \frac{V_a}{V_{dc}}\right) \quad (4.9)$$

$$CMPA_b = TBPRT_b \left(0.5 - \frac{V_b}{V_{dc}}\right) \quad (4.10)$$

$$CMPA_c = TBPRT_c \left(0.5 - \frac{V_c}{V_{dc}}\right) \quad (4.11)$$

The subscript implies the phase that the register values belong to.

Encoder Module

The enhanced quadrature encoder pulse (eQEP) module of the F28335 is used to process the digital signal from the encoder built on top of the motor [29]. There are four different modes in which the quadrature module is able to run. They are quadrature mode, direct count mode, up count and down count mode. In quadrature mode, the eQEP module receives two square wave signals from the encoder. These two square wave signals (A and B) have 90° phase shift with respect to each other, which can be used to determine the rotation direction. If square wave A is leading with respect to square wave B, then the rotation is said to be in clockwise direction and on the other side, if the square B is leading with respect to

square wave A, then the rotation is said to be in anti-clockwise direction. In direct-count mode, one square wave signal and one direction signal are sent to the eQEP module. The counter in the module will increase or decrease depending on the direction. For both modes, an index pulse signal is used to determine the absolute position of the encoder. The operating mode of the eQEP module is selected by the type of encoder. As the incremental encoder is used in this project outputs the quadrature signals, the eQEP module is set to be working in quadrature-count mode. The general block diagram of eQEP module is shown in Fig.4.15 which shows the functionality of the encoder.

Two quadrature waves are sent to the QA pin and QB pin of the decoder block as shown in the Fig.4.16. Every falling or rising edge of QA and QB will generate a clock signal (QCLK), which is passed to the position counter (QPOSCNT) from the decoder. The QPOSCNT will increase or decrease by 1 unit on each pulse of QCLK, depending on the direction signal (QDIR). If the rotation is clockwise, the QPOSCNT will increase by 1 unit for every pulse. If the rotation is anti-clockwise, the QPOSCNT will decrease by 1 unit for every pulse.

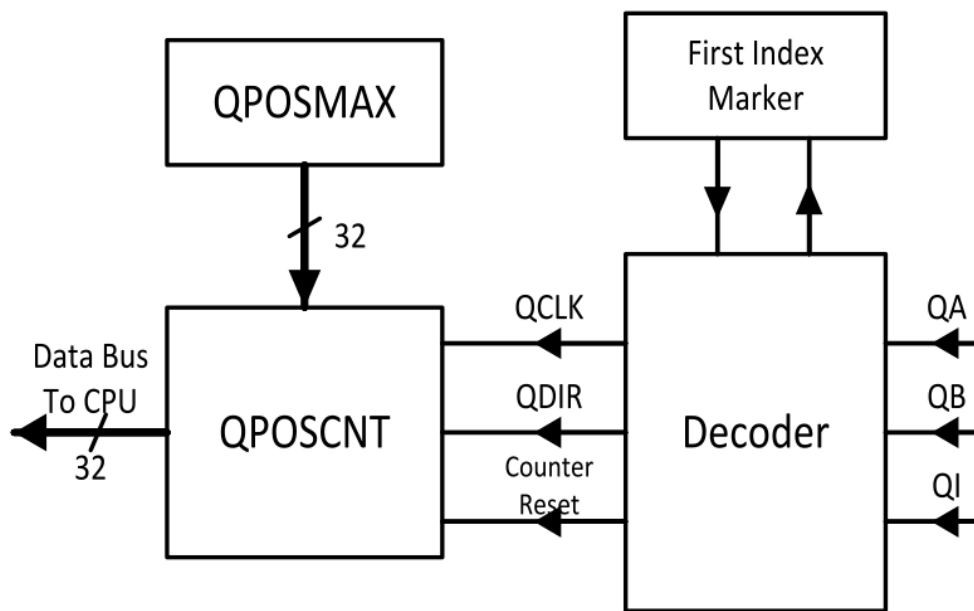


Fig 4.15: Block diagram of eQEP module

The following Table 4.2 show the details of the values of QDIR and QPOSCNT. Fig 4.16 shows the example waveform of the eQEP, which has the quadrature QA ,QB pins and index pulses. Every time the position counter (QPOSCNT) is reset by the index signal. When it

meets the index signal for the first time, the eQEP module will remember the present edge and the rotating direction in the first index marker register.

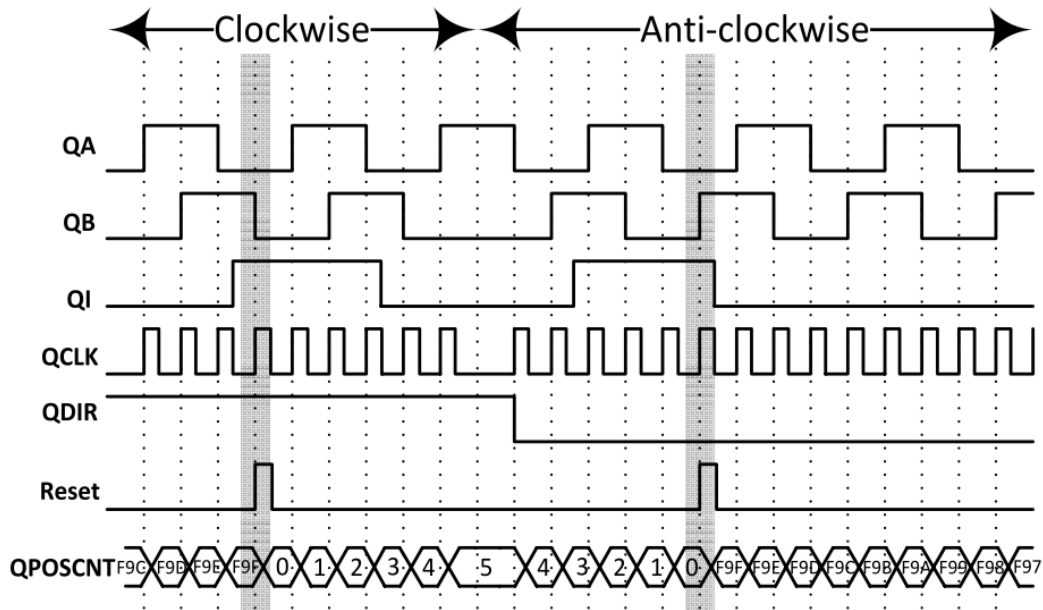


Fig 4.16: Example waveforms of the eQEP.

For instance, if the first counter reset happens on the falling edge of QB during the clockwise direction, then all the later results must be aligned with the falling edge of QB for the clockwise direction and with the rising edge of QB for the anti-clockwise direction. The position counter can be reset by the overflow or underflow of itself. For underflow the limiting value is zero. For the overflow, the upper limiting value is QPOSMAX, which is the value stored in the QPOSMAX register. for an incremental quadrature encoder with 1000 lines, the QPOSMAX should be

$$1000 \times 4 - 1 = 3999 = 0xF9F.$$

If you do not set the underflow or overflow, the counter is automatically reset to 0 during the clockwise rotation and reset to QPOSMAX during the anti-clockwise rotation. If the period of the vector control loop is set to t , then the rotating speed of the encoder can be calculated as

$$\text{Speed} = \frac{1s}{t} * 60rpm \quad (4.12)$$

Table 4.2: Encoder Truth table

Previous edge	Present edge	QDIR	QPOSCNT
QA↑	QB↑	1	increment
	QB↓	0	decrement
	QA↓	TOGGLE	increment or decrement
QA↓	QB↓	1	increment
	QB↑	0	decrement
	QA↑	TOGGLE	increment or decrement
QB↑	QA↑	0	decrement
	QA↓	1	increment
	QB↓	TOGGLE	increment or decrement
QB↓	QA↓	0	decrement
	QA↑	1	increment
	QB↑	TOGGLE	increment or decrement

This condition applies if the encoder rotates one revolution during one control loop period.

Offset Measurement

Generally, both the current and speed measurements contain a small offset, which is due to the presence of sensors or the ADC conditioning circuit. These offsets of either the currents or the speed should be measured when the machine is in standstill mode with all the other modules or devices switched on. The measured offset current from the three phases should be subtracted from the ADC results in the code to compensate for the current offset. In order to get the samples of current offset, the DSP is allowed to settle for some time, allow DSP to run in steady state and then the offset can be sent to the oscilloscope or can be measured by taking many samples per second and taking their average. The speed offset can be done using the same way as the current offset.

DATALOG Module

The DATALOG module is not a hardware module of the F28335, instead, it is a section of highly-optimized code which will realize a virtual oscilloscope in the Code Composer Studio (CCS). The DATALOG software module stores 16-bit values of up to 4 observed variables in the data RAM, which are illustrated in Fig 4.17

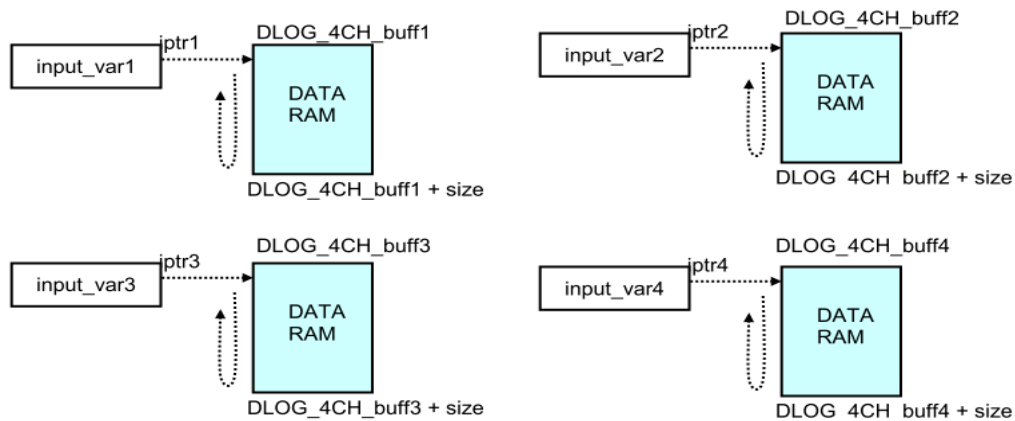


Fig 4.17: Four memory sections of DATALOG module

The values of the four data RAM sections are updated from the starting addresses to the ending addresses, with the four pointers (iptr1, iptr2, iptr3 and iptr4) moving from up to down. The data of these four data RAM sections are transmitted to CCS in real time through the JTAG port and the emulator. After a set of appropriate configurations, the graphical waveforms of the observed variables are plotted in the CCS Graph Windows as shown in Fig 4.18. The DATALOG module has brought a great convenience to the testing and the debugging of this project [30].

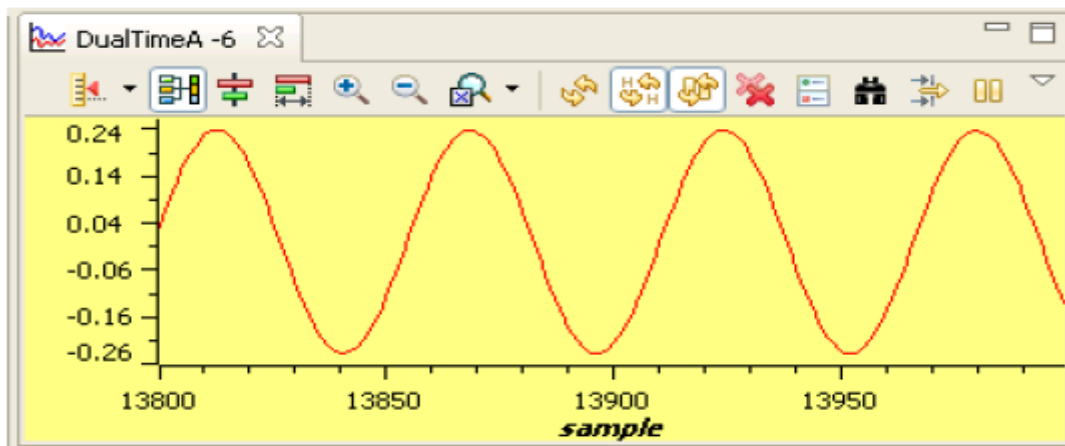


Fig 4.18: The graphical waveforms of the observed variables.

4.3 Testing and Evaluation

In the experimental part we encountered some problems such as the unavailability of speed sensor and current adapter circuit. To avoid these problems and to insure the right function of our program:

- We used internal speed estimator to get the approximate motor speed. The absence of the mechanical speed sensor improves the ruggedness of the drive and reduces the cost and the volume of the assembly.
- The ADC (current register values) is loaded directly By C-code. These values are generated by using sine table of TI.

One of the advantages of the setup we use in this project is that the user is able to access the memory, while the processor is still running.

Analysis of Results

The ADC provides the current values I_a and I_b then by using Clarke and Park transformations these currents are transformed to I_d and I_q .

The I_d and I_q are injected in the PI regulator and transformed to Clarke voltage by using inverse park transformation (V_α and V_β). The Clarke voltages (V_α and V_β) are shown in fig 4.19.

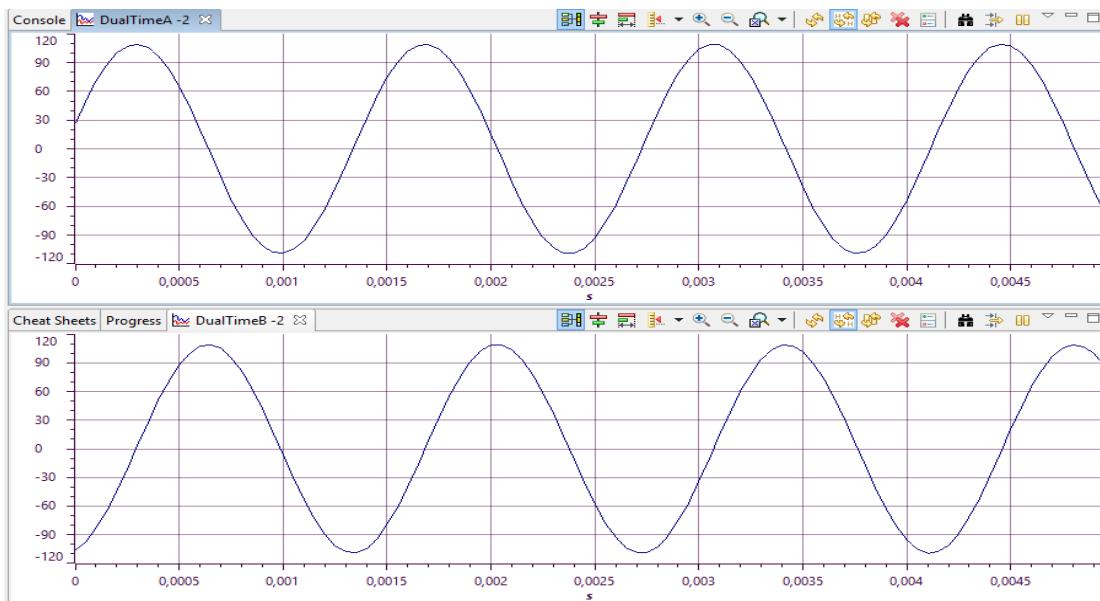


Fig 4.19: Clarke voltage (V_α and V_β).

V_α and V_β are injected in SVGEN module to get the duty cycles as shown in Fig 4.20

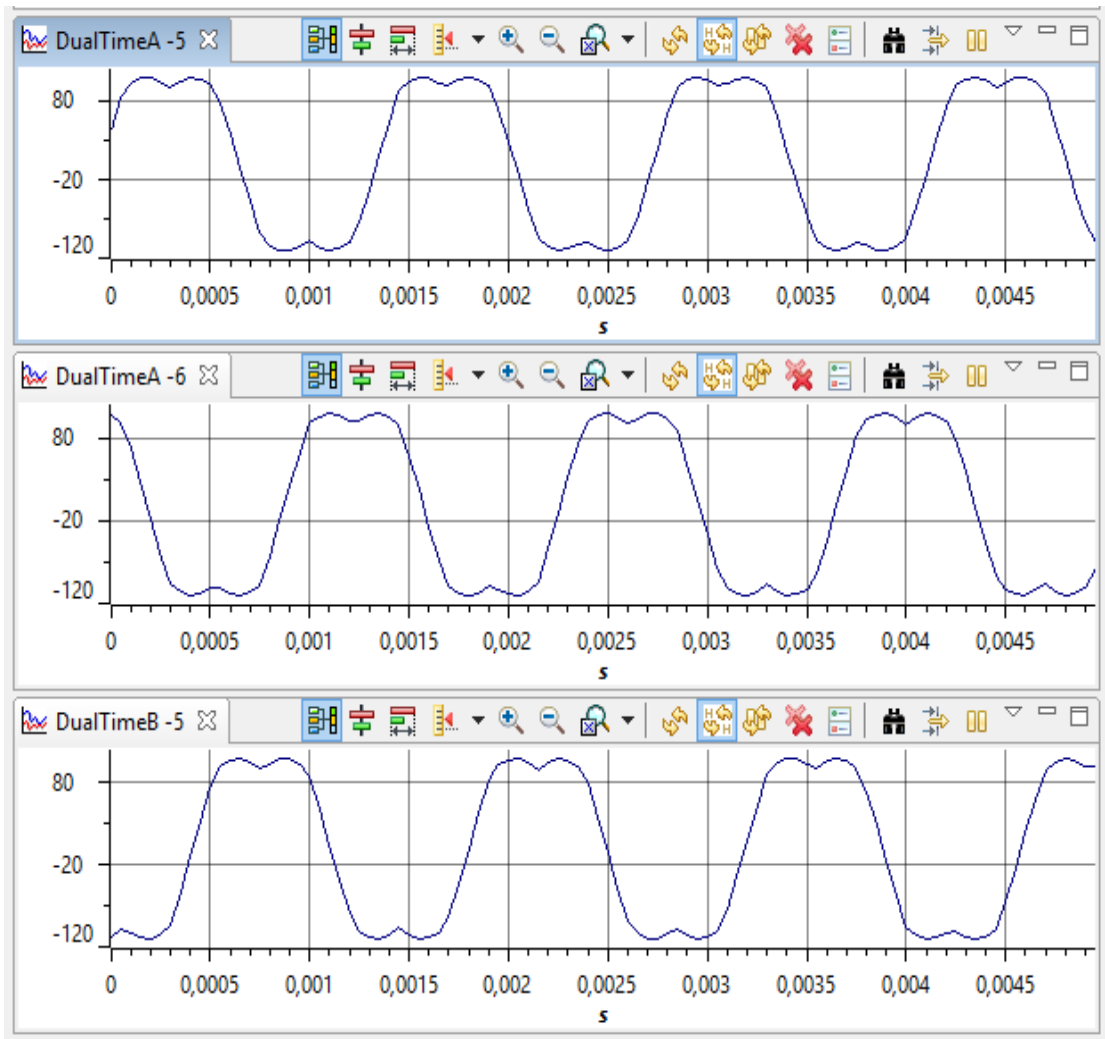


Fig 4.20: Duty cycles (T_a, T_b, T_c)

The duty cycles are used by the PWM sub-block to generate the six pwms (pwm1~pwm6) that control the six gates of the inverter. After that the inverter feeds the motor by the controlled voltages V_{abc} to reach the target speed.

Fig 4.21 shows the three upper pwms.

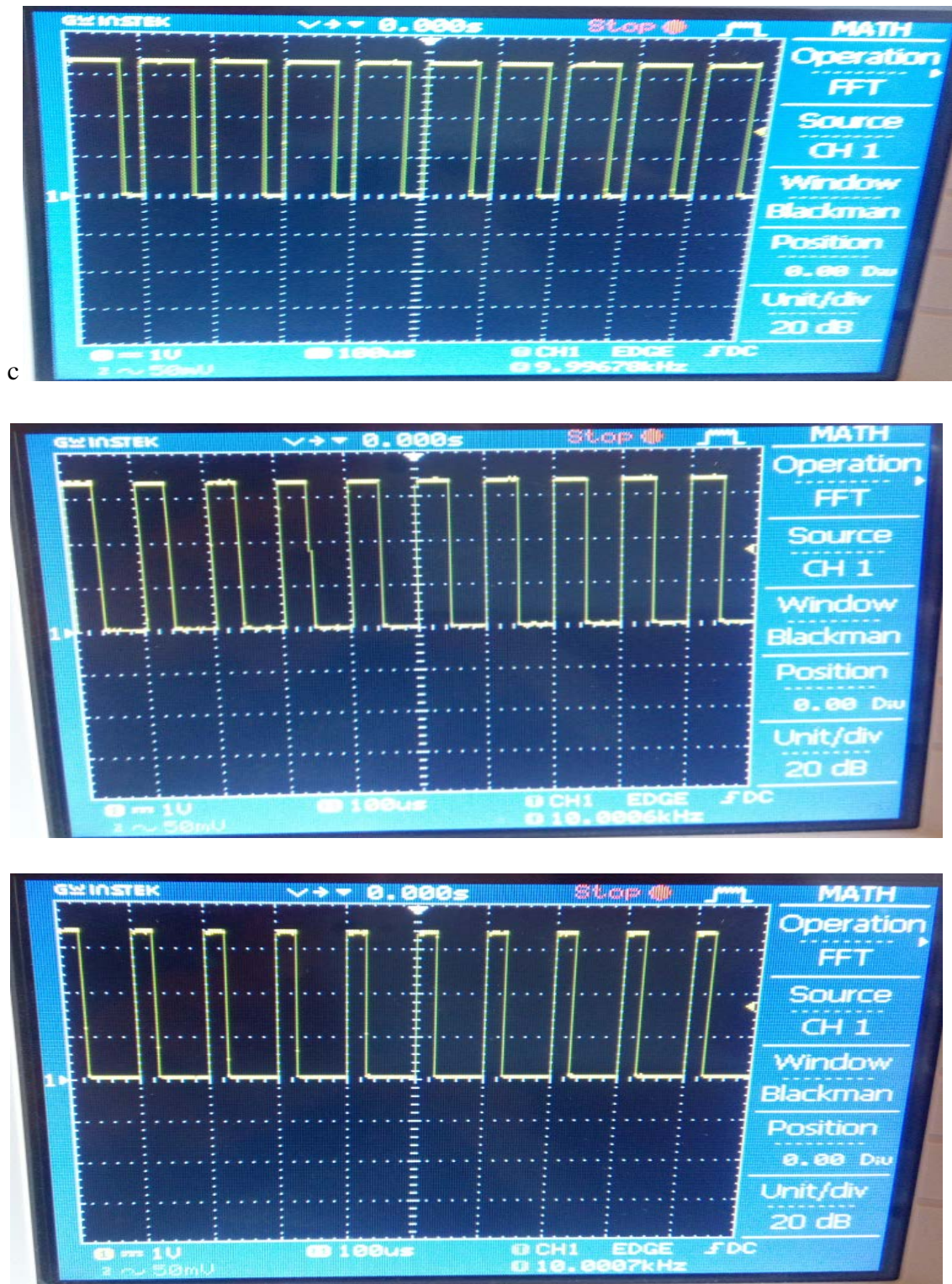


Fig 4.21: The three uppers PWM signals

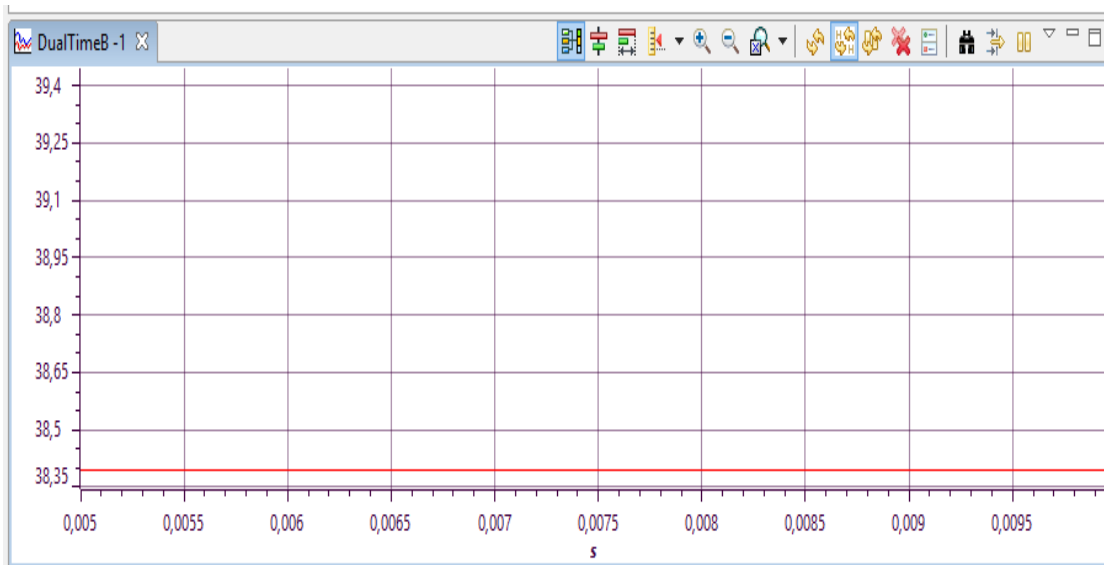


Fig 4.22: The Motor speed

The speed is kept constant at 38.4 rad/sec.

In our experimental test the currents loaded have the same values that explain the results obtained in Fig 4.22.

This test was carried out just to prove that our FOC program works and gives the right results.

4.4 Summary

The tested FOC program has shown good performances. If we used the real current signals from ADC, we will have some noise added to the measured signals. For the vector control design, the control system on the DSP manages to control the d,q currents and speed accurately. We notice also from the simulation that the FOC algorithm presents good results, the motor always reach the desired value whatever the load torque value.

CONCLUSION

A field oriented control technique of induction motor was presented in this thesis. The dynamic model of induction motor was developed in synchronous rotating frame, i.e., dq coordinate frame. The Clarke's and Park's transformations were used to convert the abc coordinate frame into the rotating dq frame. The transformation reduces greatly the complexity of the dynamic model. The 120° conduction of three-phase voltage source inverter theories are summarized in Chapter 2. The concepts of Space Vector Pulse Width Modulation (SVPWM) were discussed. The Space Vector PWM technique was developed to control the switching of three-phase inverter and is simulated with Matlab/Simulink. The theory of field oriented control was introduced and applied to control the dynamic model of induction motor. Both of the direct and indirect field control methods can be applied to calculate the rotor flux angle. The decoupled system can be achieved after applying the feed-forward control method. The developed PI controllers for speed and current control show satisfactory performances. The simulation results show the robustness and effectiveness of the designed controllers. The Texas Instruments software was used to implement the field oriented control of induction motor in hardware platform. The DSPF28335 hardware implementation demonstrated that field oriented control of induction motor can control the speed effectively.

Finally, some parts of the experimental setup still need to be improved. The parameters of the induction motor used in this test bench still need to be estimated. Some parameters are not precisely known and some parameters may vary with different operating conditions. Compensations regarding the motor parameters need to be further considered in the software program.

REFERENCES

REFERENCES

- [1] J.M. Miller, Propulsion Systems for Hybrid Vehicles, London: The Institution of Electrical Engineers, 2004.
- [2] M. Ehsani, Y. Gao, S. E. Gay, and A. Emadi, Modern Electric, Hybrid Electric, and Fuel Cell Vehicles: Fundamentals, Theory, and Design, Boca Raton: CRC Press, 2005.
- [3] Husain, Electric and Hybrid Vehicles - Design Fundamentals, Boca Raton: CRC Press, 2003.
- [4] Online source, available at http://en.wikipedia.org/wiki/Electric_motor, march 2016.
- [5] Online source, available at http://en.wikipedia.org/wiki/Reluctance_motor, march 2016.
- [6] Andrzej M.Trzynadlowski, Control of Induction Motors, Academic Press, A Harcourt Science and Technology Company, USA, 2001.
- [7] Online source, available at http://en.wikipedia.org/wiki/Induction_motor, march 2016.
- [8] W. Theodore, Electrical Machines, Drives and Power Systems, 6/E: Pearson Education India, 2007.
- [9] T. Gonen, Electrical Machines With Matlab: CRC Press, 2011.
- [10] Peter F. Ryff and David Platnick, "Electrical Machines and Transformers", Prentice-Hall, Inc., Englewood Cliffs, New Jersey, 1987.
- [11] Hi-Dong Chai, "Motion Devices and Transformers," Maple Press, San Jose, 1995.
- [12] Peter F. Ryff and David Platnick, "Electrical Machines and Transformers", Prentice-Hall, Inc., Englewood Cliffs, New Jersey, 1987..
- [13] A M. Trzynadlowski, Control of Induction Motors, Academic Press 2001
- [14] DSP-BASED ELECTROMECHANICAL MOTION CONTROL, Hamid A. Toliyat, Steven Campbell, Texas A&M University Department of Electrical Engineering College Station, Texas (chapter 13)
- [15] F. Tahri, A.Tahri, Eid A. AlRadadi and A. Draou Senior, "Analysis and Control of Advanced Static VAR compensator Based on the Theory of the Instantaneous Reactive Power," presented at ACEMP, Bodrum, Turkey, 2007.

REFERENCES

- [16] J. Lewis Blackburn, Symmetrical Components for Power Systems Engineering, Marcel Dekker, New York (1993).
- [17] Novotny, Donald and Lipo, Thomas, Vector control and dynamics of AC Drives, Oxford University Press, New York, 1996
- [18] H.A. Toliyat, ELEN689 Class Notes, Spring 2002.
- [19] R.Achouri, M.Hidouche, Engineering thesis Commande vectorielle de la machine asynchrone, ENP. June 2007
- [20] Jisha. L.K, P.Thomas, A Comparative Study on Scalar and Vector Control of Induction Motors
- [21] F. Blashke, The Principle of Field Orientation as applied to the new trans vector closed loop control system for rotating field machine, Siemens Rev, Vol 39,no.5,pp.217-220,May 1992.
- [22] S. Preitl and R-E. Precup, An extension of tuning relation after symmetrical optimum method for PI and PID controllers, Automatica 35(1999), pp.1731-1736.
- [23]Texas Instruments.<http://www.ti.com/lit/ds/symlink/tms320f28335.pages31-35>,april 2016.
- [24]Texas Instruments. <http://www.ti.com/lit/ug/sprug05a/sprug05a.pages9-15>, april 2016
- [25] D. Lewis. Fundamentals of embedded software design. Prentice Hall, 2002.
- [26]Texas Instruments. Code Composer Studio Integrated Development Environment. www.ti.com/tool/ccstudio, april 2016
- [27]Texas Instruments. F2833x analogue digital converter.Texas Instruments, Tech.Rep, april 2016
- [28]Texas Instruments. TMS320x280x, 2801x, 2804x enhanced pulse width modulator(epwm) module. Texas Instruments, Tech. Rep., July 2009.
- [29] Texas Instruments. TMS320x280x, 2801x, 2804x enhanced quadrature encoder pulse (eqep) module. Texas Instruments, Tech. Rep., December 2008.
- [30]Texas Instruments. 4-Channel Data Logging Utility Module, <http://www.ti.com>, april 2016

APPENDIX

APPENDIX A

Table A.1: The parameters of the induction motor for Matlab/Simulink simulation and DSP control implementation

Variable	value
Sn	50*746 (VA)
Un	460 (Vrms)
Rs	0.087 (ohm)
Rr	0.228 (ohm)
Ls=Lr	0.8 (mH)
Lm	34.7 (mH)
P	2
f	50 (Hz)
J	1.662 (kg.m ²)
fs	10 (KHz)

Table A.2: The calculated Kp and Ki values

	Kp	Ki
Current controller (i)	2.69732	148.34534
Speed controller (ω)	166.2	27700